2012

Body sensor network for in-home personal healthcare

Sheng Hu
Michigan Technological University

A BODY SENSOR NETWORK FOR IN-HOME PERSONAL HEALTHCARE

By

Sheng Hu

A DISSERTATION

Submitted in partial fulfillment of the requirements for the degree of

DOCTOR OF PHILOSOPHY

In Computer Engineering

MICHIGAN TECHNOLOGICAL UNIVERSITY

2012

This dissertation, "A Body Sensor Network for In-home Personal Healthcare," is hereby approved in partial fulfillment of the requirements for the Degree of DOCTOR OF PHILOSOPHY IN COMPUTER ENGINEERING.

Department of Electrical And Computer Engineering

Signatures:

Dissertation Advisor _____
Dr. Jindong Tan

Committee Member _____
Dr. Jeffrey Burl

Committee Member _____
Dr. Keat Ghee Ong

Committee Member _____
Dr. Paul Ward

Department Chair _____
Dr. Daniel R Fuhrmann

Date _____

To my wife, parents.

who didn’t hesitate to criticize my work at every stage - without which I’d neither be who I am nor would this work be what it is today.

Contents

[1] ©2009 IEEE. Portions reprinted with permission, from **Sheng Hu** and Jindong Tan, "*BioLogger: A wireless physiological monitoring and logging system*", in Proc. of IEEE Intl. Conf. on Information Processing in Sensor Networks, pp. 383 - 384, April 2009.

[2] ©2011 IEEE. Portions reprinted with permission, from **Sheng Hu**, Zhenzhou Shao and Jindong Tan, "*A Real-Time Cardiac Arrhythmia Classification System with Wearable Electrocardiogram*", in Proc. of Intl. Conf. on Body Sensor Networks, pp. 119 - 124, July 2011.

[3]

List of Figures

List of Tables

Acknowledgments

First and foremost, I would like to thank my advisor Dr. Jindong Tan for his guidance and advice of my research and study. His encouragement and support have carried me through this project. It is impossible for me to finish this dissertation without his encouragement, patience, and enthusiasm.

I would also like to thank my other committee members, Dr. Jeffrey Burl, Dr. Keat Ghee Ong and Dr. Paul Ward for taking the time to review and critique my dissertation and provide me with very valuable feedback. I would also like to thank my great labmates, who make my life in the Robotics and Embedded Systems Laboratory more colorful and enjoyable. They are Lufeng Shi, Shuo Huang, Fanyu Kong, Xi Chen, Xinying Zheng, Ya Tian and Zhenzhou Shao. I also want to say thanks to my friends at Tech, Xiaodao Chen, Jia Wang, Yonghe Guo, Xueqian Zhao for their continuous help. Specially, I want to thank Jian Lu for numerous valuable discussions on schematic and PCB design. Last but not least, I would like to thank my wife and parents for their supports and encouragement. Without their love, I could not have completed this endeavor.

Abstract

A body sensor network solution for personal healthcare under an indoor environment is developed. The system is capable of logging the physiological signals of human beings, tracking the orientations of human body, and monitoring the environmental attributes, which covers all necessary information for the personal healthcare in an indoor environment.

The major three chapters of this dissertation contain three subsystems in this work, each corresponding to one subsystem: BioLogger, PAMS and CosNet. Each chapter covers the background and motivation of the subsystem, the related theory, the hardware/software design, and the evaluation of the prototype's performance.

Chapter 1

Introduction

Fundamental biological and medical science and technology have made enormous strides over past centuries. Advanced technologies are having been aggressively applied to clinical diagnostics and treatments. X-ray Computed Tomography (CT), Nuclear Magnetic Resonance (NMR) and type-B ultrasonic are the most popular approaches assisting diagnosis - hence the length of life and quality of healthcare has significantly improved in the world. Unfortunately, the demographical trends and treatments experience are making the current healthcare system unsustainable. First of all, the United States' life expectancy has steadily increased over the years-with more than 3 percent of citizens (one in seven) are over sixty-five years old [1]. Moreover it is expected that there will be over a million people over the age of 100 in the United States by 2030. In addition, the increase in the aging population is associated with the great healthcare expenditure, which is estimated up to nearly 20 percent of the United States' Gross Domestic Product by 2010 [2], making the long-term personal healthcare a national concern, especially for the elders and the chronic disease patients. Due to this reality, improving access to healthcare and controlling the healthcare cost are the two concerns in the United States society. President Obama is committing himself to the comprehensive health care reform, and trying to achieve the following three goals during his first term: (1) reducing the healthcare cost for each family, (2) guaranteeing multiple healthcare choices, and (3) ensuring all Americans have quality, affordable healthcare. To achieve these targets, it is suggested that healthcare access has to be shifted from the clinical setting to the home, and the healthcare focuses on wellness management rather than illness diagnosis.

Coincident with an aging society is the technological revolution in sensors, VLSI, and wireless communication. The technological advances on these fields have accelerated the design of low-cost, low profile, and low-consumption sensor nodes. The sensor nodes, capable of acquiring, processing, and archiving multiple signals, can be seamlessly

integrated into a networking topology, which is termed Body Sensor Networks (BSNs). The appearance and development of BSN is paving the way for the applications of healthcare, and finding an ideal solution to ease the strain on the national budget. BSNs could support the independent lives of the elders and chronic disease patients via tracking cognitive health, detecting falls, or assisting the clinicians with physiological, biokinetic and ambient signals. With the use of BSNs, the long-term healthcare model effectively changes from a large centralized, caregiver-centric one to a distributed in-home and patient-centric one.

In this dissertation, the design and development of SmartHome is proposed , which is an innovative wireless body sensor network architecture designed for long-term in-home personal healthcare. It can monitor the health status of the subject and his or her surrounding environmental parameters in real-time.The results, in turn, will be extracted for real-time abnormality detection or delivered to a clinic sever via existing telecommunication infrastructure for further analysis and diagnostic analysis.

1.1 Personal Healthcare

Generally, different levels of healthcare service need to be provided during the different phases of the human's second-half life. From the age of 55 to 75, independent living services are enough, which may cover cognitive fitness, health aging and maintaining youth. For the next five years, assistant living services may be needed, which include daily activity monitoring, chronic disease prevention, and healthy heart. In the last stage of human life, which is above the age of 80, skilled nursing services are necessary. During this period, the subject probably needs 24/7 monitoring, active medical care and active daily activity monitoring [3]. It can be concluded that as the age increases, the requirement of more skilled, professional services are necessary.

1.1.1 Challenges

Historically, family fulfilled elders' personal healthcare. Before the 20th century, the family doctor visited the patient's home by carrying the necessary medical treatments in a doctor's bag, and the doctor conducted various tests to come out a diagnosis in the patient's home. However, this changed in the 20th century, because the patient started to need, but could not afford the rare and expensive resources. Therefore, the caregiving and healthcare became centralized in hospitals and nursing homes gradually. It was not until 1960s that personal healthcare industry emerged, when the government-run healthcare systems and commercial

nursing homes were established.

This healthcare model is "managing the illness" rather than "maintaining wellness": people do not go to the clinics or hospitals unless they feel sick, and doctors are waiting for the patients coming. In addition, the current model is inefficient for some chronic diseases. Patients visit the hospital regularly, reporting their suffered symptoms, experienced issues, and health conditions. Those repots are subjective. During each visit, multiple tests are applied to come out a diagnosis, which may not reflect the health status over the intervals.

Additionally, when society reached the 21st century, the centralized and caregiver-based model of long-term personal healthcare could not handle the imminent crisis caused by economic and demographic trends. On one hand, statistic data has shown that total health expenditure reached 2.3 trillion USD in 2008 [4], many individuals and companies have been plagued by increasing consumption on healthcare. On the other hand, baby boomers have moved into their 70's. The percentage of U.S. citizens above 65 has achieved 12.43% in 2000 [5] and is nearly 15% in 2010. Thus, the requirement for long-term healthcare services will rise dramatically. This trend is a global sensation: many countries are also suffering the increase of rising life expectancies. Therefore, it is highly necessary to fundamentally modernize the personal healthcare model into a decentralized and subject-based way, with technological improvements in wireless networking, microelectronics integration and miniaturization.

1.2 Body Sensor Networks

1.2.1 Wireless Sensor Networks

With the advances of automate sensing, embedded computing and wireless networking, it is promising to open up new opportunities in their integration at a large scale network with a low power consumption - which is termed as wireless sensor network (WSN). Typically, a WSN consists of spatially distributed autonomous nodes with sensors and a radio transceiver. The interconnections among them make the distributed in-networking processing possible. In contrast to the centralized wired networking model, separating the sensing module from the processing module via the short-term wireless connection is desirable for deployment - especially when considering biomedical, civil and other applications.

1.2.2 Body Sensor Networks

While WSNs continue to extend their broad range of applications, they do not specifically tackle the design associated with the characteristics of human body and its surroundings. Therefore, Dr. Guang-Zhong Yang, from Imperial College London, first introduced a novel term, Body Sensor Network (BSN) [6], which refers to the wireless platform suited to monitoring the human body and its surrounding environment.

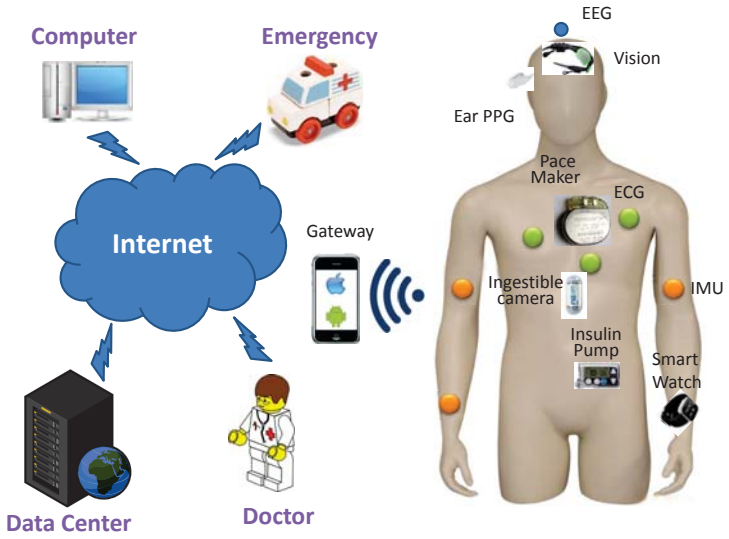

Figure 1.1: Architecture of a body sensor network.

Figure 1.1 illustrates a simplified example of a general BSN architecture. A subject is present with numerous sensors and actuators which are either implanted, worn, or in close proximity. They are able to monitor the physiological signals, such as photoplethysmophgraphy (PPG), Electrocardiography (ECG), Electromyography (EMG) and more. Each sensor is embedded with an on-board computation, storage and communication modules that forms a wireless network. This on-body network is capable of cooperating with home, office and hospital environment seamlessly to monitor the subject's physiological and biokinetic signals with environmental parameters. Prospectively, this wearable system can be integrated into a broader tele-medical system. The valuable data from the BSN is delivered to the clinic severs or clinicians to better understand the disease process and decide what therapy to start on the patient.

Following the continuous advances in WSNs, BSNs are intrinsically suitable for long-term personal healthcare. First, the integration of wireless communication, networking and information technology allows the personal healthcare to be unobtrusive. The subject is

free in an in-home environment, where the wearable sensor nodes helps to monitor his or her activity. Second, the medical information is helpful to monitor chronic illness, or detect the abnormalities in a timely manner. With the on-board computational ability, the BSN can synthesize the data from various types of sensor types, and detect the abnormalities - even before the subject feels it. The emergency notification can be sent via the short message service to the clinician. Therefore, the response time of first aid can be reduced greatly. Lastly, BSNs can be integrated into a telecommunication system or Internet, the real-time health status of the subject is able to be delivered to the clinicians remotely.and thus diagnosing the patient in a timely and efficient manner.

1.2.3 Challenges on BSN

There are still a number of obstacles as size, cost, and compatibilities before they are widespread. Although the challenges met by BSNs are similar to WSNs, intrinsic properties make BSN exposed to more challenges. For example, convenience is the first priority to the wearable sensor node design. Futurist Michio Kaku created the concept of "silently monitor" [7], referring to BSNs working in an unintrusive way, so that the subject's daily life will not be disturbed. Therefore, the life time and outline are the first concerns for the designers when considering the wearable sensor node design. In this subsection, we discuss the current challenges on BSNs in the following aspects.

1.2.3.1 Power Consumption

Compared to WSNs, power consumption is more critical in BSNs, especially for the battery-supported wearable nodes. On one hand, frequent battery replacement will annoy the patients during daily lives and what is worse, the replacement of battery in some implanted sensors is unreasonable. On the other hand, the shortage of energy will probably result in missing critical alarms on physical conditions in some vital sign monitoring applications. Therefore, to save the power and prolong the lifetime of battery are the paramount concerns in wearable node design.

Previous researches have shown that the existing short-range wireless communication techniques consume more power on average than processing the same volume of data via the microcontroller (MCU). Therefore, the common strategy for most BSNs will be to find out the balance between processing data and transmitting data, such that, the redundant data are filtered out on-node, only the valuable and necessary information are sent out in the air.

1.2.3.2 Sensors and Signal Conditioning

Basically, sensors in BSNs can be classified into two categories: physiological sensors and inertial sensors. Physiological sensors focus on measurements of human vital signs, such as blood pressure, internal body and skin temperatures, ECG, electroencephalography (EEG), and EMG. In contrast to environmental parameters in WSNs, such as indoor temperature and humidity, the unconditioned physiological signals are in the order of microvolts and always coupled with large common mode noise. This characteristic necessitates the proper analog signal conditioning circuit before the physiological signals are fed into the analog-digital converter. Moveover, the physiological signals are sensitive to the environment around the human body. Take ECG for example, ECG is a transthoracic interpretation of the electrical activity of the heart [8], which can be detected by on-body electrodes. However human motions corrupt the signal quality seriously. In hospital, a traditional Holster instrument requires the subject keep still for clear ECG waveform acquisition. However, it is unreasonable to require the patients to keep still during a long-term ECG monitoring through a wearable ECG sensor node in BSNs. Therefore, sensor design in BSNs should consider the stability of signal acquisition.

Inertial sensors, such as accelerometers and gyroscopes, which measure acceleration and rotation angulate rate of the human body, can infer the subject's position, velocity, and orientation. However, most inertial sensors have several error sources, which are more difficult to deal with. Therefore, two challenges are proposed when inertial sensors are integrated into BSNs: calibration and data filtering. Every inertial sensor is required to be calibrated after assembly in order to remove null bias error and scale factor error. Null bias error is the deviation from zero when the inertial sensor is experiencing no stimulus, and scale factor error is the deviation from ideal of the sensor's sensitivity. Orientation estimation and location tracking are more sensitive to those noise: if they are not treated properly, small errors in angular velocity readings will be integrated into progressively larger errors in orientations, and cause the rapid degrade of performance. The same situation will also occur when accelerations are integrated into positions. Therefore, data filtering is necessary once inertial sensors acquire the raw biokinetic parameters.

1.2.3.3 Wireless Communication

There is no specific standard of wireless communication for BSNs. Hence BSNs share a couple of technical challenges with WSNs, such as radio power consumption, node discovery, and quality of service. While compared with WSNs, BSNs have different concerns in communication range that are required to be restricted in a limited distance.

First of all, privacy is more concerned in BSNs. The data generated by the wearable sensor nodes are related to the physiological status of the patient, which are not allowed to access unless they are authorized. Second, the transmission range needs to be limited to reduce a node's power consumption. It has been shown that the power consumption by the radio module is dominant among all other on-node modules. Therefore, to restrict wireless communication range can prolong the lifetime of a wearable node in a sense. Third, the communication range needs to be shorten to help avoid interference among adjacent BSNs.

Another challenge in this subfield is the mechanism of radio around the human body. Typical communication techniques use the wireless channels from 850MHz to 2.4GHz. More work needs to focus on the dielectric constants of various tissue in the human body, propagation models for radio frequency communication in and around the human body, the interference by the movement of the human body and so on.

1.2.3.4 Storage

The development of Micro-Electro-Mechanical Systems (MEMS) makes the mass storage reality on a wearable sensor node. Consequently, the availability of on-node storage may extend BSNs functionalities in both realtime and delay-insensitive applications. For realtime applications, such as ECG monitoring, on-node storage is a redundant solution once the wireless connection between wearable nodes and gateways is temporally unavailable. For those longitudinal monitoring which is insensitive to time delay, caching data on node is a more reasonable strategy than transmitting all the data to a gateway.

1.3 A BSN Solution of In-home Personal Healthcare

To address the existing challenges, we propose a wireless body sensor network solution, SmartHome, for in-home personal healthcare. Figure 1.2 illustrates the layout of a SmartHome where the data acquisition and mining are fulfilled by a BSN. Data are collected according to a clinician's specifications, and sent to the clinician's side via telecommunication infrastructure, in such a way that the traveling burden can be released from the patient. Besides the persuasive monitoring, SmartHome will also assist the elders and patients during the daily lives, such as event reminders, appliance control, subject localization, and emergency alarm. Eventually, every sensor in SmartHome is going to be assigned an IPv6 address via 6LoWPAN, such that it would be integrated into Internet transparently.

SmartHome benefits both the patients and their healthcare providers. For patients, SmartHome helps improve health due to long-term monitoring, realtime diagnosis and reduction of abnormality response time. Other life quality problems, such as privacy, safety, and convenience, are solved by deploying healthcare services in the patient's own home. The patient will feel comfortable in their own house. Moreover, the patients could have their daily lives freely, which reduces the labor cost and increases the efficiency. Last, family members with the help of SmartHome would become part of the healthcare team.

On the other hand, an realtime healthcare assistant system would also benefit the care providers from the following ways. First of all, wearable sensor devices can detect the tiny variation of the vital signals, such as heart rate or blood oxygen levels, which might not be felt by the patients themselves. Notification of the abnormalities to the doctors in a realtime way greatly reduce the response time to save people's lives. In addition, the data archived by SmartHome help physicians make more informed diagnoses. Finally, both patients and caregivers do not worry about "White Coat Syndrome" which often happens in hospital.

Figure 1.2: Overview of SmarHome.

This dissertation details our hardware and software design for medical monitoring, discusses challenges, and introduces our solutions for physiological signal and inertial signal monitoring. The contributions are summarized as follows:

† Unintrusive wearable sensors for multiple physiological signals;

† Unintrusive wearable sensors for multiple inertial signals;

† Realtime heart abnormality detection;

† Assistance to the elders and chronic disease patients;

† Clinician remote diagnosis and assistance;

† Integration with the existing telecommunication infrastructure.

1.4 Publications

The work presented in the dissertation has been the basis for the following publications by the author:

1. Xi Chen, **Sheng Hu**, Zhenzhou Shao and Jindong Tan. "*Pedestrian Positioning With Physical Activity Classification for Indoors*", in Proc. of IEEE Intl. Conf. on Robotics and Automation, pp. 1311 - 1316 ,May 2011 [9].

2. **Sheng Hu**, Zhenzhou Shao and Jindong Tan. "*A Real-Time Cardiac Arrhythmia Classification System with Wearable Electrocardiogram*", in Proc. of Intl. Conf. on Body Sensor Networks, pp. 119 - 124, July 2011 [10].

3. **Sheng Hu**, Xi Chen and Jindong Tan. "*PAMS: A Wearable Physical Activity Monitoring System for Continuous Motion Capture in Free-living Environments*", in Proc. of Intl. Conf. on Body Area Networks, pp. 233 - 239, September 2010 [11].

4. **Sheng Hu** and Jindong Tan. "*BioLogger: A Wireless Physiological Sensing and Logging System with Applications in Poultry Science*", in Proc. of Intl. Conf. of the IEEE Engineering in Medicine and Biology Society, pp. 4828 - 4831, September 2009 [12].

5. **Sheng Hu** and Jindong Tan. "*BioLogger: A wireless physiological monitoring and logging system*", in Proc. of IEEE Intl. Conf. on Information Processing in Sensor Networks, pp. 383 - 384, April 2009 [13].

6. Jin He, **Sheng Hu** and Jindong Tan. "*Layered hidden Markov models for real-time daily activity monitoring using body sensor networks*", in Proc. of the 5th Intl. Summer School and Symposium on Medical Devices and Biosensors, pp. 326 - 329, June 2008 [14].

7. **Sheng Hu** and Jindong Tan. "*Compressive mobile sensing for robotic mapping*", in Proc. of IEEE Intl. Conf. on the Automation Science and Engineering, pp. 139 - 144, August 2008 [15].

8. Rex Wong, **Sheng Hu**, Cabrera-Mora, Jizhong Xiao and Jindong Tan. "*A Distributed*

algorithm for mobile robot localization and mapping in wireless sensor networks", in Proc. of Intl. Conf. on Information and Automation, pp. 560 - 566, June 2008 [16].

1.5 Organization

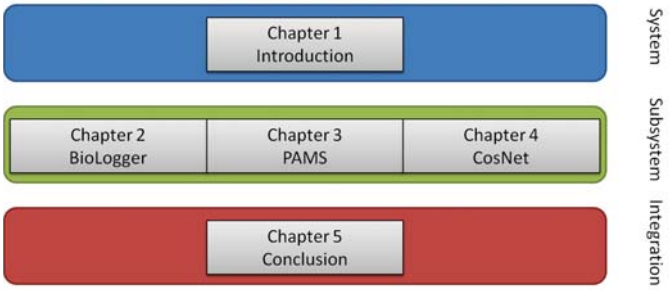

Figure 1.3: The structure of dissertation.

This dissertation are organized into three parts:

Chapter 1 gives the overview of this dissertation, discussing the background and challenges of in-home personal healthcare. After that, we propose body sensor network to be a solution for this issue.

From Chapter 2 to Chapter 4, three subsystems in SmartHome are proposed respectively , which address the monitoring of physiological signals , inertial signals, and environmental signals. Chapter 2 presents the design and development of BioLogger, a wireless physiological signal sensing and logging system. BioLogger can simultaneously monitor and record various types of physiological signals and the patient is continuously monitored in a free living environment. In addition, the electrocardiogram (ECG) front-end is carefully designed to guarantee clean and reliable analog ECG fed into the analog-to-digital convertor. Moreover, long term continuous monitoring of ECG in a free living environment provides valuable information for the prevention on the heart attack and other high risk diseases. But previous works only provide the function of ECG recording or ECG diagnosis in an in-hospital environment. Therefore, a realtime cardiac arrhythmia classification algorithm is also proposed in Chapter 2, in which a novel layered hidden Markov model is introduced to classify multiple cardiac arrhythmias in realtime.

Long term continuously monitoring of human physical activities in free living environments provides valuable information for a wide range of applications. And Chapter 3 presents the design and implementation of a physical activity monitoring system (PAMS).

It can capture human motions which potentially provide many new types of human health assessment and intervention mechanisms for obesity management, rehabilitation, assisted living and human robot interaction. A low power design is applied for PAMS in the hardware/middleware design and the signal processing/filtering algorithms to reduce the number of packets transmitted to the gateway. A full 6-DoF inertial measurement unit is integrated in PAMS to achieve highly reliable inertial data. With highly reliable inertial data, PAMS is designed for a spectrum of applications in healthcare monitoring, electronic entertainment and biokinetics researches. Case studies of realtime human motion tracking via PAMS are demonstrated and performances are evaluated.

Chapter 4 introduces the prototype of a static sensor network, which is used for the environmental monitoring around the human beings (CosNet). The auxiliary information acquired by CosNet will support SmartHome to understand the health status of human beings. Also a case study is presented in the end of this chapter that the ultrasonic sensors are used for localize the subject in an indoor environments.

Chapter 5 summarizes the contributions of the current work and their points of strength, compared with previous works. In addition, some of possible directions of research are also discussed as open problems for future studies. Figure 1.3 depicts the conceptual links between the different chapters.

Chapter 2

BioLogger: A Wireless Physiological Sensing and Logging System[1][2]

2.1 Introduction

Several factors have converged to create new opportunities to address the efficient in-home healthcare system. First, more and more people are suffering the chronic deceases. Cardiovascular diseases (CVDs) have become one of the leading underlying causes of death in both developing and developed countries. A recent report from American Heart Association claims that 81.1 million American adults (more than one third) are estimated having one or more types of CVDs, and they account for 34.3% deaths in 2009 as the underlying causes [2]. Moreover, the health expenditure with established healthcare delivery has been dramatically rising. United States is one of the developed countries that have highest growth rates in the healthcare costs. The share of GDP devoted to healthcare has grown from 9 percents in 1980 to 16 percents in 2008 [17]. Last, the aging of population is one of the urgent social issue in developed countries. In United States, the baby-boomers have reached their retiring age [1], their long term in-home care is becoming an concern recent years. Therefore, efficient long term monitoring systems are motivated for personal in-home healthcare.

[1] ©2009 IEEE. Portions reprinted with permission, from **Sheng Hu** and Jindong Tan, "*BioLogger: A wireless physiological monitoring and logging system*", in Proc. of IEEE Intl. Conf. on Information Processing in Sensor Networks, pp. 383 - 384, April 2009.

[2] ©2011 IEEE. Portions reprinted with permission, from **Sheng Hu**, Zhenzhou Shao and Jindong Tan, "*A Real-Time Cardiac Arrhythmia Classification System with Wearable Electrocardiogram*", in Proc. of Intl. Conf. on Body Sensor Networks, pp. 119 - 124, July 2011.

The prerequisite of healthcare is to understand the health status of the subject. A traditional monitoring system usually uses a direct-wired connection between the subject and the instrument, the subject is therefore confined to the monitoring instrument. Hence wearable wireless sensors for health status monitoring attracts more and more attentions. It detaches the sensing unit from the processing unit, such that the subject with wearable sensors can be monitored in a free living environment. Moreover, a conventional monitoring system is usually only used for collecting data, while the data processing and diagnosis are done offline [18]. In contrast, the on-body sensor in the wireless monitoring system can detect early abnormities by local computational capacity, even when the subject is unaware and unconscious [19]. For the aging people with heart deceases, emergencies often occur when the patients are sleeping. Hence it is critical that the medical disorders can be detected early. Finally, using the telecommunication infrastructure [20], data can be directly delivered to the clinics, where doctors can remotely analyze realtime physiological status of the subject, and make correct diagnosis timely.

Unfortunately, there still exist technical challenges for the application of wearable wireless sensors in biology science and healthcare. First, the clear and stable signal is the paramount concern in healthcare applications. Taking ECG as an example, the accuracy of ECG processing and cardiac arrhythmia classification are all based on the quality of raw ECG morphology. Therefore, the analog front-end for physiological signal sensing should be carefully designed such that most coupled noises are canceled out before they are fed into an analog-to-digital convertor (ADC). Second, most of the existing systems only consider monitoring one single physiological signal [21][22], while multiple physiological statuses are required simultaneously in reality. For example, a subject's heart rate is detected higher than normal. It is possible that the subject is having exercise at that time, or the subject is suffering heart attacks. In this scenario, only heart rate is not enough to infer the reason. Other information are required for the correct judgement. Third, the wearable ECG sensor node is an energy-limit system. Energy efficiency considerations on a wearable system includes low power hardware/software codesign, power efficient networking, and so on. All the components in this system are carefully chosen with the sleep mode, such that they can be configured into sleep mode according to the requirements of applications. Last, the wearable sensor node needs to be low profile in weight and size, such that the patient's daily life will not be annoyed.

To address these technical challenges, BioLogger, a system prototype for biological monitoring and logging, is proposed. The subject is monitored by a wearable sensor node in such an un-obstructive way that his daily life will not be interrupted. All physiological signals are digitalized by an on-node ADC module and transmitted to a smart phone via Bluetooth. On the smart phone, the waveforms are visualized and corresponding diagnosis approaches are applied to infer the human health status. Once the system detects the patient's abnormalities, the alarm message will be sent to the caregivers or clinics via the embedded WiFi or 3G interface on the phone. The high-level goal of this system is to

enable the long-term continuous physiological signal monitoring and realtime detection of multiple cardiac arrhythmias. The contributions of this system are highlighted as follows:

† BioLogger is able to collect the various realtime physiological signals simultaneously: electrocardiogram (ECG), electroencephalogram (EEG), respiration rate and skin temperature. Moreover, an extension socket is available for additional signals;

† Energy efficiency considerations of BioLogger include low power hardware and software design, and power efficient networking;

† An improved ECG analog front-end circuit is designed aiming at enhancing the anti-noise ability;

† A novel layered hidden Markov model is proposed to detect cardiac arrhythmia from sensor readings directly;

† The physiological signals and human health status are visualized on a smart phone in real time;

† The smart phone could access the remote clinical database using its WiFi or 3G interface.

2.2 Systematical Design Overview

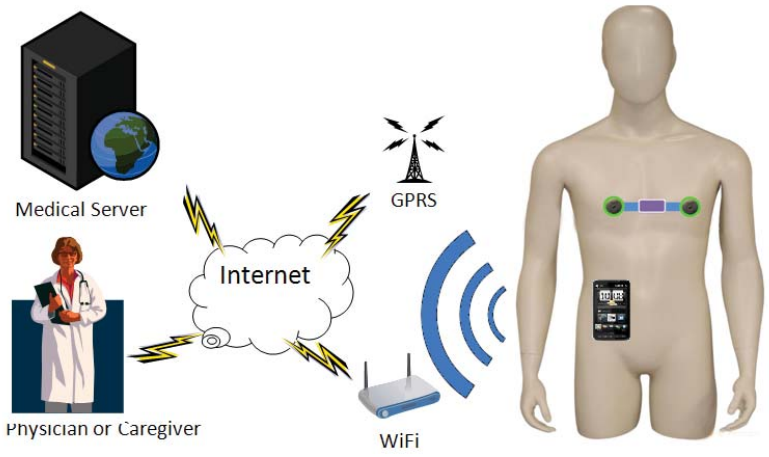

Figure 2.1: The architecture of BioLogger.

The BioLogger system consists of two parts: multiple wearable sensor nodes and a smart phone as a Gateway, as shown in Figure 2.1. Sensor node (Figure 2.2) attached to the subject's body acquires the physiological signals from the subject, and converts them to digital data. These data can be stored in MicroSD card on sensor node, preprocessed using the on-board computational capability, or transmitted to gateway using Bluetooth technology.

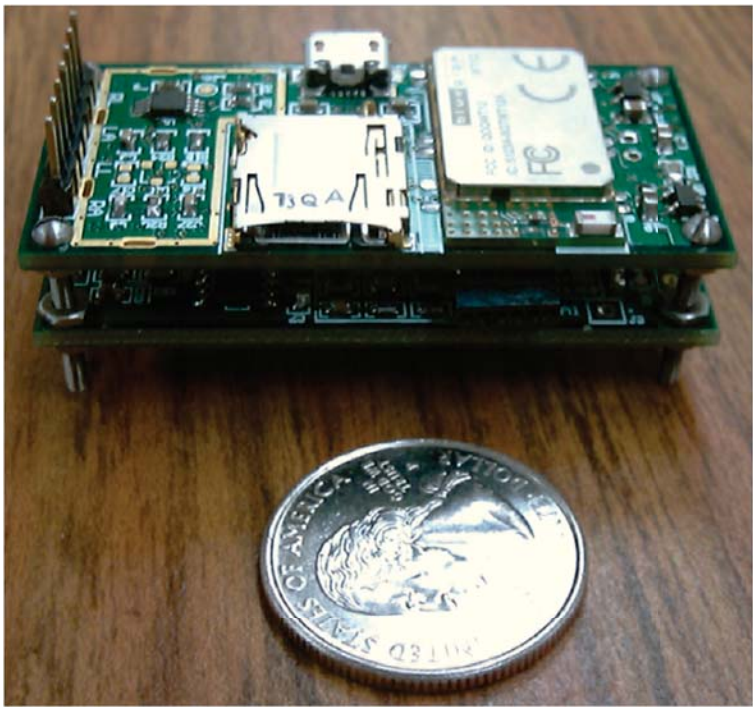

Figure 2.2: One sensor node in BioLogger.

Gateway visualizes the physiological signals and is open for various realtime physiological signal based approaches for diagnosis. Once BioLogger detects the subject's abnormalities, the alarm message will be sent to the caregivers or clinics by the embedded WiFi or 3G interface on gateway.

The following of this chapter will be organized as follows. Each module on sensor node will be discussed sequently, and then we will introduce how gateway receives the data and how it processes these data. After that, a case study of cardiac arrhythmia classification by BioLogger will be presented.

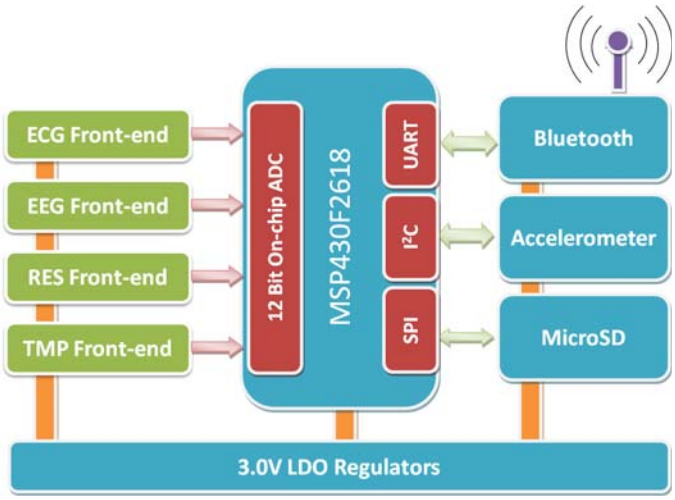

Figure 2.3: The block diagram of sensor node in BioLogger.

2.2.1 Sensor Node Design Overview

The wearable sensor node consists of seven modules: analog front-end circuits for four physiological signals, a radio communication module, a storage module, and a microcontroller unit (MCU), as shown in Figure 2.3. The raw signals from the electrodes are fed into corresponding analog front-end circuit for noise decoupling, and then they are amplified to a proper dynamic range and fed into the on-chip ADC. After that, the MCU can process the data on the specific requirements. The storage module can store all the data on a MicroSD card and the radio module can transmit data wirelessly to gateway. The specifications are summarized in Table 2.1.

2.2.2 Gateway Design Overview

The gateway in BioLogger has three functions. First, it serves as a data sink which gathers all the data from sensor nodes. Second, it is capable of analyzing the data from sensor node and making the correct diagnosis. Last, it behaves as an interface to the telecommunication infrastructure via WiFi and 3G network, from which the physiological signal is able to be transferred to the medical care service for further diagnosis or the physician can realtime monitor the subject remotely. Therefore, four requirements are proposed for the gateway. First, the gateway have to support both the short range wireless communication with sensor node and wireless Internet access respectively. Second, it has powerful computational capability to deal with the physiological signal in real time. Third, it must be a portable device such that there is no impact on the subject's daily life. Before the prototype is

Table 2.1
Specifications of the sensor node.

Module	Parameter	Specification
ECG	Gain	120
	Sampling rate	100Hz
	Low pass cutoff frequency	40Hz
	High pass cutoff frequency	0.1Hz
EEG	Gain	7680
	Sampling rate	100Hz
	Low pass cutoff frequency	30Hz
	High pass cutoff frequency	0.1Hz
Temperature	Sampling rate	1Hz
	Sensing Range	-80 to +150°C
Respiration	Sampling rate	10Hz
On-chip ADC	Resolution	10 bit
Radio	Data rate	250Kbps
Storage	Capacity	2GB
Power	Voltage	3.0V

brought up, we choose the smart phone to serve as Gateway rather than developing a brand new evaluation board. A few factors are concerned during the decision. First, the smart phone on the market meets the requirements mentioned above. Second, using the existing smart phone can reduce the cost of development. Last, carrying a smart phone has been a part of human's daily life, other forms of gateways will be an extra burden for the subject.

Among the amount of the off-the-shelf smart phones, we choose windows mobile based HD2 rather than other operating system phones, like iPhone or Android phones. Window mobile operating system offers almost the same API with the ones on the desktop version, therefore we can transplant the desktop software to the mobile device easily. In addition, Visual Studio have already supported the embedded system development, we can develop the user interface on the smart phone seamlessly. Last, the development on the Windows mobile is free, the developer does not need to pay for the authority.

Currently there are the two functionalities implemented on gateway:

Realtime Physiological Signal Display

As realtime digitalized data reach the gateway, HD2 in BioLogger, radio communication thread dumps the data on air to the memory, the display thread are used to plot them on the screen. The ECG waveform is visualized on screen, as shown in Figure 2.4. The

waveform can be zoomed in/out by sliding the screen such that the user is able to examine the physiological signal in a close way. The scale of the axis for ECG plotting follows the clinical standard of a resting ECG machine: the unit for the vertical voltage axis is 0.5mV/Div, and the unit of the horizontal time axis is 200ms/Div. Meanwhile, each beat is classified and annotated by two read line showing each QRS complex.

Realtime Diagnosis Platform// The framework of the user interface only provides the basic functionality to communication setup and waveform visualization. More realtime diagnosis approaches can be embedded into this framework as a plugin. These approaches could be implemented as a separate dynamic linked library (dll) out of the main framework and has its own thread. Using this framework, multiple dll plugins would be developed for different vital sign analysis and realtime diagnosis without changing the main framework.

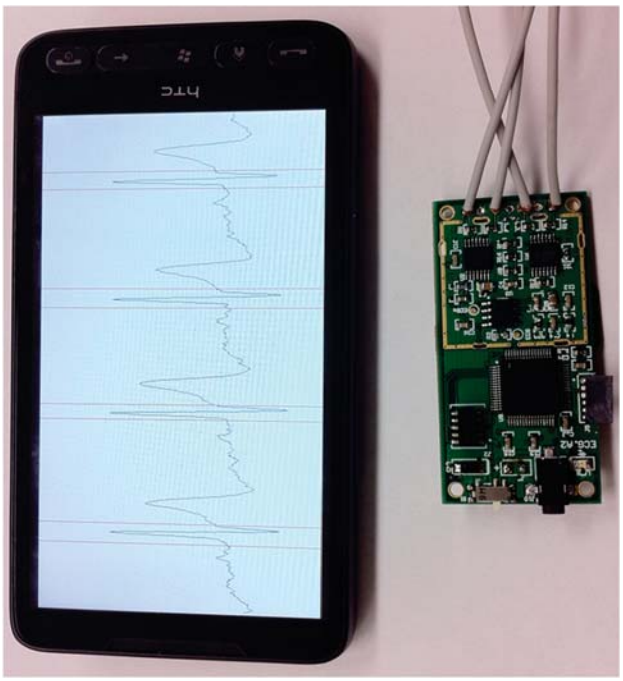

Figure 2.4: HTC HD2 is collecting data from sensor node.

2.3 Physiological Signal Processing

In order to acquire accurate and stable analog signals, it is critical to grantee the firm connection and proper grounding for any mix-signal embedded systems. Therefore, the analog front-end, as the direct touch of the raw signal, is the first concern in a system design. If the analog front-end is not well designed, the reconfigurability of the entire

system is at stake. Therefore we will focus on the analog front-end design in senor node in this section.

2.3.1 Electrocardiography

2.3.1.1 Noise Handling and Grounding

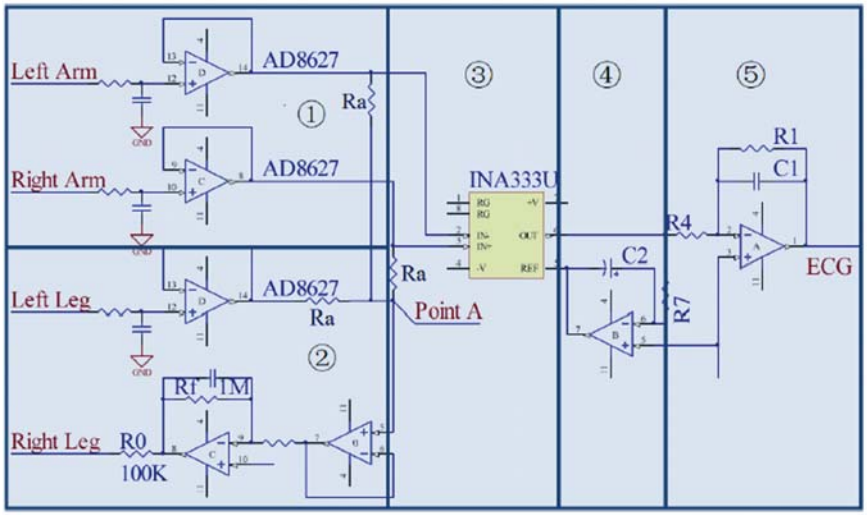

Figure 2.5: The schematic design of the ECG analog front-end circuit. (1) Two JFET input voltage followers. (2) The driven right leg circuit. (3) Instrumental amplifier, INA333. (4) An AC coupled circuit. (5) An active filter.

For an ECG monitoring and diagnosis system, any noise on ECG waveforms will limit the resolution of further analysis and diagnosis. Hence, the ECG analog front-end design is the paramount concern in most ECG systems. The unconditioned ECG from the electrode is an extremely weak signal ranging from 0.5mV to 5.0mV, while the magnitude of the coupled noises could be up to $\pm$300mV. Therefore, the noise must be handled carefully in order to pick up the valid ECG waveform. Most noise of wearable ECG are associated with the following resources:

† The large common mode noise results from the voltage potential between the electrodes and ground.

† The great DC offset resulting from the electrode-skin contact limits performance of

the instrumentation amplifier.

† The system can pick up the electrical noise (50Hz in Americas and 60Hz in most parts of the world) at any point along with the signal flow.

† The changes of the impedance and capacitance are sensed by the ECG electrode and result in motion artifacts.

† The radio frequency interference (RFI) can be coupled into ECG along the leads.

To deal with these noises, the ECG analog front-end design in sensor node gives the complete solution, as shown in Figure 2.5. A voltage follower in Figure 2.5(1) is plugged in the each input channel. This is due to the fact that the input bias current (I_b) of the front-end amplifiers can polarize the electrode if there is poor skin contact: $\Delta v_e = I_b \cdot \Delta z_e$, where Δv_e is variation of the voltage at the electrode site and Δz_e is the equivalent impedance variation. Therefore, AD8627, a JFET input operational amplifier with input bias currents less than 1pA, is selected here to reduce the influence by the impedance variation at the electrode site. The RC network before AD8627 is used for electro-static discharge (ESD) protection.

By plugging in these two voltage followers, the interference of motion artifact will reduce a lot. Figure 2.6 depicts degradation of the ECG waveforms under different stress conditions. The digital filter on node is disabled to concentrate on the performance of the front-end. It can be concluded from this figure that key features can be still identified with slight activities. However, when the patient is jogging, only QRS complex in the ECG waveform can be detected reliably.

Moreover, most ECG front-ends are 3-lead configuration circuits, in which the third lead is a driven right leg circuit for injecting the inverted common mode noise back into the body to cancel them out. Unfortunately, the reason why the driven right leg circuit is required and how it works are not well explored in many designs, which results in non-optimality in these designs. Actually, the driven right leg circuit [23] can provide a low impedance path between the patient and the amplifier, such that less common mode noise will be transformed by the amplifier. If G is defined as the resistor ratio of the inverting amplifier, $G = \frac{2 \cdot R_f}{R_a}$ in the traditional driven right leg circuit (Figure 1 in [23]). G needs to be set as large as possible to minimize the common mode voltage v_c.

In contrast to the typical driven right leg circuit, a novel driven right leg circuit is proposed here, in Figure 2.5(2). We name the circuit 4-lead configuration front-end, where the fourth lead connected to the left leg of the body. The signal along this channel will not be amplified but only provide an bias at point A. Therefore, G is modified to $G' = \frac{3 \cdot R_f}{R_a}$ due to the third input channel, such that G' is 1.5 time to G when other parameters do not

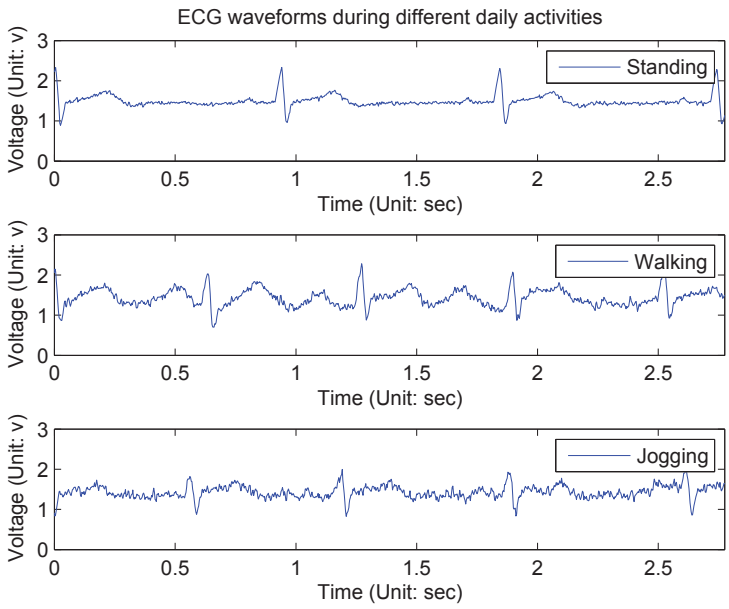

Figure 2.6: ECG waveforms captured during different daily activities. The charts show a three-second snapshot.

change. Empirically, we find that 100 is a proper value for the gain, since a higher value will affect the stability of the system. Therefore, R_0 is set to 10kΩ and R_f is set to 1MΩ in this design. From the experimental results shown in Figure 2.7 and Figure 2.8 (These waveforms are not processed by the digital filter on node). It can be concluded that in an clear and noise-free environment, the performance of the modified driven right leg circuit is the similar to the traditional one [23]. However, when the wearable sensor node is placed in a high interference environment, the proposed circuit largely outperforms the traditional one.

Other methods for suppressing the noise and removing DC offset include:

† One INA333 with a high common mode rejection ratio (100dB) is placed in the first stage of amplification, as shown in Figure 2.5(3). Its structure with three operational amplifiers makes it reject the common mode noise. In addition, it contains an internal RFI filter to get rid of most RFI.

† An AC coupled circuit in Figure 2.5(4) is designed to remove the large DC offset, such that the gain of operational amplifier in Figure 2.5(5) can be set as large as possible. According to our experience, setting the cutoff frequency, $f_c = \frac{1}{2\pi C_2 R_7}$, to be 0.5Hz has the best performance. If the frequency were lower than 0.5Hz, the capacitor would be charged for a long time, resulting in saturation of the operational

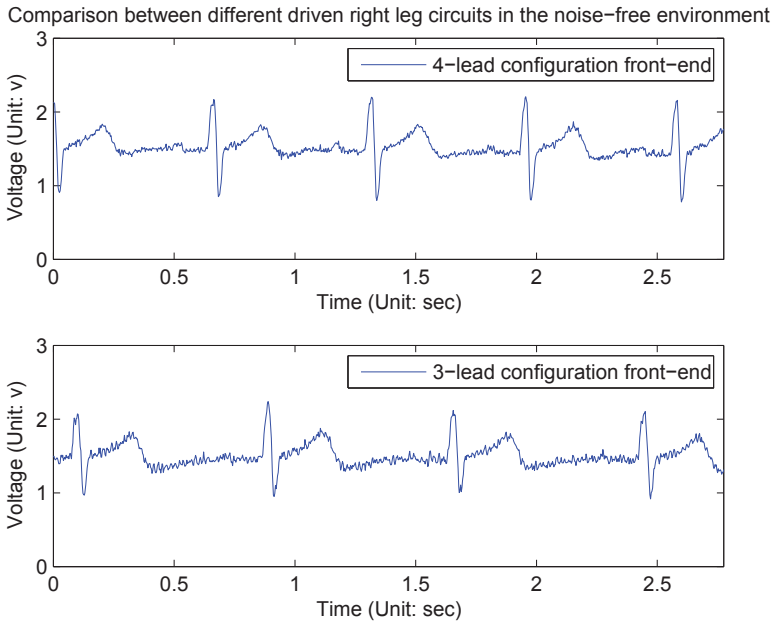

Figure 2.7: ECG waveforms using different driven right leg circuits in the noise free environment. The charts show a three-second snapshot.

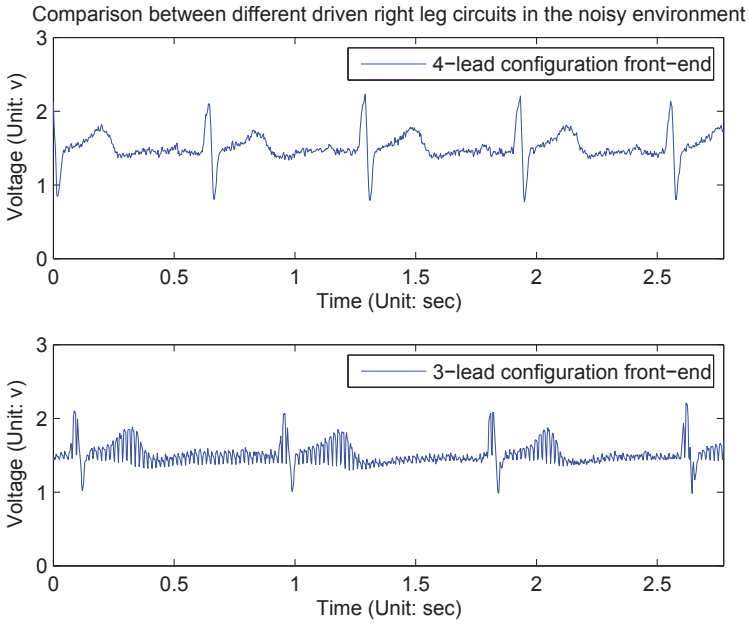

Figure 2.8: ECG waveforms using different driven right leg circuits in the noisy environment. The charts show a three-second snapshot.

amplifier.

† An active filter is shown in Figure 2.5(5). Its cut-off frequency is set to be 0.5-150Hz [24] and the gain is set to be 100, such that the dynamic range of conditioned ECG waveform would be 2 volts, which is two third of the rail-to-tail voltage of the amplifier.

† The proper layout grounding can reduce the level of 50/60Hz noise, especially in a severe environment.

2.3.1.2 ECG On-node Filtering

Although many approaches are explored in the analog front-end circuit to remove the 50/60Hz noise, the noise may still be coupled into analog signal flow at any point. Therefore, a digital filter is a better solution than the filer in analog domain. Due to the limit of computational capability, one second order IIR with a notch frequency at 50/60Hz and a 3-dB notch bandwidth of 6Hz [25] is implemented on the node. Taking the 50Hz filter as an example and assuming a sampling frequency of 360Hz, the normalized angular notch frequency and the normalized angular 3-dB bandwidth can be calculated as

$$\omega_0 = 2\pi(\frac{50}{360}) = \frac{5\pi}{18} \ , \ \omega_0 = 2\pi(\frac{6}{360}) = \frac{\pi}{30} \ . \tag{2.1}$$

Therefore, the desired transfer function can be obtained by

$$H(z) = \frac{1 - 1.287z^{-1} + z^{-2}}{1 - 1.223z^{-1} + 0.900z^{-2}} \ . \tag{2.2}$$

However, the output of this notch filter contains some small ripples along the signal, which is called the Gibbs phenomenon. It shows that these ripples can not be suppressed by increasing the order of the filter. Therefore, a Savitzky - Golay smoothing filter (SG filter) [26] is also integrated on the node. Its main purpose is to preserve features of ECG, such that P subwave will not be lost, while removing those Gibbs ripples. According to our experience, the SG filter with the zero-order polynomial regression and 15-point sliding window is optimal when considering the tradeoff between ripple amplitude and subwave

preservation. Figure 2.9 shows the comparison between the SG filter's input and output. It can be conclude that although the amplitude of QRS complex is shrunk, most ripples are removed and all the key features are preserved.

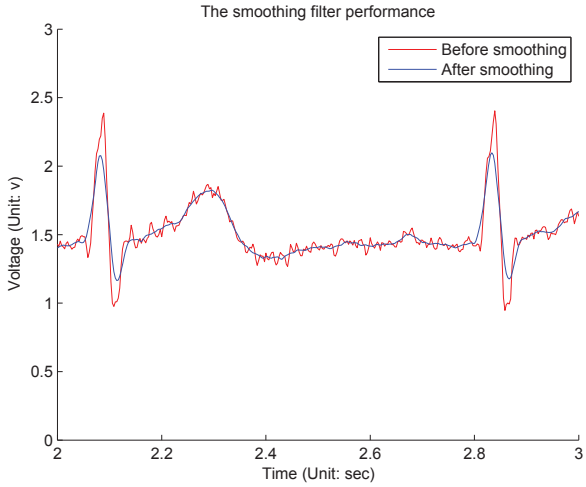

Figure 2.9: The performance of the SG filter. The chart shows a one-second snapshot.

2.3.2 Electroencephalography

2.3.2.1 Analysis of the EEG Waveform Characteristics

Electroencephalography (EEG), as shown in Figure 2.10 [27], is the recording of the oscillations of brain electric potentials along the scalp, which reflects the brain activities. In 1924, German psychiatrist Hans Berger accomplished the first human EEG recordings. After that EEG based diagnosis approaches are more and more introduced into the neurological practice. The typical clinical application is epilepsy diagnosis, as epileptic activities can lead to an abnormal waveform on a EEG stream [28]. It can be used to identify epileptic seizures from others and localize the area of the brain where the epilepsy originates. Other applications include the anesthesia monitoring and the brain function monitoring.

Typically, the EEG waveform can be mainly classified into the following patterns corresponding to different brain activities.

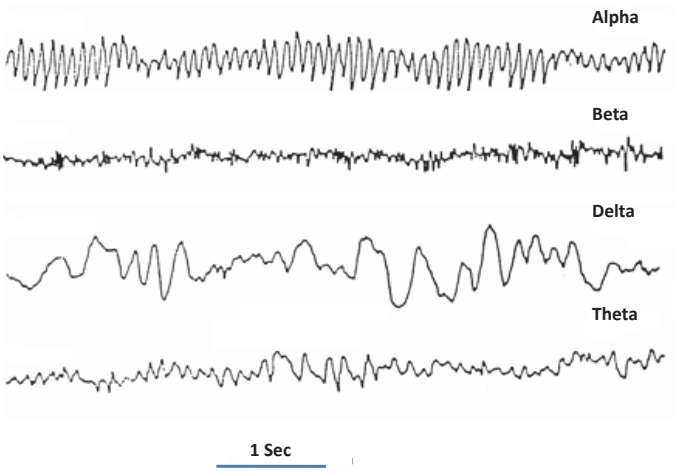

Figure 2.10: The typical waveform patterns of EEG.

† Alpha is the waveform ranging from 8Hz to 12Hz [29]. It can be detected in the posterior regions of the head: higher in amplitude on the dominant side, and weaker signal on the other side. It appears when the eyes are closed or when the subject is relaxing. It is lower than 8 Hz for young children [30].

† Beta is about from 12Hz to 30Hz. It can be seen on both sides in the symmetrical distribution. The rhythm with multiple frequencies and the low amplitude is often associated with the conditions of active, busy or anxious. It may occur among various pathologies and drug effects [30].

† Delta is a high amplitude brain wave with a frequency of oscillation up to 4 hertz. It is the strongest wave among all other wave patterns. It is detected during the slow wave sleep on both adults and children. It may be associated with subcortical lesions, diffuse lesions or deep midline lesions.

2.3.2.2 EEG Acquisition

Before the test, the scalp area should be handled by light abrasion, because the death cells would increase the impedance and corrupt the EEG signal. After that, the subject wears the multiple individual electrodes that contact the scalp with the conductive gel or paste. In some tests, a cap with fixed electrodes may be worn on the subject rather than multiple individual electrodes. General electrode locations have been standardized, as shown in Figure 2.11, for the reproduction reason that the acquiring results could be compared with other studies over time [31]. By contrast with the normal EEG, the ambulatory EEG allows the subject to move around and monitors long periods of time in recording of EEG. However, the ambulatory EEG has fewer electrodes than the regular one generally, due to

the cost and ease for operation. The recording may last for a full day or even longer, and the subject is allowed to have his own daily life rather than to limit in the hospital.

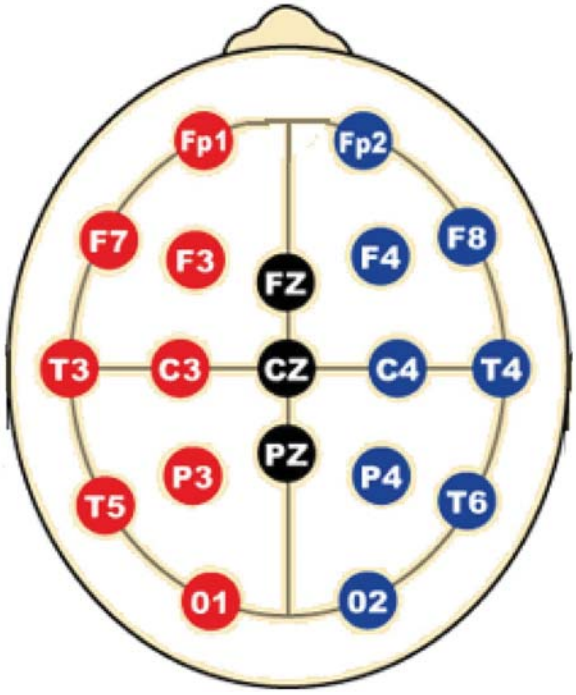

Figure 2.11: International 10-20 system for EEG electrode placement.

Each pair of electrodes is connected to one differential input of the front-end amplifier, and there is a common electrode serving as a system reference. The amplitude of a normal adult human EEG is in the range of 100 - 200μV when directly acquired from the scalp and is about 10 - 20mV when acquired from subdural electrodes, so the front-end gain is set to from 1,000 to 100,000 times (or from 60 to 100dB of voltage gain), and typically is partitioned to two stages. In order to suppress the noise and the offset that locate in the different frequency area of the spectrum, the typical design of a high-pass filter and a low-pass filter are set to 0.5-1Hz and 35-70Hz, respectively. The high-pass filter is integrated for slow artifacts, such as electrogalvanic signals and movement artifact, while the low-pass filter is designed for the high frequency noise. In addition, a notch filter typically filters out the noise from electrical power lines (60Hz in the United States and 50Hz in many other countries). After that, the amplified and filtered signal is digitized via an ADC, which benefits for analyze, achieve and display. Analog-to-digital sampling rate typically locates at the range of 256-512Hz in clinical scalp EEG, and some research applications requires sampling rates of up to 20kHz.

2.3.2.3 EEG Analog Front-end Circuit

Per EEG characteristics, we design the analog front-end circuit similar to ECG's circuit, while the gain and the cut off frequency of the filter are modified accordingly.

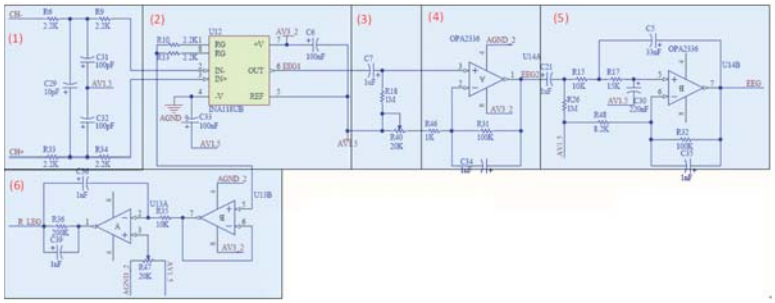

Figure 2.12: EEG Analog Front-end Circuit. (1) The protection circuit. (2) The instrumentation amplifier. (3) The RC highpass filter. (4) The non-inverting amplifier. (5) The second amplification stage. (6) The right leg driven circuit.

Figure 2.12(1) shows the protection circuit after the raw signal is penetrated the circuit. The RC network is integrated to reduce radio-frequency signals coupled the system via the electrode. Sometimes clamping diodes are also used to prevent the current injecting to the human body. The signal from the protection circuit is fed to the instrumentation amplifier with 12 times gain, as shown in Figure 2.12(2). Also the output impedance is also lowered by this instrumentation amplifier, which helps the next stage of the circuit draw the energy. The gain is set by the $R216$ and $R217$ according to $G = 1 + 50k\Omega/Rg$, where $Rg = R10 + R13$.

Some of the metal electrode materials are easy to be polarized, which means that electric charge can accumulate on the surface of the electrode, leading to a relatively high voltage compared to the original signal. If the gain of this stage was set too high, the amplifier would be saturated due to the great DC-voltage offsets. Therefore, a highpass filter with 0.16Hz cutoff frequency is depicted in Figure 2.12(3) after the instrumentation amplifier. It is a purely RC network of $C7$ and $R18$, which is designed to remove this greate DC bias.

After that, the EEG signal is amplified about 40 times by a non-inverting amplifier, as shown in Figure 2.12(4). Actually the gain is set as $G = (Ra + Rb)/Ra$, where $Ra = R40 + R46$, ranging from $1k\Omega$ to $21k\Omega$, and $Rb = R31 = 100k\Omega$, setting the gain to from 6 to 100. Figure 2.12(5) shows an active filter, which contains an amplification unit with 16 times gain and one third order lowpass filter. This amplification is used to adapt the dynamic range of the ADC, where the signal is digitized.

2.3.2.4 EEG Acquisition Experiments on Broilers

We have successfully demonstrated EEG analog front-end on broilers(Figure 2.13) in a broiler poultry welfare experiment.

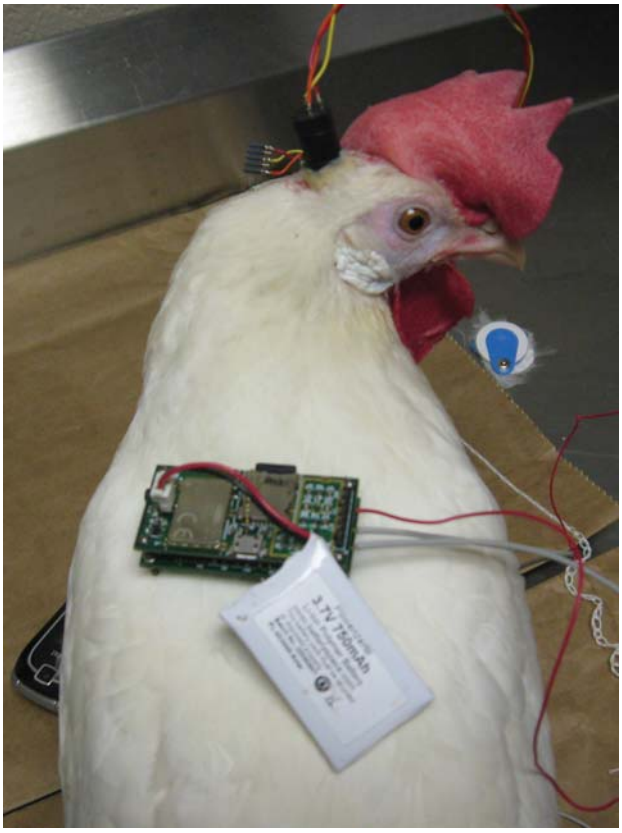

Figure 2.13: Chicken welfare experiment setup for EEG waveform acquisition.

This experiment was to observe the EEG waveform when a hen is placed in CO_2 environment. Before the welfare experiment, a three-lead EEG electrode was implanted in every hen, and hens are then recovered from the operation for four days. All the EEG data were acquired by BioLogger EEG analog front-end and analyzed by Spike2 [32], as shown in Figure 2.14. The part of the waveform before the red line in the top chart shows the EEG of a relaxed hen. And at time point of the red line, we stimulated the bird for one time, the hen was alert and the EEG waveform pattern changed immediately from low to high frequency and from large to small amplitude. The top chart illustrates that the hen responded to external stimulations in terms of EEG. Then we placed the hen in CO_2 environment for 15 seconds. The middle chart records the EEG waveform after the hen was taken out of CO_2. At first, the bird was unconscious and then waked up. The EEG

waveform of the wake-up moment is denoted by the blue line, as shown in the middle chart. Last, we placed the hen in CO_2 environment till dead, the bottom chart shows the hen's EEG waveform after its death.

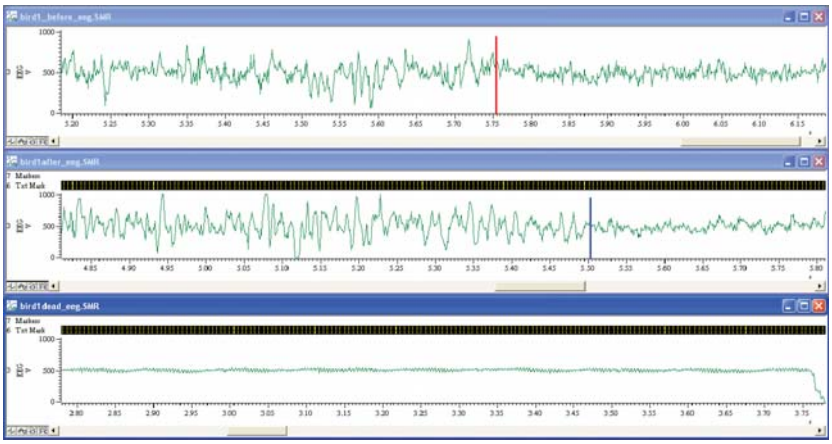

Figure 2.14: EEG waveform in the welfare experiment.

2.3.3 Respiration Rate

Many approaches are used for respiration rate measurement, while the piezo file is selected in current sensor node design. 100 year ago, the Curie brothers found that quartz changes its dimension when placed in an electrical field, and reversely, generates electrical charge when it is distorted mechanically. They named this piezoelectricity, Greek for "pressure" electricity [33]. This piezo film can be applied to measure chest and abdominal expansion associated with respiratory effort. The systems takes advantage of the piezo electric sensor's ability to generate a small voltage under the stress. For each breath the sensor is deformed by the expansion of the chest or abdomen and the produced voltage is amplified by the physiograph to produce a clean, reliable respiratory signal.

In BioLogger, a strip piezo film serves as the respiratory sensor. The voltage generated by the piezo film will decay if the exerted force remains unchanged for a while. This property is quantified by *Time Constant*, which is defined as the period when a signal decays to 70.7% of its original amplitude [34]. The frequency of adults' respiration rate normally ranges from 0.2 to 0.5Hz [35]. Therefore, on sensor node, $TimeConstant = R401 \times C_{Piezo}$ = 0.1s, and it guarantees that the signal does not decay too fast, as shown in Figure 2.15. The simple RC network at the end of the circuit is to remove the coupled high frequency noise.

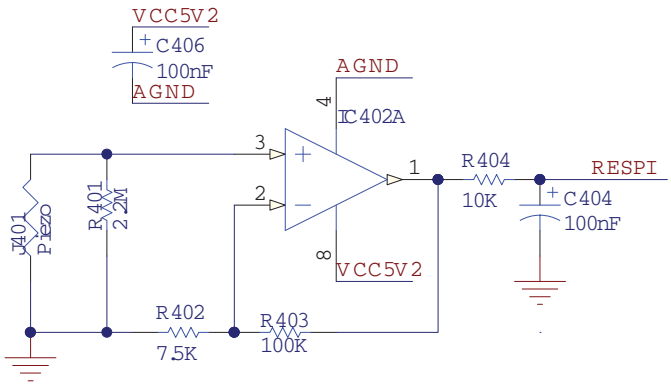

Figure 2.15: Respiration conditioning circuit.

2.3.4 Skin Temperature

The temperature conditioning circuit mainly consists of a voltage divider, a voltage follower, and a RC network, as shown in Figure 2.16. The voltage divider includes a temperature sensor and a resistor. $J402$ is a 10K3NTC temperature sensor from Betatherm Ireland Ltd. $10K3NTC$ has wide linear scope, which is from -80°C to +150°C. Its R/T relation follows $R_T \propto \exp(\frac{1}{T})$ [36], where R_T is the resistance of the thermistor at a particular temperature T (Unit: Kelvin). $R407$ is an ultra-small temperature coefficient resistor, whose resistance keeps invariant when the temperature changes. At the consequent two stages, a voltage follower decreases the output resistance, and the RC network decouples the high frequency noise. In the real implementation, V_{cc} is also sampled to compensate for its drift.

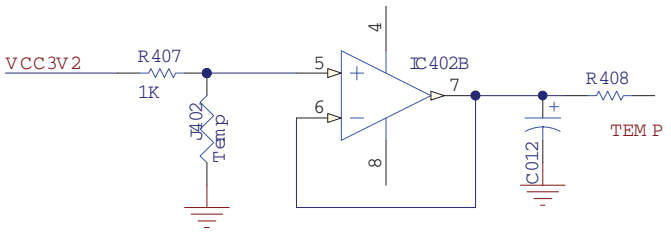

Figure 2.16: Temperature conditioning circuit.

In order to convert the digitized ADC readings to true temperature values, it is necessary to calibrate the sensors in advance. Sensor node constructs a look-up table that contains all the values of temperature corresponding to the ADC readings, which will trade the time by on memory space. This is a reasonable option due to that the flash memory on the MCU is large enough for the look-up table, but computation time is critical in the realtime monitoring system.

2.4 Firmware

Firmware is the program running on the MCU, which interacts with all other hardware modules on the MCU. According to the general embedded system developing principle, the hierarchical architecture is applied to the firmware on sensor node as shown in Figure 2.17. The firmware is hierarchized into multiple layers per their functionality. This is a multi layer structure, each layer fulfils their own functionalities by the service from the underneath layer and provide the service to the upper layer. And the communication between two layers are based on the interface. This makes most codes independent on the hardware, and helps implant across different hardware platforms.

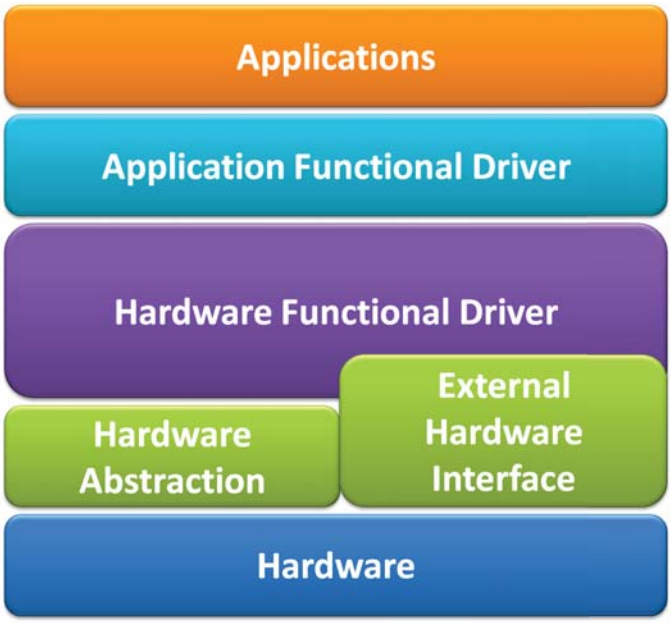

Figure 2.17: The architecture of the firmware on sensor node.

2.4.1 Hardware Layer

The hardware layer is lying on the bottom of the system. It contains the physical on-chip functional modules, peripheral sensors and the electrical connections among them.

2.4.2 Hardware Abstraction Layer

The hardware abstraction layer (HAL) is one layer just above the physical hardware and under the driver layer. It is used to hide the details of multiple hardware platforms from the functional driver, such that most of the driver codes are able to scale to other platforms. In sensor node, the HAL is much simpler: it generally abstracts register write/read operations and interrupt handling.

2.4.3 Hardware Functional Driver Layer

This layer envelops the basic on-chip module primitive operations, and provides the interface to the upper layer. Take the SPI module in the MSP430 as an example, the hardware functional driver layer contains functions like SPIStart(), SPIWriteByte(), SPIReadByte() and SPIStop(). Meanwhile, this level also contains the external sensor interface, which provides the way to access the peripheral sensor on the board.

2.4.4 Application Functional Driver Layer

This layer offers the APIs for the applications on the top level. In this level, all the hardware related access are mapped into the memory space. The MCU accesses it as the memory access. The applications can call those functions in this layer easily. For example, the accelerometer operations and data exchange, like InitialACC() and getACCData() and stopACC(), are placed in this layer.

2.4.5 Application Layer

A simple realtime task scheduler is implemented on sensor node to manage three periodic tasks: 1) acquiring physiological signals; 2) preprocessing the digitalized signals and 3) encoding and transmitting the data to base station. In addition, if some abnormalities are detected in the second task, a non-exemptible sporadic task with a higher priority is released to sound alarm. The abnormalities can be defined by the users in advance.

2.5 Cardiac Arrhythmia Classification with BioLogger

This is a case study in which we develop a novel realtime cardiac arrhythmia classification approach on gateway. Gateway receives clear and reliable ECG for visualization and cardiac arrhythmia detection. Among the numerous cardiac arrhythmia classification paradigms, we focus on the hidden Markov model (HMM) based algorithms. First, a typical ECG period as shown in Figure 2.18 always consists of a P subwave, a QRS complex, a T subwave and isoelectrics between those subwaves, where HMM is able to preserve the ECG structural nature. Second, the HMM is more adaptive to the dynamics than the heuristic rules. The HMM belongs to a probabilistic module, hence it would not be limited by an absolute threshold. Third, the HMM has relatively low cost in time complexity, which is more favored in an embedded system. Finally, the HMM can be used to the non-linear system, while the extra errors are introduced during the linearization of KF methods [37].

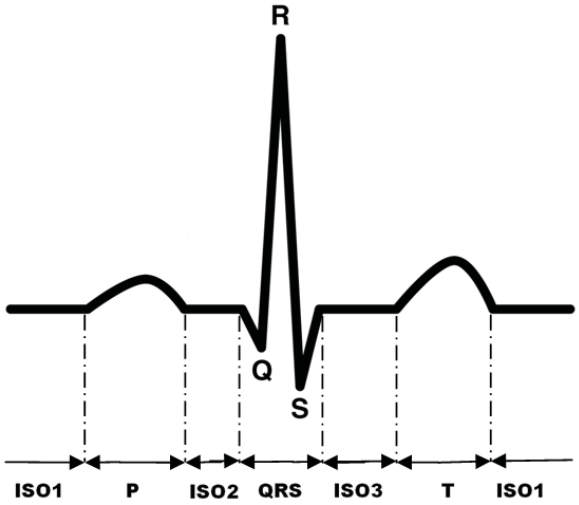

Figure 2.18: ECG waveform and its subwaves (P subwave, QRS complex, T subwave and isoelectrics) in a cardiac cycle.

However, two issues are required to address in the existing HMM-based algorithms [38][39][40]. One is the interference from motion artifacts. Motion artifacts also can distort the morphology of the waveforms, thus false alarm will be triggered if they are not treated properly. In our design, an accelerometer is introduced in the algorithm to classify the human motion, such that the ECG waveform distorted by the artifacts cannot be identified as an arrhythmia. Another problem is the big time delay. Generally, the process of cardiac arrhythmia detection contains two steps: the first round is ECG segmentation or ECG feature extraction, the second one is to classify the type of arrhythmias based on the results inferred from the first round. In this way, the response

time would be increased, and the abnormalities could not be found timely. To deal with this problem, a novel layered hidden Markov model (LHMM) framework is proposed in BioLogger to realtime identify multiple cardiac arrhythmias.

The LHMM is derived from the normal HMM, where primitive observation symbols will be yielded directly from observations of the modeled process on the lower layer, and the upper layer corresponds to observation symbols or probability generators from the lower layer. The proposed model consists of two layers of HMMs. The ECG waveform is fed into Layer 1 HMM, and used to segment the ECG waveform. Meanwhile, Layer 2 HMM is responsible for detecting the types of cardiac arrhythmias using the ECG clinical features and information from the accelerometer as observations, as shown in Figure 2.19.

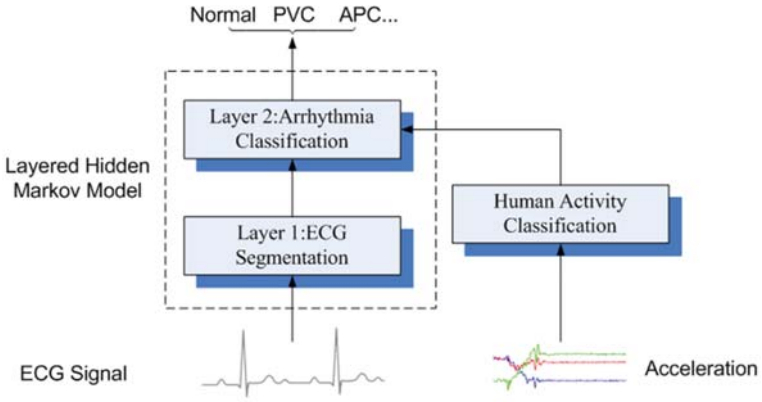

Figure 2.19: The block diagram of the proposed LHMM framework.

2.5.1 Layer 1: ECG Segmentation

ECG segmentation is the first step to diagnose the cardiac arrhythmias. The onsets and offsets of characteristic subwaves need to be localized precisely from the periodic ECG signals. Layer 1 HMM is used to fulfill this task and extract clinical ECG features.

2.5.1.1 Model Description

Figure 2.18 shows a typical period of ECG waveform, which can be partitioned into six characteristic subwaves: Isoelectric1 (ISO1), P subwave, ISO2, QRS complex, ISO3, T subwave. Therefore, the mapping of ECG waveform to hidden states in the HMM can be done by associating each sample (ADC reading) with a hidden state representing a

characteristic subwave. Figure 2.20 shows the six element state space defined in Layer 1 HMM. As to the observation space in Layer 1 HMM, the 12-bit ADC readings can not be fed into HMM directly, since the value the observation space ranging from 0 to 4095 is too large for a realtime HMM algorithm. Hence ECG signal is classified into 4 levels according to the magnitude of the corresponding voltage value. Each level associates with a distinct observation symbol (O_1, O_2, O_3 , O_4) respectively, as shown in Figure 2.20.

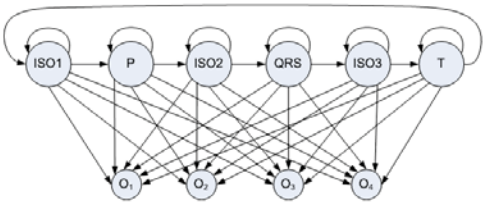

Figure 2.20: State space and observation space in Layer 1 HMM. "P" stands for P subwave, "QRS" for QRS complex, and "T" for T subwave. Readings from 0 to 1023 correspond to O_1, readings from 1024 to 2047 corresponds to O_2.

The model in Figure 2.20 is able to represent the normal cardiac sinus beats well, but can not cover the situations of cardiac arrhythmias. On one hand, there exists a problem called double-beat segmentation, in which two or more heat beats are detected incorrectly, when there is only one beat present. To address this problem, a duration constraint is incorporated into Layer 1 HMM. Every state has an empirical minimum duration, such that the HMM cannot generate false heart beat in the constraint range. In our experiment, the minimum state duration is calculated as 60% of the minimum duration in the training data. On the other hand, sometimes P wave would be missing, when cardiac arrhythmia happens. In this case, transition between ISO1 and ISO2 could be possible in terms of the HMM chain. Accordingly, Figure 2.21 shows the modified chain to adapt more situations.

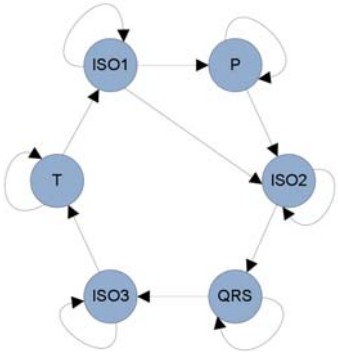

Figure 2.21: The revised Layer 1 HMM. A connection is added between ISO1 and ISO2.

During the training process of this LHMM, the triplet $\lambda = (A, B, \pi)$ [37] is constructed

by a sequence of observations unsupervised. In the experiments, the training data is ten-second ECG waveform from the wearable ECG sensor node or from the ECG emulator, which contains ten to twelve cardiac beats. During the training of model, the optimal parameters are obtained by maximizing the local likelihood $P(O|\lambda)$ iteratively using classic Baum-Welch algorithm [41].

2.5.1.2 Automatic ECG Segmentation

The results deducted from Layer 1 in the entire framework is backed up, and Figure 2.22 shows the four-beat normal ECG waveform and its subwaves (P, QRS, T) in every period. In this figure, the onset and offset of all the subwaves are identified by red lines, the letter on the top indicates the type of the subwave.

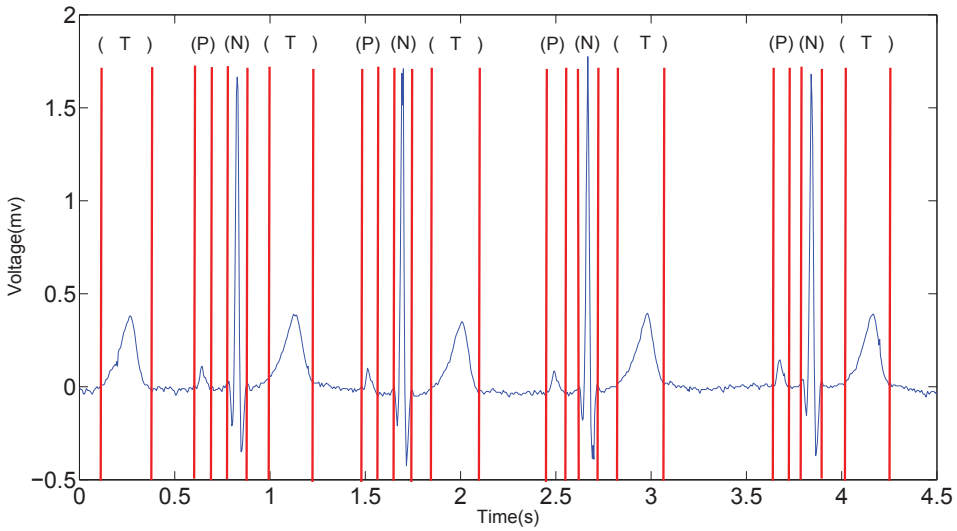

Figure 2.22: ECG segmentation using Layer 1 HMM. "P" stands for P subwave, "N" for a normal QRS complex, and "T" for T subwave.

2.5.2 Layer 2: Cardiac Arrhythmia Classification

2.5.2.1 State Space

There are a variety of cardiac arrhythmias, such as Premature Ventricular Contraction (PVC), Atrial Premature Contraction (APC), Right Bundle Branch Block (RBBB) and Left

Bundle Branch Block (LBBB). In Layer 2 HMM, two common cardiac arrhythmias are considered: PVC and APC. In contrast to the normal sinus heart beat, they have their own characteristics in terms of the ECG morphology.

† PVC has an wider QRS complexes than the normal ones, which might last more than 120 ms. Sometimes its QRS complex is not followed by a P subwave, and additionally the T subwave is usually larger.

† APC has an abnormal P wave. Normally P subwave are smaller and rather shapeless. In addition, P subwave occurs earlier than expected, which means P-Q interval is larger than the normal ones.

Generally, these two types of arrhythmias could occur intermittently. Hence, an fully-connected ergodic model is constructed, as shown in Figure 2.23. In this model, besides the two cardiac arrhythmias, two other hidden states exist: one is the normal sinus beat, and the other one is invalid beat. Invalid beat means the system has detected strong motion artifacts, where the ECG waveform acquired from sensor node can not represent the real heart status.

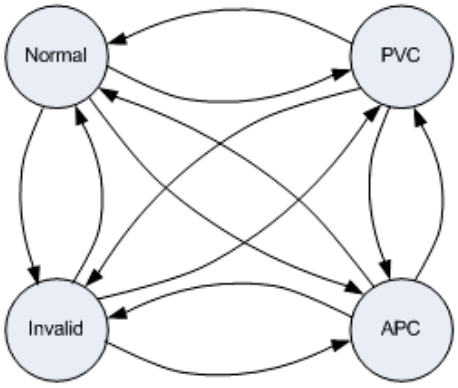

Figure 2.23: The structure of Layer 2 HMM for cardiac arrhythmia detection. "Normal" means a normal beat, and "Invalid" means an invalid beat.

2.5.2.2 Observation Space

The Observation Space of Layer 2 HMM contains two parts, as shown in Figure 2.19. Per definition, the hidden state sequence of Layer 1 HMM should serve the observation of Layer 2 HMM. However, PVC and APC classifications do not require the onset and

offset of all the subwaves. Therefore, valuable clinical features are extracted from ECG segmentations, such as QRS duration, P-R interval and R-R interval. Sometimes, P wave is skipped, R-R interval will make more contributions to arrhythmia classification.

Another part of observations comes from the tri-axis accelerometer. Its Z axis is perpendicular to the earth and points to the earth. Three common activities are concerned during human's daily life: standing, walking and lying, and is considered as an element in Layer 2 HMM's observation space. A simple heuristic-rule algorithm is employed to classify these three activities (Algorithm 1), in which three features are calculated from the accelerometer readings, the acceleration value of Z axis, the sum of squares of accelerations along three axes, and acceleration variance along three axes. The sliding window is about three seconds, which may contain about three to four cardiac periods. If the patient is still or moving slowly, the sum of tri-axis acceleration square should be one G (Gravitational constant). If it goes beyond this value, and the variance is also greater than a particular threshold, the patient is defined to be walking, and ECG segmentation is going to be concerned invalid. Otherwise, the patient is classified to be standing, when Z axis value is close to one G, and be lying, when its value is close to zero. Under the later two situations, the ECG waveform is considered reliable.

Algorithm 1 Human Activity Classification Algorithm.

while true do
  Acquire accelerometer readings, $A_x\ A_y\ A_z$ are three components along three axes;
  Calculate acceleration $A = \sqrt{A_x^2 + A_y^2 + A_z^2}$;
  Calculate σ, covariance of A in a 3sec sliding window;
  if $A \geq \delta_1$ **and** $\sigma \geq \delta_2$ **then**
    {δ_1 and δ_2 are two thresholds.}
    return Walking;
  else
    if $|A_z| \leq \varepsilon$ **then**
      {ε is a small number closed to zero.}
      return Lying;
    else
      return Standing;
    end if
  end if
end while

Figure 2.24 shows the relationship between ECG and acceleration: the upper chart shows a snapshot of the subject's ECG waveform; the middle chart displays the corresponding accelerometer measurements; the lower chart depicts the classification result of Algorithm 1. It can be summarized that the subject experiences four stages during the period of more than 25 seconds. Moreover, the ECG waveform is corrupted during the walking stage.

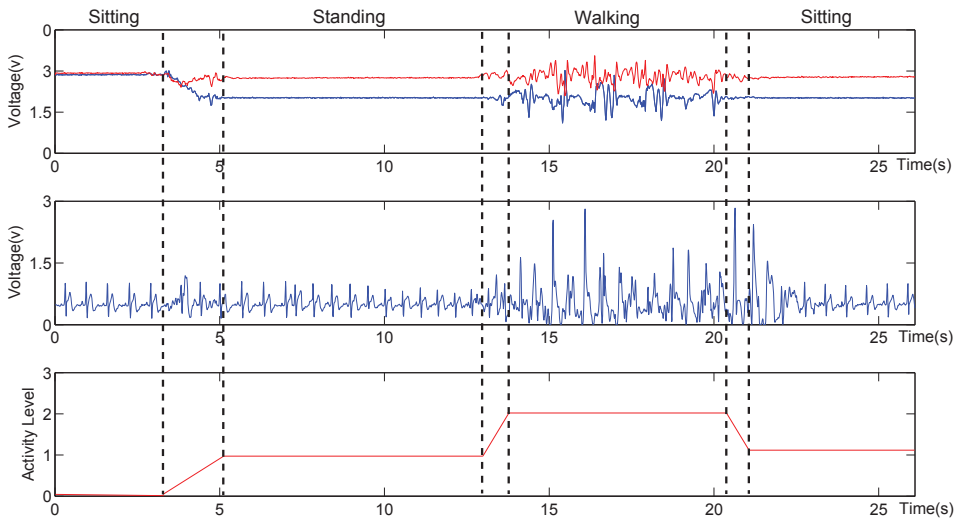

Figure 2.24: Human activity classification based on the accelerometer measurements. The dashed lines represent the human activities and the transitions between them.

2.5.3 Experiments and Performance Evaluation

2.5.3.1 Experimental Results

The proposed algorithm is implemented on the smart phone using Visual Studio 2008. Figure 2.25 demonstrates the effectiveness of the system: the ECG waveform is captured by the wearable ECG sensor node. No PVC or APC is present in the waveform during this six second snapshot.

To compare the reliability and accuracy with other benchmarks, an ECG emulator is also developed on the laptop. It behaves like a wearable sensor node, except that the data are from MIT-BIH Arrhythmia Database [42, 43] which is loaded in advance. The ECG emulator also employs the embedded Bluetooth module on the laptop to transmit the data using both the same data format and sending rate with the wearable ECG sensor node. Figure 2.26 illustrates a snapshot of ECG in Record 119 in [43] and the classification result. In this record, there are 1987 beats in total, 1543 normal beats and 444 PVCs respectively. The red bars in the lower chart identify the PVCs in the ECG waveform, which are wider than normal beat. Similar to PVC detection, Record 220 in [43] is used for APC detection and the result is shown in Figure 2.27.

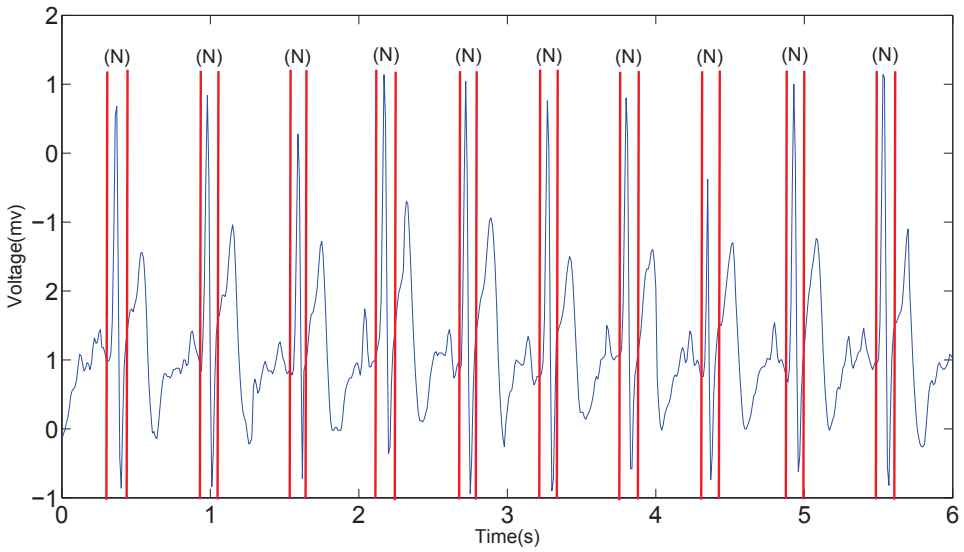

Figure 2.25: ECG analysis for the wearable ECG sensor node. All the normal beats are annoted as "N".

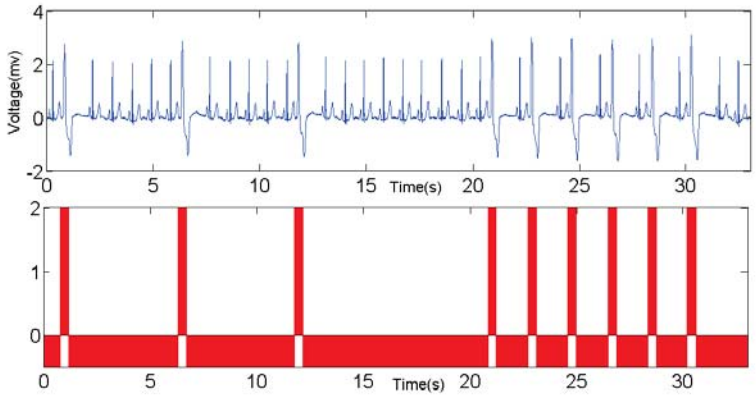

Figure 2.26: PVC detection based on the proposed LHMM.

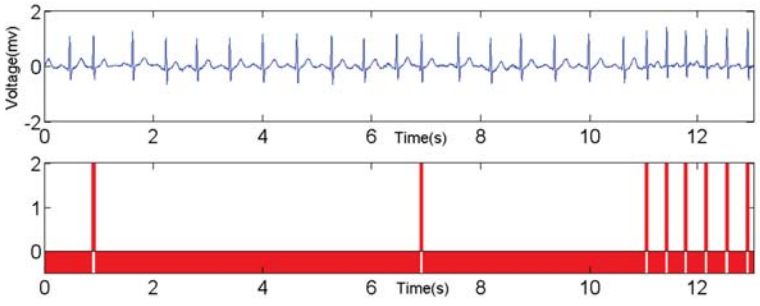

Figure 2.27: APC detection based on the proposed LHMM.

2.5.3.2 Evaluation Metrics

The performance of arrhythmia classification is quantified using the widely accepted statistical metrics: accuracy, sensitivity and positive predictivity. Accuracy (Ac), as the most crucial metric, is used to evaluate the overall performance for all kinds of beats. This overall parameter is defined as

$$Ac = \frac{N_t - N_e}{N_t} \times 100\% \ , \tag{2.3}$$

where N_t represents the beat number in the record, and N_e is the the total number of classification errors. To express the ability of detecting the fraction of events and true events correctly, the sensitivity (Se) and positive predictivity (+P) are defined as follows:

$$Se = \frac{TP}{TP + FN} \times 100\% \ , \tag{2.4}$$

$$+P = \frac{TP}{TP + FP} \times 100\% \ , \tag{2.5}$$

where TP, FN and FP denote the number of true positives, false negatives and false positives respectively [44]. True positive means the detection is corresponding to the annotations labeled by experts. False negatives are beats that should be detected, but they are missed and assigned to another state. A false positive happens, when the beat is assigned incorrectly.

To evaluate the overall performance for all records, the weighted measure [45] is used according to the number of beats of each state that exist in the record. It is defined as

$$M^{WA} = \frac{\sum_{i=1}^{n_f} n_{b_i} * M_i^C}{\sum_{i=1}^{n_f} nb_i} \times 100\% \ , \tag{2.6}$$

where M denotes the sensitivity or positive predictivity, n_{b_i} is the number of beats for the ith record, n_f is the total number of records, and M_i^C is the value of a specific measure for the ith record in the class "C", which might be one of Normal, PVC and APC.

2.5.3.3 Performance

For overall performance evaluation, 16 ECG records are selected from the Arrhythmia group in [43]. These records are all acquired from the modified Lead II. For ease of presentation, these records are divided into 4 types: records with only normal beats (type I), records with normal beats and PVCs (type II), records with normal beats and APCs (type III) and records consisting normal beats, PVCs and APCs (type IV). Three common statistical metrics, accuracy, sensitivity and positive predictivity, are adopted to quantified the algorithm performance.

Table 2.2 shows the comprehensive results for PVC and APC detection. For type I, the normal beats are detected accurately. It shows the proposed algorithm is competent for arrhythmia classification. The evaluation results of type II demonstrates that the PVCs are abstracted from the normal beats. The accuracy, sensitivity and positive predictivity even achieve 100% for the records 119 and 230 using the proposed algorithm. Therefore, the algorithm is fully suitable for PVC detection. Similarly, during the APC detection, shown in type III, the algorithm works with the sensitivity of 100%. The performance is better than PVC detection. Because morphology of ECG changes a little when APC occurs, while the change of ECG waveform will be significant when there are continuous double PVCs existing especially. The last type is a mixture of PVCs and APCs. In most cases, the sensitivity and positive predictivity are equal to 100%. The overall performance shows the capability of the arrhythmia detection with a weighted average Se and $+P$ of 99.72% and 99.64% respectively.

Table 2.2
Results for cardiac arrhythmia classification using the LHMM. N_b denotes the number of beats.

Type	Record	N_t	Ac(%)	Normal			PVC			APC		
				N_b	Se(%)	+P(%)	N_b	Se(%)	+P(%)	N_b	Se(%)	+P(%)
I	115	1952	100.00	1952	100.00	100.00	0	N/A	N/A	0	N/A	N/A
	122	2474	100.00	2474	100.00	100.00	0	N/A	N/A	0	N/A	N/A
II	106	2027	93.73	1507	99.54	96.21	520	98.07	96.15	0	N/A	N/A
	119	1987	100.00	1543	100.00	100.00	444	100.00	100.00	0	N/A	N/A
	123	1517	99.01	1514	100.00	99.08	3	100.00	75.00	0	N/A	N/A
	221	2427	99.56	2031	99.46	99.93	396	99.24	95.96	0	N/A	N/A
	230	2255	99.65	2254	100.00	99.65	1	100.00	100.00	0	N/A	N/A
III	101	1864	99.30	1859	100.00	99.31	0	N/A	N/A	5	100.00	100.00
	103	2083	99.95	2081	100.00	100.00	0	N/A	N/A	2	100.00	66.67
	112	2537	99.40	2535	100.00	99.41	0	N/A	N/A	2	100.00	25.00
	117	1534	100.00	1533	100.00	100.00	0	N/A	N/A	1	100.00	100.00
	220	2046	100.00	1952	100.00	100.00	0	N/A	N/A	94	100.00	100.00
IV	100	2271	99.87	2237	100.00	100.00	1	100.00	100.00	33	100.00	89.63
	116	2411	99.34	2301	99.52	100.00	109	91.74	86.96	1	100.00	50.00
	215	3361	98.51	3194	98.62	100.00	164	93.29	90.00	3	100.00	100.00
	228	2053	99.10	1688	98.93	99.52	362	96.69	100.00	3	75.00	100.00
Total		34799	N/A	32655	N/A	N/A	2000	N/A	N/A	144	N/A	N/A
Weighted Average		N/A	99.20	N/A	99.72	99.64	N/A	97.75	96.63	N/A	99.48	95.77

Further, our algorithm is compared with other benchmarks proposed in the literature, as shown in Table 2.3. Due to the fact that most of them is used for PVC detection, the lateral comparison only concerns PVC detection. It can be seen that the proposed method yields a higher sensitivity, while the positive predictivity of 96.63% is achieved in the acceptable range.

Table 2.3
Performance comparison on PVC detection. N is denoted as the number of records used in the test and N_{PVC} is the total number of PVCs which have been annotated.

Algorithm	Database		Evaluation		
	N	N_{PVC}	Ac(%)	Se(%)	+P(%)
Temporal statistics [46]	20	5677	N/A	91.90	89.46
	44	6731	N/A	74.51	97.36
PCA [47]	20	5677	N/A	93.12	94.76
	44	6731	N/A	92.73	96.92
NNs [45][40][48]	40	6958	95.20	85.20	92.40
	44	6958	97.00	93.40	93.30
	7	953	97.04	96.67	97.04
KNN classifier [49]	20	5677	N/A	97.30	97.70
	44	6731	N/A	81.60	78.03
Gaussian process [50]	18	2720	97.10	97.60	97.00
	27	4080	96.90	84.70	97.50
LHMM	16	6956	99.20	97.75	96.63

2.6 Summary

In this chapter, we present BioLogger, a wireless physiological monitoring and logging system. It can simultaneously monitor and log various types of physiological signals including ECG, EEG, respiration rate and skin temperature. We focus on improving the ECG signal quality by hardware design and propose a realtime cardiac arrhythmia classification algorithm, which successfully monitors the patient's ECG and identifies its cardiac arrhythmia in real time. The ECG waveform and the cardiac arrhythmia classification result are displayed in a smart phone, rather than a bulky resting ECG instrument. The plug-in algorithm can detect the normal sinus beat, PVC and APC at the same time. Once the abnormalities are detected, the alarm message will notify the patient or clinicians via telecommunication infrastructure. Further, the patient can utilize this system to monitor their heart status when the daily lifestyle changes, in such a way that the patient can adjust to living in a comfortable lifestyle and potential risk would be

decreased.

We are planning to apply this system to the clinical experiments, instead of using the ECG database. Additionally, we are developing scalable algorithm that can detect more types of cardiac arrhythmia, such as left bundle branch block (LBBB) and right bundle branch block (RBBB). Moreover, more efficient algorithms are being developed to enhance the classification accuracy. Finally, more physiological sensors are planning to be integrated, so the system's capability of diagnosis will be increased.

Chapter 3

PAMS: A Wearable Physical Activity Monitoring System[1]

3.1 Introduction

Physical Activity Monitoring, or motion capture, is defined as using sensors to track and record the position, velocity, acceleration and impulse of an activity, especially human's motion [51]. Early physical activity research can be traced back to the motion capture via photography developed by Etienne-Jules Marey (1830 - 1904). His technique made it possible to record the multiple phases of movement on a single photographic surface [52]. As the development of techniques, current state-of-art physical activity monitoring systems are capable of tracking many points at very high speed, with great accuracy, even in three dimensions.

3.1.1 Motion Capture Applications

Motion capture systems can be applied in many different disciplines to capture movement and gesture of the human body.

[1] ©2010 ACM. Portions reprinted with permission, from **Sheng Hu**, Xi Chen and Jindong Tan, "*PAMS: A Wearable Physical Activity Monitoring System for Continuous Motion Capture in Free-living Environments*", in Proc. of Intl. Conf. on Body Area Networks, pp. 233 - 239, September 2010.

† Biomechanics: In the clinical gait domain, medical professionals employ motion capture systems to determine whether an individual's gait pattern has been affected by the disorder [53]. Also in the rehabilitation domain, available facilities are used to calibrate the patient's any unintentional movement to assist them to reach an expected location. [54][55].

† Biology: Motion capture systems help biological scientists to understand the mechanisms how muscular contractions and articulating joints are translated to functional movements.

† Surgery: Motion capture systems are used to monitor and track the exact position, orientation and movement of instruments relative to the object in real-time. In addition, doctors and medical technicians can trained in the proper use of endoscopic instruments during surgical procedures [56].

† Sport: Athletes and coaches use motion analysis techniques which provide real-time data to measure physical movement for improvements in performance. Proper examples include the analysis of a golf swing [57], batter's swing and soccer kicks [58].

† Entertainment: Video games may use motion tracking approaches to animate in-game characters rather than done by the joystick. Movie industry has already used motion capture for CG effects, for creating the virtual characters rather than the traditional cel animation. Moreover, motion tracking is serving currently as a popular interaction with video games, such as Wii and Kinect [59].

3.1.2 Motion Capture Approaches

Current motion capture systems have advanced far beyond the early designs. Over years, motion tracking has been developed into many branches, each with its own advantages and disadvantages. Basically they are able to be classified into optimal based systems and the non-optimal ones.

3.1.2.1 Optical Motion Capture

Optical Motion Capture systems use data acquired from image sensors to localize the 3D position of a subject among multiple cameras which have been calibrated to provide overlapping projections. Subject wears passive (reflective) or active (inferred emitting) markers, and the tracking system employs several cameras, usually between 3 and 16,

to triangulate and track the 3D position of the markers within a specific 3D volume [60]. Current advanced systems are able to track surface features to identify the particular subject realtime [61].

The most attractive advantage of optical based system is that the subject feels free to move due to no cables connecting, and the marker is light profile in both dimension and weight. However, it suffers by the following disadvantages. Primarily, motion tracking will always be limited in the volume covered by the image cameras, the outdoor tracking is difficult to realize. In addition, environmental light have an impact on the performance. Therefore, tracking systems are always deployed in the studio and lab, while it is inappropriate to deploy them in the home environment. Moreover, the reflective markers can be blocked by other structures, resulting in the loss of data. The short time blocking be compensated by estimation of the position using the kinematic models [62], but the long term data missing will seriously corrupt the system performance. Last, modern optical tracking solutions are far beyond the burden of individual researchers or even small companies [62].

3.1.2.2 Mechanical Motion Capture

Mechanical capture approaches employ potentiometers and rotational encoders to track the human body joint angles. Therefore these system are often referred as exoskeleton motion capture systems. The subject wears a skeletal-like structure hooked onto his back. The exoskeleton follows the subject's movement and detects the rotation in each joint. Similarly, other types of mechanical motion capture include the mechanical gloves and arms which concentrate on finger or arm movements respectively.

Compared to other techniques, mechanical systems have the advantage that they are self-contained systems, allowing tracking in a large area without the external infrastructure. In addition, they are realtime and relatively low cost. Nevertheless, the limitations are summarized as follows: First, they are typically cumbersome to wear, which is not proper for the daily life monitoring. Second, the sensors only sense the rotation of the joint, so absolute positions are not obtained directly. Last, it presents serious difficulties in aligning external infrastructure. Fourth, it is limited to one dimension tracking. It encounters the particular challenge when considering the joints with multiple degrees of freedom, such as the shoulder. The mechanical structure can not follow the rotation in more than one dimension.

3.1.2.3 Magnetic Motion Capture

Magnetic systems calculate position and orientation by utilizing sensors placed on the body to measure a generated magnetic field [63]. The sensors and magnetic transmitter are cabled to an unit that relies their locations within the field. Generally the magnetic systems use 6 to 11 sensors to track the entire body motion. Those systems have the advantages that the human body is transparent to the magnetic field, hence the blocking in the optical systems will not occur in the magnetic ones. Another advantage is that positions and rotations are measured absolutely, therefore no accumulated error should be taken into account. However, the disadvantages are also obvious: First, the magnetic sensor measurement is not linear, and the magnetic distortion occurs as distance increases. Second, the earth magnetic field might be effected by other fields generated by ferrous objects in the surrounding area. Last, the low frequency noise results in the lower sampling rates, which makes them not fit for the high rate applications.

3.1.2.4 Acoustic Motion Capture

The acoustic motion capture approaches rely on the fight duration of an ultrasonic pulse or the phase shift of a continuous-wave source to determine the distance [64]. However acoustic signals are extremely affected by the multi-path issue that the signal received from the direct sender is often mixed with several times reflected signals. The trick to avoid such a problem is to only accept the first impulse and block others, because the direct sent signal travels the shortest distance. Most acoustic systems are classified into two types [64]. One is based on time-delay: the receiver detects the time-of-arrival or time-difference-of-arrival to determine the distance between the object and the transmitter. Such systems are the dominant methods with relatively high accuracy (1-30 cm), but low range. Another method is based on Doppler shift. Acoustic Motion Capture shares the same shortcomings of optical systems that they require line-of-sight links and have limited coverage areas. Therefore, they are mostly applied to tracking the location of the target, and seldom used to motion tracking.

3.1.2.5 Inertial Motion Capture

Inertial based navigation systems have already widely applied to vehicles, ships and aircrafts in the early 1950s. It employs three kinds of inertial sensors, gyroscope, accelerometer and magnetometer, to capture the point associated with the sensors. Current

MEMS techniques make them light, compact and packaged with the driver circuits, such that they can directly provide digital outputs. Therefore, the portable devices and wearable sensors are able to carry them to provide valuable inertial information.

Gyroscope

A gyroscope measures the orientation, based on the fact that angular momentum is constant in a closed system. The gyroscope used in wireless sensor networks is referred to the MEMS gyroscope, which takes the idea that a vibrating object tends to keep its motion constant in the same plane. Per Coriolis effect, suppose the acceleration on the proof masses is equal to $a_c = -2(v \times \Omega)$, where v is a velocity and Ω is an rotational rate. The out-of-plane motion y_{op} is given by:

$$y_{op} = \frac{F_c}{k_{op}} = \frac{2m\Omega X_{ip}\omega_r \cos(\omega_r t)}{k_{op}}, \tag{3.1}$$

where m is a mass of the proof mass, k_op is a spring constant, and Ω is a magnitude of a rotation vector perpendicular to the driven proof mass motion [65].

Accelerometer

An accelerometer is a device that measures proper acceleration, which is relative to the free-fall under the inertial coordinate [66]. Therefore, when an accelerometer is sitting still, it measures a value of 1g ($\approx 9.8 ms^{-2}$). However, an accelerometer will measure a value of zero, if it is in gravitational free fall. Current MEMS accelerometers are based on surface micromachined capacitive feature. When a force applies, the mass of the beam moves closer to one of the fixed outer plates than other side, making the differential capacitance change. An comparator converts the capacitance difference, and streams out the voltage signal which is proportional to the acceleration [67]. This type of capacitive accelerometer outperforms the piezoelectric-type in terms of the DC acceleration measuring. Therefore, MEMS accelerometers is also able to measure tilt while sitting on the ground [68], as shown in Figure 3.1.

Magnetometer

A magnetometers is the sensor for magnetic field detection, which is often employed in industrial, oceanographic and biomedical fields [69]. In inertial applications, magnetometers are often used to provide the absolute orientation rather than the specific magnetic flux density [70]. The magnetic field of the earth originates at the south magnetic pole and terminates at the north pole. Per the relationship between the magnetic and geographical poles, we can figure out the absolute pointing. In North America the earth's

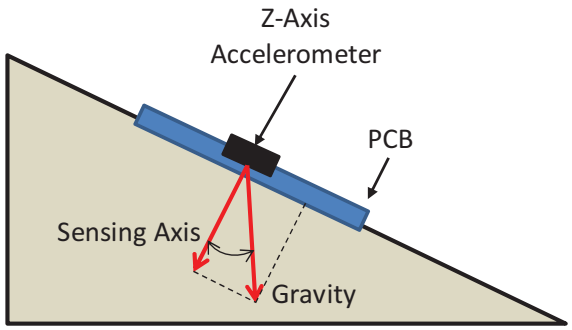

Figure 3.1: Tilt measurement using the accelerometer.

magnetic field is not horizontal, but has an inclined angle (Φ) about 70 degrees into the earth's surface, shown in Figure 3.2.

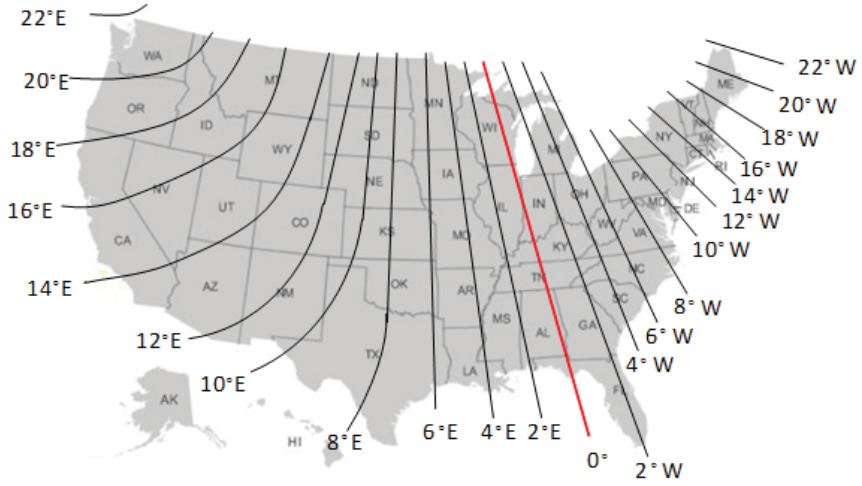

Figure 3.2: Earth magnetic field over United States.

Therefore, the earth's magnetic field vector h can be factored into three axis values h_x, h_y, and h_z. The ratio of h_x and h_y can be inferred the absolute heading under the earth coordinate, as shown in Figure 3.3.

Current MEMS magnetometers are based on anisotropic magnetoresistance (AMR) found by Lord Kelvin. He observed the resistance of iron increased 0.2% when applied a magnetic field along the direction of the current [71]. AMR based magnetometer exceeds the Hall Effect based ones in terms of simple structure and convenience for minimization and integration. Also high sensitivity and low-noise signal enable AMR sensors to operate in a large distance from the magnet, while Hall sensors are limited to the near field of the magnet. However, AMR is high possible disturbed by the external magnetic fields.

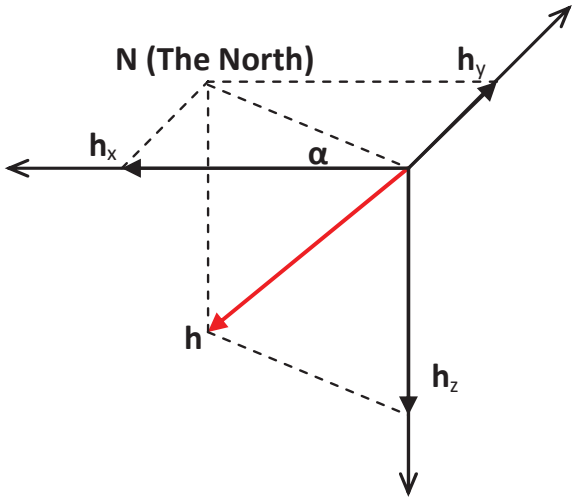

Figure 3.3: Absolute heading calculation under the a magnetometer coordinate frame.

Most current inertial systems employ accelerometers to measure accelerations and gyroscopes to measure rotational rates. Further, the relative position could be calculated by double-integration of accelerations, and the rotation could be calculated by integration of the angular rates. Finally, the magnetometer will assist to obtain the absolute heading. They are especially fit for out-door tracking and daily life tracking because there is no external infrastructure required. With multiple inertial measurement units (IMUs), inertial mocap systems realtime capture the human body motion with the full six degrees of freedom. Other benefits of using inertial based systems include: it is a self-contained system, and inertial sensors cost much less than other systems. However, most critical disadvantage is that use of low cost sensors limits the accuracy of such systems, as integration of noisy sensed data causes cumulative errors to build up. Another drawback is that the IMU is annoying during the long term monitoring, compared to the optical markers.

3.1.3 Summary

Human motion capture systems are designed to yield realtime data, which dynamically represent the gesture changes of a human body. Figure 3.4 illustrates a classification of current available sensing approaches. Performance of the systems based on these methods is listed in Table 3.1.

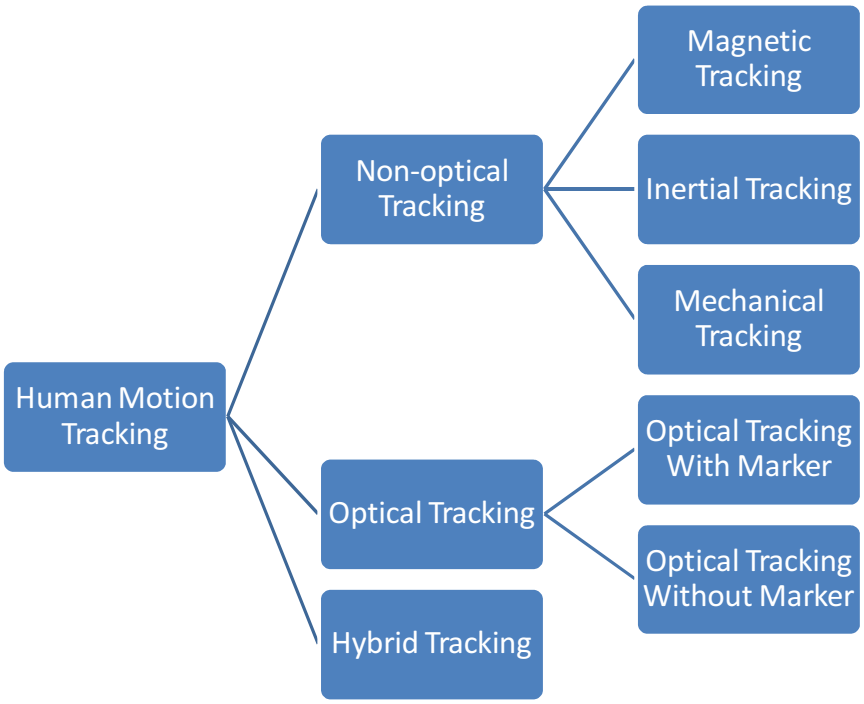

Figure 3.4: Human motion tracking approach classification.

Table 3.1
Performance comparison among different motion tracking approaches.

Approach	Accuracy	Cost	Pros	Cons
Inertial	High	Low	Outdoor	Offset
Marker	Very High	High	Studio	Occlusion
Non-marker	Medium	Medium	unintrusive	Occlusion
Magnetic	Medium	Low	No infrastructure	Ferromagnetic materials

3.2 Related Works

More and more research communities and commercial companies are involved in developing the off-the-shelf motion tracking systems. In this section, we overview the existing products on the market and academic research progress in the related areas. We compare their specifications and discuss the limitations.

3.2.1 Commercial Motion Trackers

InterSense

Wireless InertiaCube3 [72] from InterSense is the latest product in the InertiaCube family of sensors, which provides full tracking of six-degree-of-freedom (6-DoF). It employs advanced Kalman filter to abstract nine discrete inertial sensors. A maximum of four cubes can be tracked using a single receiver, while multiple receivers are able to support up to thirty-two cubes. An external processor unit is available to reduce processing load on the host PC by offloading the processing of the orientation filter. 180Hz update rate with 6 ms of latency would meet requirements from most applications.

Xsens

MTw SDK [73] provides an entire solution of human motion tracking. MTw has the sensor, providing drift-free 3D orientation, acceleration, angular velocity, magnetic field as well as static pressure. When one MTw is in the sensor network, the wireless data rate would be up to 120 Hz, while the data rate will lower down to 20Hz, when 32 MTw are in the single one network. AwINDA station is the data gateway which supports up to 32 MTws's data simultaneously. The entire wireless network is based on IEEE 802.15.4 PHY. The wireless protocol proposed by Xsens guarantees the time-synchronization less than $10\mu s$ between each MTw.

Trivisio

Colibri-Wireless [74] is the wireless motion tracker from Tribiso. It contains a standard IMU, which includes one accelerometer, one gyroscope and one magnetometer. A on-board temperature sensor helps to remove the temperature bias. It supports up to 10 Colibri-Wireless to be connected to one single USB receiver. The sampling frequency is 100 Hz for every Colibri-Wireless.

Vicon

Vicon [75]has developed an entire solution of optical motion tracking, which contains its optical sensors, software and hardware. The cutting edge T40s is a high speed and resolution camera, which captures 515 frames per second (fps) at full frame resolution 2336×1728 (4 Megapixels). This camera is capable of capturing with the speed of up to 2,000 fps by sacrificing the resolution. Vicon system can mix and match different lens and strobe combinations for each camera, increasing strobe efficiency and maximizing marker

clarity on any environment.

Optotrak Certus

Optotrak 3020 [76] provides an accuracy of up to 0.1 mm and resolution of 0.01mm, while a maximum marker frequency of 4600 Hz is enabled to capture data at even higher speeds. Optotrak Certus acclaims the data is research-grade data, which is objective and accurate. However, the tracking volume is much less than Vicon, which is 1126mm$\times$200mm$\times$161mm.

3.2.2 Motion Tracking in Research

The research communities are concentrating overcoming the flaws and improving the performance by proposing different methods. For optical based systems, people are developing marker-free systems, which is motivated by the drawbacks of the systems based on the marker: identification of markers is not reliable and the subject can get rid of the markers completely. Several prototypes have been proposed, but the accuracy is much worse than the maker based systems. Although more and more magnetic based systems have been applied for the tracking issues, magnetic approach has the inherent disadvantage, like latency and jitter. Multiple researches have been involved these issues, using Kalman filtering or any other non-linear filters. Ultrasonic systems are aiming at dealing with the muti-path issue and how to enlarge the tracking range. For inertial based system, several factors are related to the final performance, therefore people are addressing the issues from the following aspects: hardware, wireless protocol, data processing and applications.

3.2.2.1 Hardware

The subject wears multiple IMUs on the body, so IMUs should be installed in a non-intrusive way to avoid the interruption of subject's daily life, if it is a long term tracking. The intuitive way is to increase the functional density, which requires careful design of the hardware. BodyANT [77] and Eco [78] have the smallest size in the existing sensor nodes. However, they contain only one X-Y accelerometer and do not have local storage capability, which are constrained to applications of daily activities monitoring and classifications. TEMP3.1 [79] integrates a tri-axis accelerometer and a tri-axis gyroscope for acquiring more information. Similarly, Mercury [80] and SHIMMER [81] describe a wireless sensor platform for motion analysis of patients with neuromotor disorders. Mobile phones can be an ideal and portable processing platform. Little Rock [82] is a

coprocessor-like subsystem, which is embedded into a cell phone to sense and preprocess the motion data sampled by an IMU in the phone. It helps activate the phone to receive the filtered data and reduce the power consumption.

3.2.2.2 Wireless Protocol

Although the microelectronics industry has faithfully catched up to Moore's law, researchers are proposing efficient wireless protocols to reduce the power consumption, since the average power consumption of wireless transceivers is much higher other parts on the IMU. Most MAC protocols are based on the policy of B-MAC [83]: sensor nodes sleep most of time, and only wake up when detecting a beacon. H-MAC [84] is a Time Division Multiple Access (TDMA) based MAC protocol designed for BSN, which operates on human heartbeat rhythm. Z-MAC [85] is a hybrid protocol, which combines contention-based control slots within TDMA schemes. It can be adaptive to sudden changes in the network environment.

3.2.2.3 Data Processing

The most critical drawback of inertial sensors is that the offset would be accumulated during the calculation of the position and angle by an integration of the inertial sensors' readings. The goal of the current research activities is to design a drift-free inertial system or a self-calibration one. Extended Kalman filters and complimentary filters are the common approaches that are applied for multi sensor calibration. [86] discovered a novel tracking approaches for human upper limb by the employment of a linear encoder.

3.3 Inertial Tracking Theory

Human motion tracking using inertial information is to estimate the orientation of the subject's limbs per the kinematic model of the human beings. The orientation is inferred from the inertial sensors attached to the joint of the limbs. Current developed inertial sensors are accelerometers and gyroscopes, which measures acceleration and rotating rate. If absolute direction is needed, the magnetometer is also involved in motion tracking. This section presents the theoretical foundation of orientation estimation by the inertial sensors.

3.3.1 Coordinate Frame

Normally a generic skeleton frame can be modeled as a set of rotational joints connected by bones arranged in a tree-like structure [87], as shown in Figure 3.5. To capture the human gesture or motions, it is necessary to track the joints in a coordinate frame. And the motion can be considered the complex rotations in the corresponding coordinate frame. In order to describe the human motions, three coordinate frames or even four should be introduced, which are the earth frame, the sensor frame, the body frame, and the screen frame as well.

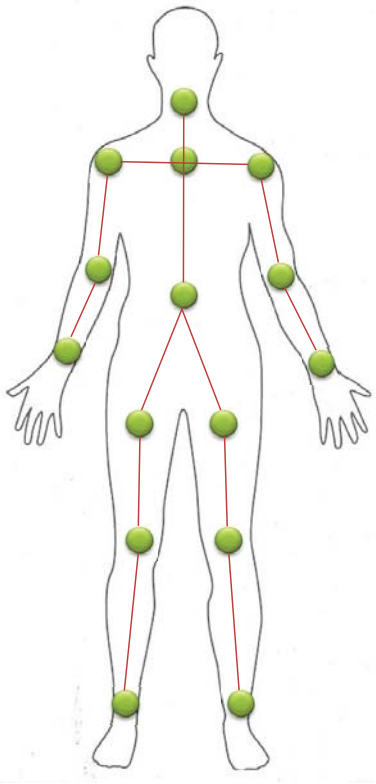

Figure 3.5: Human's skeleton frame.

Earth Coordinate Frame

The earth coordinate frame is used for a reference co-ordinate frame in which all other coordinate systems can coexist. Therefore. we define it as a right-hand cartesian coordinate system with positive X-axis pointing in the direction of magnetic North, positive Y-axis pointing East and positive Z-axis pointing down towards the center of the Earth, where "North" means the direction of magnetic induction line rather than the geographic north. Here it is supposed that the magnetic north is a constant direction in a local area. This assumption would simply the rotation model and do not affect the tracking result. Actually,

there are two Earth bounded axes conventions, the one mentioned above is referred as NED (North, East, Down), used specially in aerospace; another one is named ENU (East, North, Up).

Body Coordinate Frame

The body coordinate Frame is also called the joint frame because of its representation of the local coordinate of a joint in the body model. In practice, if only one joint needs to be tracked, the body frame can be identical to the sensor frame. However, during the full body tracking, there exists multiple joints frame.

Sensor Coordinate Frame

Every sensing device has its own sensor coordinate frame, as shown in Figure 3.10, on which sensor measures the inertial information based . For accelerometers and magnetometers, they measure corresponding parameters relative to the earth frame, while the gyroscopes measure angular rate relative to the body frame. The sensor coordinate frames have been defined after assembly. Therefore the multiple inertial sensors should be coaxial in one IMU in order to simply the calculation. In addition, most off-the-shelf sensors use right-hand coordinate system.

Screen Coordinate Frame

In most motion tracking application, the tracking results will be visualized on the computer's screen. Therefore, it is necessary to project the orientation in the earth frame to the screen frame with positive X-axis points right, positive Y pointing up and positive Z pointing into the screen.

3.3.2 Rotations in 3D Space

Assume the human body is a rigid body structure, the gesture capture is converted to the joint rotation tracking. Take the upper limb for example, the upper limb can be modeled as a simple two-joint segments, as shown in Figure 3.6.

Point O is the shoulder, which is assumed a fixed point. A is the elbow joint, whose movement is considered the 3D rotation around the shoulder. By the same token, the wrist's movement B is also considered the rotation around A. Suppose IMUs are placed on A and B, we can estimate their locations if given the lengths of two segments $\|OA\|$ and

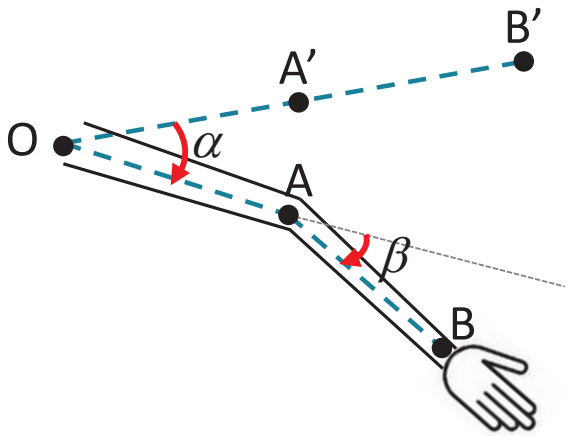

Figure 3.6: Upper limb rotation model.

$\|AB\|$ and the rotations α and β measured from the IMUs. Therefore, before the motion tracking solutions are given, rotation representations are present first in this subsection.

3.3.2.1 Rotation Matrix

A rotation matrix is defined as a matrix that is used to perform a rotation in Euclidean space. First, a 2D rotation is considered, as shown in Figure 3.7.

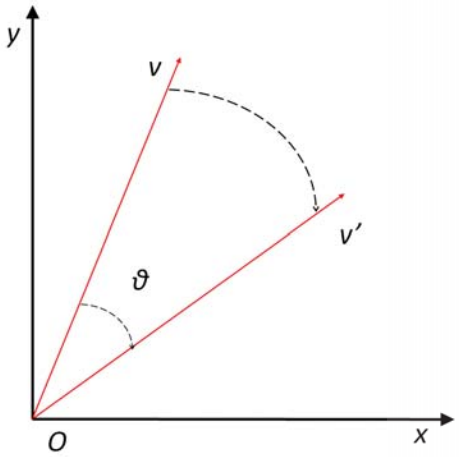

Figure 3.7: Rotation matrix in a 2D coordinate.

Assume $\mathbf{v} = (v_x, v_y)'$ is a column vector that contains the coordinates of the point, a rotated vector $\mathbf{v}'$ is obtained by using the matrix multiplication $\mathbf{Rv}$, where $\mathbf{R}$ is the rotation matrix. Suppose the rotation is through an angle θ about the origin of the Cartesian coordinate

system, the rotation matrix $\mathbf{R}$ can be written by

$$\mathbf{R}(\theta) = \begin{pmatrix} \cos\theta & -\sin\theta \\ \sin\theta & \cos\theta \end{pmatrix}. \tag{3.2}$$

Rotation under a 3D space is extended to an arbitrary axis, not limited to a coordinate axis, as shown in Figure 3.8.

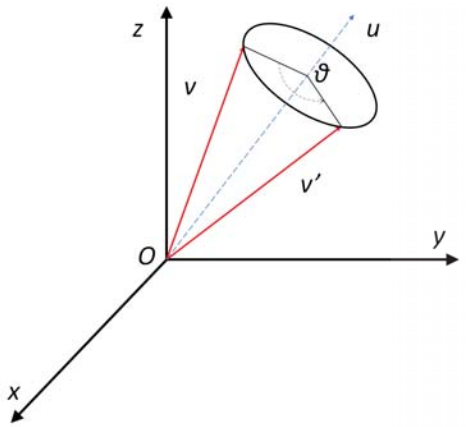

Figure 3.8: Rotation matrix in a 3D coordinate.

Suppose a vector $\mathbf{v} = (v_x, v_y, v_z)$ rotates an angle of θ along the unit vector $\mathbf{u} = (v_u, u_y, u_z)$, where $u_x^2 + u_y^2 + u_z^2 = 1$, the vector after the rotation can be denoted $\mathbf{v}' = \mathbf{R}\mathbf{v}$. Under this condition, the rotation matrix can be written by

$$\mathbf{R} = \begin{pmatrix} \cos\theta + u_x^2(1-\cos\theta) & u_x u_y(1-\cos\theta) - u_z\sin\theta & u_x u_z(1-\cos\theta) + u_y\sin\theta \\ u_y u_x(1-\cos\theta) + u_z\sin\theta & \cos\theta + u_y^2(1-\cos\theta) & u_y u_z(1-\cos\theta) - u_x\sin\theta \\ u_z u_x(1-\cos\theta) - u_y\sin\theta & u_z u_y(1-\cos\theta) + u_x\sin\theta & \cos\theta + u_z^2(1-\cos\theta) \end{pmatrix}. \tag{3.3}$$

According to Equation 3.3, the features of $\mathbf{R}$ can be summarized:

† $\mathbf{R}$ is an orthogonal matrix, whose inverse matrix is equal to its transpose, i.e., $\mathbf{R}\mathbf{R}^T = \mathbf{R}\mathbf{R}^{-1} = \mathbf{I}$.

† The determinant of $\mathbf{R}$ is 1: $det(\mathbf{R}) = 1$.

† Three eigenvalues of $\mathbf{R}$ are 1, $cos\theta + \mathbf{i}sin\theta$ and $cos\theta - \mathbf{i}sin\theta$.

Moreover, we can also inversely infer the mount of rotation θ and the rotation axis $\mathbf{u}$, given a rotation matrix $\mathbf{R}$.

$$\begin{aligned} & \mathbf{Ru} = \mathbf{u} \\ \Rightarrow \quad & (\mathbf{R} - \mathbf{I})\mathbf{u} = 0, \end{aligned} \tag{3.4}$$

which shows that $\mathbf{u}$ is an eigenvector of $\mathbf{R}$ corresponding to the eigenvalue $\lambda = 1$. In addition, the trace of $\mathbf{R}$ is equale to $1 + 2\cos\theta$, per Equation 3.3. Therefore,

$$\theta = \frac{tr(\mathbf{R}) - 1}{2}. \tag{3.5}$$

3.3.2.2 Euler Angles

Leonhard Euler $(1707 - 1783)$ introduced Euler angles to describe the orientation of a rigid body [88]. A set of Euler angles could infer that any orientation in 3D can be achieved by composing three elemental rotations, therefore any orientation can be represented by three independent angles, which is more compacted than the rotation matrix. Suppose the fixed system (or the reference system) is denoted in $O(x,y,z)$, and the rotating system (or the rigid body local system) is denoted in $O(X,Y,Z)$, the two systems are exactly same before the rotations. First, $O(X,Y,Z)$ rotates around z-axis by α, which is also named "yaw". The rotation matrix can be written by

$$\mathbf{R}_z(\alpha) = \begin{pmatrix} \cos\alpha & -\sin\alpha & 0 \\ \sin\alpha & \cos\alpha & 0 \\ 0 & 0 & 1 \end{pmatrix}. \tag{3.6}$$

The X-axis in the rotating system rotates to line N. Second, $O(X,Y,Z)$ rotates around y-axis by β, which is named "pitch". The rotation matrix can be written by

$$\mathbf{R}_y(\beta) = \begin{pmatrix} \cos\beta & 0 & \sin\beta \\ 0 & 1 & 0 \\ -\sin\beta & 0 & \cos\beta \end{pmatrix}. \tag{3.7}$$

Last, the rotating system rotates around x-axis by γ, which is called "roll". The rotation matrix can be written by

$$\mathbf{R}_x(\gamma) = \begin{pmatrix} 1 & 0 & 0 \\ 0 & \cos\gamma & -\sin\gamma \\ 0 & \sin\gamma & \cos\gamma \end{pmatrix}. \tag{3.8}$$

Therefore, the complex rotation in 3D space determined by yaw, pitch and roll can be written by

$$\begin{aligned} & \mathbf{R}(\alpha,\beta,\gamma) \\ = \; & \mathbf{R}_z(\alpha)\mathbf{R}_y(\beta)\mathbf{R}_x(\gamma) \\ = \; & \begin{pmatrix} C_\alpha C_\beta & C_\alpha S_\beta S_\gamma - S_\alpha C_\gamma & C_\alpha S_\beta C_\gamma + S_\alpha S_\gamma \\ S_\alpha C_\beta & S_\alpha S_\beta S_\gamma + C_\alpha C_\gamma & S_\alpha S_\beta C_\gamma - C_\alpha S_\gamma \\ -S_\beta & C_\beta S_\gamma & C_\beta C_\gamma \end{pmatrix}, \end{aligned} \tag{3.9}$$

where C_*=cos $(*)$ and S_*=sin $(*)$. Note that the order of the matrices can not be swapped since matrix multiplication is non-commutative.

Compared with other rotation representation,the euler angle can be directly measured from a gimbal mounted in a vehicle, which can simply much calculation. Although simple to understand, the euler angles also have the most significant disadvantages. First, there are discontinuities in the tracking of subjects which are over 360 degrees. Moreover another

substantial problem occurs when a gimbal lock happens, in which one degree of freedom is missed when the axes of two of the three gimbals are driven into a parallel configuration. Last, there are multiple axis conventions existing. In one system, the axis convention should be consistent. The identical euler angles in different axis conventions would result in different orientation.

3.3.2.3 Quaternion

Quaternion is the third approach for rotation expression. In mathematics, it is original used for extending the complex numbers, which is first introduced by William Rowan Hamilton [89]. A quaternion

$$\mathbf{q} = q_0 + q_1\mathbf{i} + q_2\mathbf{j} + q_3\mathbf{k} \tag{3.10}$$

is a four-dimensional vector space over the real numbers, where $\mathbf{i}^2 = \mathbf{j}^2 = \mathbf{k}^2 = \mathbf{ijk} = -1$. Unit quaternion provides a convenient mathematical presentation for orientation and rotation in three dimensions. Suppose a vector $\mathbf{v}(v_x, v_y, v_z)$ is fit into a quaternion by $\mathbf{q_v} = 0 + v_x\mathbf{i} + v_y\mathbf{j} + v_z\mathbf{k}$, and the vector $\mathbf{v}'(v'_x, v'_y, v'_z)$ after rotation about unit vector $\mathbf{u}(u_x, u_y, u_z)$ by α can be denoted as:

$$\mathbf{v}' = \mathbf{qvq^{-1}}, \tag{3.11}$$

where $\mathbf{q} = \cos\frac{\alpha}{2} + \mathbf{u}\sin\frac{\alpha}{2}$ and $\mathbf{q^{-1}} = \cos\frac{\alpha}{2} - \mathbf{u}\sin\frac{\alpha}{2}$. For a composition of rotations, the expression over quaternions is straight forward. For example, suppose $\mathbf{p}$ and $\mathbf{q}$ are quaternions representing single rotations, then rotation by $\mathbf{pq}$ is equivalent to the complex rotation by $\mathbf{p}$ and then by $\mathbf{q}$:

$$\mathbf{pqv}(\mathbf{pq})^{-1} = \mathbf{pqvq^{-1}p^{-1}} = \mathbf{p}(\mathbf{qvq^{-1}})\mathbf{p^{-1}}. \tag{3.12}$$

Meantime, the quaternion representation can be converted to Euler angles:

$$
\begin{aligned}
\mathbf{q} &= \mathbf{R}_z(\alpha)\mathbf{R}_y(\beta)\mathbf{R}_x(\gamma) \\
&= [\cos\frac{\alpha}{2} + \mathbf{k}\sin\frac{\alpha}{2}][\cos\frac{\beta}{2} + \mathbf{j}\sin\frac{\beta}{2}][\cos\frac{\gamma}{2} + \mathbf{i}\sin\frac{\gamma}{2}] \\
&= [\cos\frac{\gamma}{2}\cos\frac{\beta}{2}\cos\frac{\alpha}{2} + \sin\frac{\gamma}{2}\sin\frac{\beta}{2}\sin\frac{\alpha}{2}] \\
&\quad + [\sin\frac{\gamma}{2}\cos\frac{\beta}{2}\cos\frac{\alpha}{2} - \cos\frac{\gamma}{2}\sin\frac{\beta}{2}\sin\frac{\alpha}{2}]\mathbf{i} \\
&\quad + [\cos\frac{\gamma}{2}\sin\frac{\beta}{2}\cos\frac{\alpha}{2} + \sin\frac{\gamma}{2}\cos\frac{\beta}{2}\sin\frac{\alpha}{2}]\mathbf{j} \\
&\quad + [\cos\frac{\gamma}{2}\cos\frac{\beta}{2}\sin\frac{\alpha}{2} - \sin\frac{\gamma}{2}\sin\frac{\beta}{2}\cos\frac{\alpha}{2}]\mathbf{k}. \qquad (3.13)
\end{aligned}
$$

Inversely, we can obtain the Euler angles from the quaternion, which is:

$$
\begin{aligned}
\gamma &= \arctan\left(2(q_0q_1 + q_2q_3), 1 - 2(q_1q_1 + q_2q_2)\right) \\
\beta &= \arcsin 2(q_0q_2 - q_3q_1) \\
\alpha &= \arctan\left(2(q_0q_3 + q_1q_2), 1 - 2(q_2q_2 + q_3q_3)\right). \qquad (3.14)
\end{aligned}
$$

3.3.2.4 Summary

Among these three representations, the euler angles are the most efficient one which only have three independent variables, and no other redundant variables. Moreover, the meaning of the euler angles are straight forward which represent the angles of three successive rotations. However, the drawbacks are critical: its limit on smooth tracking through all orientations due to the discontinuities. Rotation matrices are computational efficient, nevertheless the nine elements actually has three independent variable, and the values can not tell the relationship to the rotation explicitly. Quaternions overcome the disadvantages of the previous two. Compared to the euler angles, they are easy to compose and avoid gimbal lock. Also in contrast to rotation matrices, they have more numerical stability and may be more efficient in term of only four elements, while rotation matrices have nine.

Therefore, more and more numerical calculation in computer graphic and motion modeling employ quaternions to express the rotation in 3D space.

3.3.3 Orientation Estimation Filter

3.3.3.1 Two Intuitive Approaches

The primary purpose of a filter to decouple the valuable signal from noise. For example, the low pass filter is utilized to remove the low frequency noise from the signal in terms of the spectrum. The similar one contains high pass filter, band pass filter, notch filter and so on. More sophisticated filters can filter the "optimal" value from multiple sources with respect to some criteria. Wiener Filter, Kalman Filter are belong to this type of filters, which are based on one certain probabilistic model.

If the gyroscope was the ideal one that could stream out the accurate angular rate along three axes, according to the rotational differential Equation 3.15 [90],

$$\dot{\mathbf{q}} = \frac{1}{2}\omega\mathbf{q}, \tag{3.15}$$

We would calculate the precise orientation. However, the actual sensors reading differs from the real inertial value. The purpose of introducing a filter is to remove or reduce the noise and the bias from the sensor measurements. Therefore, we first model the measurement of inertial sensors, and then construct the filtering algorithms to remove the unnecessary noise or offset from the ground truth.

A gyroscopes measures the rotational rate in the sensor frame. The measured gyroscope vector, $\mathbf{G}$, can be considered to be

$$\mathbf{G} = S_G(\omega + \mathbf{O}_G + \mathbf{n}_G) \tag{3.16}$$

where ω is the actual angular rate vector, $\mathbf{O}_G$ is the offset readings while the gyroscope

keeps still, and $\mathbf{n}_G$ again denotes an additive noise. S_G is used as a scaling factor matrix for normalization. The scaling factor S_G would result in under- or overestimate the rotational rate, if it is not equal to $\mathbf{I}$. Further, this will in turn lead to the orientation under- or overestimation.

According to Equation 3.15, we can infer that

$$\dot{\mathbf{q}} = \frac{1}{2}\mathbf{G}\mathbf{q}. \tag{3.17}$$

Suppose the time period of two gyroscope measurement is Δt, then

$$\dot{\mathbf{q}}(t) = \frac{1}{2}\mathbf{G}(t)\mathbf{q}(t)\Delta t \tag{3.18}$$

where $*(t)$ denotes this is subject to variation with time. Finally, the discrete orientation quaternion $\mathbf{q}(t+1)$ can be expressed by

$$\mathbf{q}(t+1) = \frac{\dot{\mathbf{q}}(t)+\mathbf{q}(t)}{\|\dot{\mathbf{q}}(t)+\mathbf{q}(t)\|}, \tag{3.19}$$

in which $\mathbf{q}(t+1)$ has been normalized.

This intuitive approach of orientation estimation suffers from the non-zero $\mathbf{O}_G$. Due to the integration, the gyroscope will be under a constant rotation even then it is placed still.

Another approach is to estimate the orientation from the observation of the accelerometer and the magnetometer. An accelerometer measures the acceleration in the sensor frame. Its measurement, $\mathbf{A}$, can be represented by

$$\mathbf{A} = S_A(\mathbf{a}+\mathbf{g}+\mathbf{O}_A+\mathbf{n}_A), \tag{3.20}$$

where **a** denotes the dynamic acceleration under the earth coordinate frame, **g** is the gravity vector, $\mathbf{O}_A$ is the sensor's intrinsic offset, $\mathbf{n}_A$ is the probabilistic additive noise and S_A is a matrix representing for a scaling factor. Here the model of accelerometer is simplified without considering the scaling factor:

$$\mathbf{A} = \mathbf{a} + \mathbf{g} + \mathbf{O}_A + \mathbf{n}_A, \tag{3.21}$$

because the accelerometer measurements could be normalized to 1g when placed still.

A magnetometer measures the local magnetic field in the sensor frame. The measured magnetic vector, **M** can be modeled by

$$\mathbf{M} = S_M(\mathbf{m} + \mathbf{m}_F + \mathbf{O}_M + \mathbf{n}_M). \tag{3.22}$$

In this formula, **m** denotes the field generated by the earth, $\mathbf{m}_F$ denotes the field by other resources, $\mathbf{O}_M$ is the measurement offset, $\mathbf{n}_M$ is the probabilistic additive noise, and S_M is a scaling factor matrix. Suppose we are in a open space, there is no other magnetic field, which $\mathbf{m}_F$ is equal to 0, then Equation 3.22 can be simplified to

$$\mathbf{M} = S_M(\mathbf{m} + \mathbf{O}_M + \mathbf{n}_M). \tag{3.23}$$

Many methods [91][87] are able to derive the orientation estimation using the measurements of the accelerometer and the magnetometer. Here we summary the deduction of FQA introduced in [91]. Suppose the sensors are under a North−East−Down (NED) coordinate system convention. Regardless the noise and offset, the normalized measurements of the accelerometer can be expressed by

$$\bar{\mathbf{A}} = \frac{\mathbf{A}}{\|\mathbf{A}\|} = (\bar{A}_x, \bar{A}_y, \bar{A}_z) = (\sin\theta, -\cos\theta\sin\phi, -\cos\theta\cos\phi) \tag{3.24}$$

where the accelerometer is pitched up through an angle of θ, and then is rolled with an angle of ϕ. Therefore, we can infer the two quaternoins representing these two rotations.

$$\mathbf{q}_p = \cos\frac{\theta}{2} + \sin\frac{\theta}{2}\mathbf{i} + \sin\frac{\theta}{2}\mathbf{j} + \sin\frac{\theta}{2}\mathbf{k}. \tag{3.25}$$

and

$$\mathbf{q}_r = \cos\frac{\phi}{2} + \sin\frac{\phi}{2}\mathbf{i} + \sin\frac{\phi}{2}\mathbf{j} + \sin\frac{\phi}{2}\mathbf{k}. \tag{3.26}$$

Similarly, the yaw rotation ψ can be inferred from the measurements of the magnetometer.

$$\mathbf{q}_y = \cos\frac{\psi}{2} + \sin\frac{\psi}{2}\mathbf{i} + \sin\frac{\psi}{2}\mathbf{j} + \sin\frac{\psi}{2}\mathbf{k}. \tag{3.27}$$

Having obtained all three rotation quaternions, the quaternion representing the orientation of the sensor over the complex rotation can be given by

$$\mathbf{q} = \mathbf{q}_y\mathbf{q}_r\mathbf{q}_p \tag{3.28}$$

Regardless the noise and offset of the sensor measurements, this approach has a prerequisite that the accelerometer only measures the gravity acceleration $\mathbf{g}$, therefore the existence of dynamic acceleration will invalidate this FQA. Further the rigid body is required to be still or move constantly under the earth frame. However this precondition is not always true, when this approach is applied to human motion tracking.

3.3.3.2 Kalman Filter and Extension

Both these two naive approaches discussed above have their own drawbacks, therefore many efforts are involved to fuse the two independent results. Kalman Filter and its extensions are one of the sophisticated filters that are applied to orientation or attitude estimation. The Kalman filter addresses a linear stochastic process estimation problem using the transition model

$$\begin{aligned} \mathbf{x}_k &= \mathbf{A}\mathbf{x}_{k-1} + \mathbf{B}\mathbf{u}_{k-1} + \mathbf{w}_{k-1} \\ p(\mathbf{w}) &\sim \mathbf{N}(0, \mathbf{Q}), \end{aligned} \tag{3.29}$$

and measurement model

$$\begin{aligned} \mathbf{z}_k &= \mathbf{H}\mathbf{x}_k + \mathbf{v}_k \\ p(\mathbf{v}) &\sim \mathbf{N}(0, \mathbf{R}), \end{aligned} \tag{3.30}$$

where

- † $\mathbf{x}_k \in \Re^n$ is a state vector of the discrete-time controlled process at time k,
- † $\mathbf{A}$ is the linear state transition model, applied to the last state $\mathbf{x}_{k-1}$,
- † $\mathbf{B}$ is the linear input model which is applied to the control vector $\mathbf{u}$,
- † $\mathbf{z}_k$ is the measurement vector defined by measurement model $\mathbf{H}$ at time k,
- † The random variables $\mathbf{w}_k$ and $\mathbf{v}_k$ are independent random variables, which represent the Gaussian white noise of the transition process and measurement.

In practice, Equation 3.29 can be simplified by removing the control input $\mathbf{u}$, when the system is a closed system. And the process noise covariance $\mathbf{Q}$ and measurement noise covariance $\mathbf{R}$ may be time-variant matrices, however they can be simplified to be constant under most situations.

Both of transition model (Equation 3.29) and measurement model (Equation 3.30) are able to predict the current state of the system. However, the noise introduce some uncertainty about the inferred current system state. The Kalman filter gives the optimal prediction of a system's state using a weighted average, which can reduce the uncertainty from the transition and measurement models.

$$\begin{aligned}
\mathbf{K}_k &= \mathbf{A}\mathbf{P}_{k-1}\mathbf{H}^T(\mathbf{H}\mathbf{P}_{k-1}\mathbf{H}^T + \mathbf{R}_{k-1})^{-1} \\
\hat{\mathbf{x}}_k &= \mathbf{A}\hat{\mathbf{x}}_{k-1} + \mathbf{K}_{k-1}(\mathbf{z}_k - \mathbf{H}\hat{\mathbf{x}}_{k-1}) \\
\mathbf{P}_k &= \mathbf{A}\mathbf{P}_{k-1}\mathbf{A}^T + \mathbf{Q}_{k-1} + \mathbf{A}\mathbf{P}_{k-1}\mathbf{H}^T\mathbf{R}_{k-1}^{-1}\mathbf{H}\mathbf{P}_{k-1}\mathbf{A}^T,
\end{aligned} \tag{3.31}$$

where $\mathbf{K}$ is the Kalman gain and $\mathbf{P}$ is the posteriori estimate covariance.

Kalman filter is only suitable for the linear system, which can be represented by $\mathbf{A}$, if a non-linear system is addressed, an extended Kalman filter can be plugged into the estimation procedure. In the extended Kalman filter, the state transition 3.32 and observation 3.33 models are not required to be linear functions but differentiable functions instead.

$$\mathbf{x}_k = \mathbf{f}(\mathbf{x}_{k-1},\ \mathbf{u}_{k-1}) + \mathbf{w}_{k-1} \tag{3.32}$$

$$\mathbf{z}_k = \mathbf{h}(\mathbf{x}_k) + \mathbf{v}_k \tag{3.33}$$

where the denotation is the same as the Kalman filter except that $\mathbf{f}$ the nonlinear function is used to describe the transition model and similarly $\mathbf{h}$ is the nonlinear function to decribe the measurement model. The core of EKF is to linearize both the transition and measurement

models using Taylor expansion. The non-linear relations denoted by **f** and **h** can be approximated into the linear relation represented by a Jacobian matrices:

$$\mathbf{F}_{k-1} = \frac{\partial \mathbf{f}}{\partial \mathbf{x}}\Big|_{\hat{\mathbf{x}}_{k-1|k-1},\, \mathbf{u}_{k-1}}$$
$$\mathbf{H}_k = \frac{\partial \mathbf{h}}{\partial \mathbf{x}}\Big|_{\hat{\mathbf{x}}_{k|k-1}} \tag{3.34}$$

The extended Kalman filter can give reasonable performance under more situations than the regular Kalman filter, however, it is not an optimal estimator owing to the Taylor expansion. In addition, linearization also leads to diverge if the initial state is not estimated correctly.

3.4 PAMS Implementation

3.4.1 Introduction

Various IMUs have been developed with the advances in wireless sensor networks and especially the growing interests in body sensor networks. In contrast to other tracking systems, wearable IMU do not require any infrastructure or reference source. In addition to their differences in size and weight, these sensors use different networking technologies such as Bluetooth and IEEE 802.15.4. The selection varies from simple fall detection devices based on accelerometers and orientation tracking devices comprising sensor of accelerometers, magnetometers and gyroscopes, according to different design goals and application scenarios [87].

There are a number of challenges to achieve long term continuous monitoring of physical activities and human motion capture. These include sensor size, weight, cost, wireless networks, battery life, and system robustness. First, minimization of the dimension and weight is necessary to a wearable sensor platform. An unobtrusive style of daily life is preferred while the subject is monitored. Fortunately, the development of MEMS enables the possibilities on node miniaturization, which leads a state-of-the-art design of such systems. Secondly, power efficiency of wearable sensor nodes is a paramount concern.

The long-term monitoring requires durable runtime between cycles of battery replacement. Frequent battery replacement would annoy the subject during daily living and probably miss critical information on physical conditions. Thus, low power chips should be chosen and efficient algorithms are considered to be implemented on body-worn nodes. More importantly, the sensor data should be able to provide adequate information of subjects, in order to better understand their health conditions.

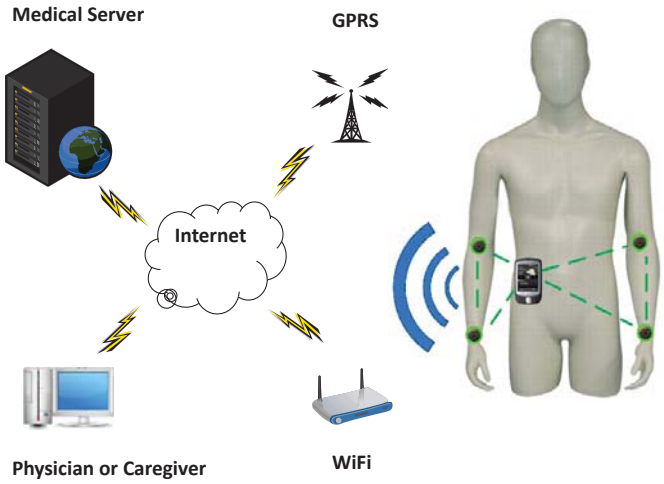

Figure 3.9: PAMS system architecure.

To address the challenges above, PAMS, a wearable physical activity monitoring system is proposed in this chapter. The architecture in Figure 3.9 shows the concept of PAMS with a cell phones as gateway to the Internet. PAMS is a 6-DoF wearable IMU, which can detect tri-axis acceleration, tri-axis angular rate and tri-axis magnetic field. PAMS only weights 8.4 gram, with a miniature outline of 40mm$\times$30mm. Moreover, a high-performance Bluetooth module and one MicroSD card slot enable PAMS to be capable of both durable real-time monitoring and off-line data analysis. Wireless communication via Bluetooth can support interaction with cell phone users on real-time PA monitoring. Embedded large storage can record substantial sensor data later analysis. Critical information will be transmitted to the gateway (cell phone) while substantial data will be recorded on the device for later processing. PAMS can be applied to a spectrum of applications, e.g. human motion tracking, daily activities monitoring/classification and navigation. A motion tracking algorithm is also proposed to demonstrate its applicability and reliable data acquisition from on-board sensors.

3.4.2 System Design

3.4.2.1 Design Goals

Three major issues are involved in building an energy efficient wearable sensor node in a PA monitoring system. First, lifetime is the most critical concern for a battery supported sensor node. Recharging the battery frequently would annoy the subject's daily life and corrupt the integrity of the sensing data. Previous research shows that wireless communication dominates the power consumption among all the modules on the wearable sensor node. Therefore, only power efficient wireless protocols can be taken into account in the system design. Furthermore, local preprocessing ability is required to abstract essential information from raw sensor readings and reduce the volume of data in the air, because relaying all the sensing data to a gateway is a heavy load for most battery supported sensor nodes. Finally, due to the importance of the further off-line analysis, the storage module on-board is also highly necessary.

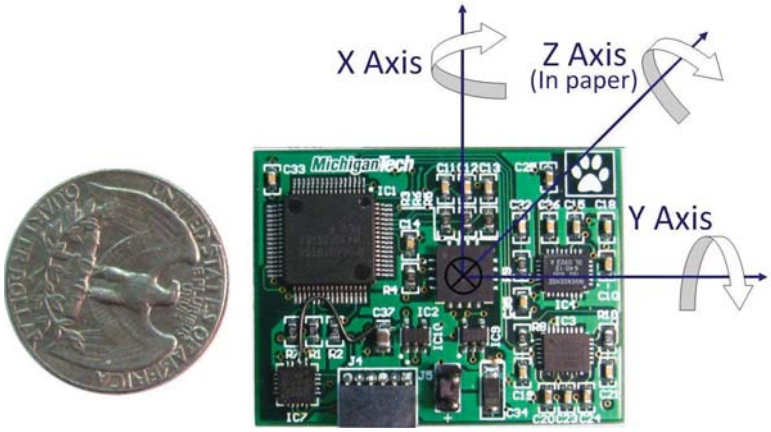

Figure 3.10: The top view of a wearable sensor node in PAMS and its coordinate.

To handle these issues, the wearable sensors node (Figure 3.10) in PAMS is highlighted in four modules: an ultra low power microcontroller, a complete 6-DoF IMU, a wireless communication module and an extendable storage module. The block diagram of the wearable sensor node is illustrated in Figure 3.11. Wearable sensor nodes acquire the inertial parameters from the subject, and convert them to digital data. These data can be stored in a MicroSD card locally for the off-line analysis, or preprocessed by on-board computational capability and then transmitted to a gateway via Bluetooth. The software on the gateway is able to visualize digitalized signals real-time, or operating specific algorithms on demand.

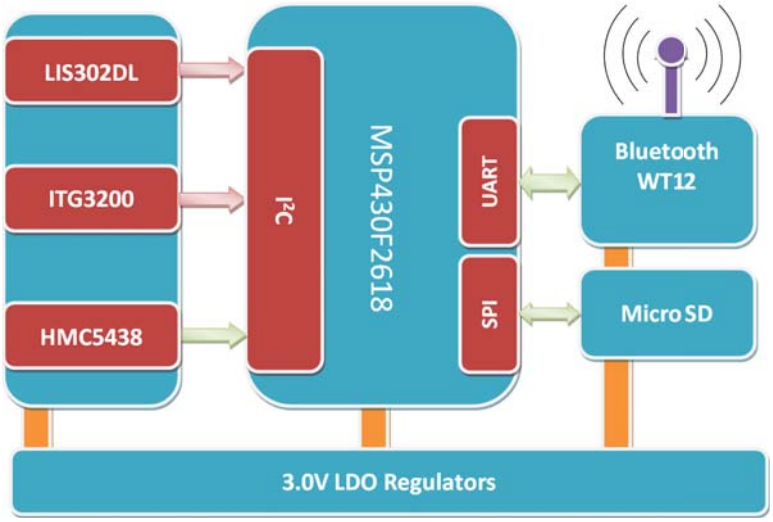

Figure 3.11: The block diagram of the wearable sensor node in PAMS. Each module is powered by a 3.0v regulator.

3.4.2.2 Microcontroller

Although the microcontroller market offers various solutions for different domains, the requirement of the PA monitoring applications narrows down the options into ones with low power consumption, small size and rich peripheral modules. MSP430F2618 from TI is chosen for our proposed PAMS due to its outstanding properties as follows. MSP430F2618 consumes only 450μA current in the active mode, which is one order of magnitude lower than any other commercial microcontrollers. Additionally, four sleeping modes on MSP430F2618 offer more flexibility to the developers on power saving strategies. What's more, the numerous on-chip modules, such as 12-bit ADC and SPI, I^2C, will facilitate the connections to the inertial sensors and miniaturization of the on-body node design.

3.4.2.3 Inertial Measurement Unit

A complete IMU is required to sense linear accelerations, angular rates and magnetic fields along three axes. Even though an off-the-shelf IMU, ADIS14500 from Analog Device, supports all functionalities with higher resolution, the unacceptable high power consumption and its large size suppress the deployment on BSN applications. Meanwhile, ADIS14500 does not support the flexible power control strategies: it can not turn the specific sensors off when they are not needed. Therefore, the design of IMU in PAMS addresses the problems above by combining multiple solo-function inertial sensor chips

with simple profiles. The vendors have offered a variety of accelerometers, gyroscopes, and magnetometers, and PAMS chooses the optimal ones based on their characteristics.

Tri-axis accelerometers, ADXL345 and LIS302DL outperform the available ones on the market in metrics of size, power consumption, etc. But ADXL345 has a 16-bit digital interface, which is not compatible with the 8-bit SPI on MSP430F2618. Although a compatible interface using General Purpose Input and Output (GPIO) pins can be implemented, it is not fast enough and occupies too much resource of MSP430F2618. Therefore, the analog tri-axis accelerometer LIS302DL is adopted, and its output can be discretized by the on-chip ADC module in MSP430F2618.

In contrast to accelerometers, the choices of gyroscopes are less competitive.ITG3200 from ST Microelectronics is the first tri-axis gyroscope on the market, while most other solutions are given by one bi-axis gyroscope plus one single-axis gyroscope.

HMC5843 and HMC1053 are both popular magnetometers in magnetic field sensing designs. However, the decision on HMC5843 in PAMS is inspired by the following factors. First, HMC5843 has already integrated a calibration circuit, which needs to be implemented externally in HMC1053's reference design. Moreover, HMC5843 supports the digital output, while HMC1053 only provides the analog output. Last, HMC1053 is more costly and bigger than HMC5843 in size.

3.4.2.4 Wireless Communication and Extendable Storage Module

There are various choices of network protocols existing in 2.4GHz bandwidth for wireless communication under different working conditions, as shown in Figure 3.12. But Bluetooth is widely used in BSN community, since its design goals fit for the BSN requirements. PAMS also follows the mainstream to choose Bluetooth as the wireless communication protocol. In detail, Bluetooth is defined as a low power short-range wireless technique focusing on power consumption and profile simplicity, while Wi-Fi and Wireless USB more care about throughput, reliability and scalability of networks. Therefore, even they can provide longer communication range and higher throughput, power efficient Bluetooth is proper to the low data rate applications. Additionally, Bluetooth also has a few of advanced features compared to Zigbee. First, most cell phones and laptops have already embedded a Bluetooth module, the hardware development on the gateway is unnecessary. As a result, the cost and period of the whole system development can be reduced significantly. In addition, another temptation of Bluetooth comes from the various profiles it provides. For example, the communication between two Bluetooth ends can be transparent as a UART communication when both of them are configured into Serial Port Profile. In this way,

developers do not need to care about the protocol on Transport Layer in OSI Model, and can focus on the Application Layer design. Last, PAMS only requires a simple wireless topology, which a star-like one is enough. The gateway like the laptop or the smartphone would be the network coordinate in this topology and the wearable sensors are the leaf nodes in this network.

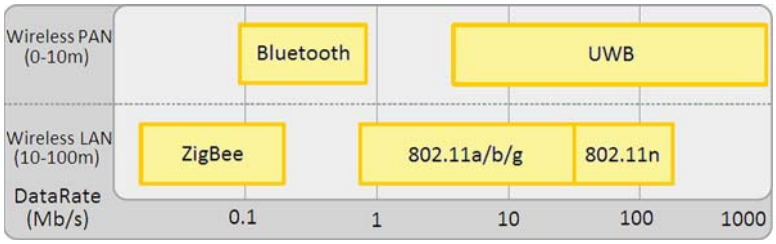

Figure 3.12: Comparison of short range radios.

Currently a lot of commercial Bluetooth modules are on the market. Most of them have the similar size, functionalities and interfaces, as shown in Table 3.2. Therefore transmitting energy consumption becomes a major concern. By this standard, WT12 from BlueGiga would be an optimal choice, since it consumes the lowest transmitting current. In addition, Received Signal Strength Indicator (RSSI) of each package can be tracked for different transmitting power configurations. Hence PAMS benefits from WT12 to enable dynamic transmitting power control and carry out efficient power consumption strategies.

Table 3.2
Features of Bluetooth modules available. TX refers to transmitting.

	TX Current (mA)	Dimension (mm^3)	Price
LMX9838	65.0	10.0×17.0×2.0	$24
BTM410	32.0	12.5×22.0×1.6	$19
RN-41	65.0	13.2×25.8×2.1	$45
WT12	31.5	14.0×25.6×2.4	$23
BTR310	35.0	15.0×24.5×2.8	N/A

Finally, PAMS supports up to 2G byte storage space by integrating a MicroSD card slot. The microcontroller can write and read data to/from the MicroSD card via a bidirectional SPI.

3.4.2.5 Laboratory System Evaluation

In this section, the lifetime of PAMS is evaluated in the laboratory environment in order to compare the power consumption of a wearable sensor node under different configuration.

In this evaluation, lifetime of the on-body node is defined as the period from the time when the first package is sent out to the time when the last correct package is accepted by gateway. Meanwhile, given the same external conditions, PAMS is operated under different configurations and tested its life-time to see how the following factors influence power consuming: the sampling rate, power dissipation of IMU, read/wirte operations of the MicroSD card, wireless communication, and filtering algorithms in the firmware.

Before the evaluation, the power supply is fixed to a 750mAh rechargeable polymer battery and wireless communication is setup to the 0dBm transmission power. For the first round, we start PAMS with 30Hz sampling rate, and turn on different combinations of the sensors on the wearable sensor node. The inertial signals are accordingly sent out using Bluetooth or archived locally on a MicroSD card. There is not any filtering or estimation algorithms integrated. During the second round, the sensor node operated in the same condition except for a 100Hz sampling rate, so that the tradeoff can be assessed between the precision and the lifetime. For the last round, the proposed orientation estimation algorithm is plugged into the firmware, and the sensor node only sends out the estimated orientations. Figure 3.13 summaries the data collected in the evaluation.

From C1 and C2, it can be observed that gyroscopes are more power hunger than the other two types of sensors, which can also be verified from their datasheets. It also can be observed that lowing the sampling frequency could prolong the lifetime, but the influence is not apparent (C2 and C3). In addition, from C3 and C4, it can be inferred that the power consumption by the MicroSD card can be neglected. This fact will guide the developers to store the data locally rather than sending them out by Bluetooth. Finally, it is worth noting that under the C5 condition, the wearable sensor node with the orientation estimation operates much longer than the one without it (C4), because the orientation estimation algorithm reduce the volume of data in the air apparently.

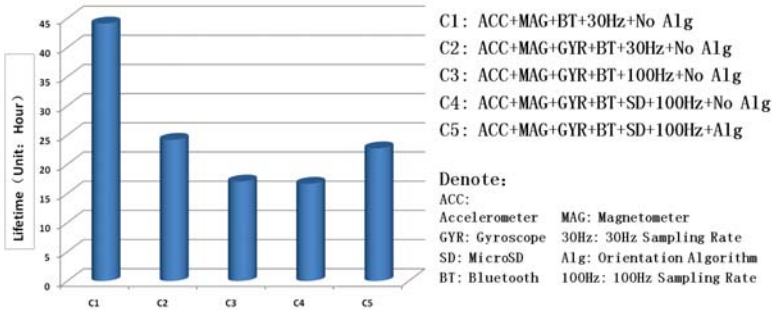

Figure 3.13: The lifetime of PAMS under different conditions.

3.5 Orientation Estimation on PAMS

In most PA applications, accelerations and angular rates are considered as mediate steps. The users actually concern estimating the subject's position, velocity, and orientation. Another merit lies on the fact the orientation estimating on sensor nodes would filter out the redundant data. In this case, the wearable sensor node's lifetime would be prolonged by relieving the load of the wireless communication module. However, if they are not treated properly, small errors in angular velocity readings are integrated into progressively larger errors in orientations, causing rapid degrade of performance. Researches have shown that the noise from which most inertial sensors suffer can be modeled by the linear or high order nonlinear stochastic processes [92]. They can be handled respectively according to the bandwidths: on one hand, the high-frequency noise can be simply filtered out using a low-pass filter; on the other hand, the low-frequency part can be modeled as a first-order Gauss-Markov process. Hence PAMS utilizes Kalman filters to provide optimized estimation naturally.

3.5.1 Extended Kalman Filter

The low pass filter is able to remove most high frequency noise, but is helpless to the low frequency noise which is mixed with the signal in the spectrum. Until recently, many literatures have addressed the orientation estimation using complementary filters and Kalman filters [93][91][94][95][96] to filter the noise and bias out. However, most algorithms require powerful computational capability, which can not be offered on the on-body nodes. Therefore, an efficient quaternion-based Extended Kalman Filter (EKF) is proposed in this section. First, the observations in our filter design do not come from the sensor measurements directly, while a simple algorithm is plugged before sensor measurements are fed into the EKF, so that the system observation model can be simplified. Second, compared to rotation matrices and Euler angles, quaternions outperform for their compact representation and explicit relation to the spacial rotation. Third, no trigonometric function subroutines are needed in this EKF design, which is suitable for implementation on MSP430F2618.

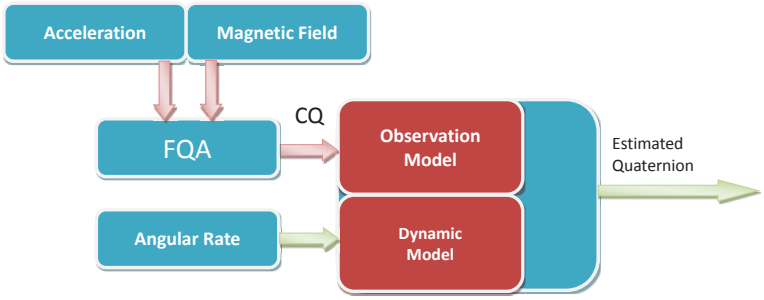

Figure 3.14: The architecture of the EKF designs. CQ stands for Computed Quaternion.

3.5.1.1 System Dynamic Model

Let $\vec{\omega}$=[ω_x ω_y ω_z]^T denote the angular rate from the gyroscopes' reading along three orthogonal axes in the IMU coordinate, and the quaternion representation of the subject's corresponding orientation is denoted by $\mathring{q} = q_1 + q_2\vec{i} + q_3\vec{j} + q_4\vec{k}$ in the earth coordinate. Hence, in the EKF design of PAMS, the state vector can be represented as a 7-D column vector $\vec{X} = [\omega_x\ \omega_y\ \omega_z\ q_1\ q_2\ q_3\ q_4]^T$. Supposing the human body is moving at a constant velocity, the system can be modeled as a first order linear system as follows,

$$\dot{\vec{\omega}} = -\frac{1}{\tau}(\vec{\omega} + \vec{w}) \tag{3.35}$$

and

$$\dot{\mathring{q}} = \frac{1}{2}\mathring{q} \bigotimes \vec{\omega}, \tag{3.36}$$

where τ is a time constant, $\vec{w}$ is supposed to be an zero-mean and Q covariance gaussian white noise, and $\bigotimes$ represents quaternion multiplication.

3.5.1.2 System Observation Model

Traditional quaternion-based EKFs are fed the IMU measurements as the observations directly, which leads to the nonlinear system observation model and high computational requirements. In PAMS, we introduce Factored Quaternion Algorithm (FQA) [91] to synthesize the IMU readings, and treat the outputs of FQA, *Computed Quaternion*s ($\mathring{q}_c$), as observations of the proposed EKF, shown in Figure 3.14. In this case, the observations of the EKF is proportional to the state vector$\vec{X}$. Although extra cost is needed for the FQA implementation, the overall computational requirement is still less than before. Therefore, supposing the observation vector $\vec{Z} = [z_1\ z_2\ z_3\ z_4\ z_5\ z_6\ z_7]^T$ and denoting $\mathring{q}_c = q_{c1} + q_{c2}\vec{i} + q_{c3}\vec{j} + q_{c4}\vec{k}$, the system observation model could be simplified as follows:

$$\begin{bmatrix} z_1 \\ z_2 \\ z_3 \end{bmatrix} = \vec{\omega} + \vec{v}\,, \quad \begin{bmatrix} z_4 \\ z_5 \\ z_6 \\ z_7 \end{bmatrix} = \begin{bmatrix} q_{c1} \\ q_{c2} \\ q_{c3} \\ q_{c4} \end{bmatrix}\,, \tag{3.37}$$

where $\vec{v}$ is a zero-mean and R covariance gaussian white noise.

After the system dynamic model (Equation 3.35, Equation 3.36) and the observation model (Equation 3.37) are constructed, an standard EKF algorithm can be employed to recursively estimate the current state vector, which contains the estimated orientation.

3.5.2 Experimental Results

To evaluate the performance and accuracy of the orientation estimation, the entire algorithm is firstly implemented in Matlab for performance evaluation. The PAMS is attached to the subject's forearm, all the data acquired by PAMS are transmitted to a desktop running the algorithm, we can track the trace of error covariance matrix P_k of the state vector $\vec{X}_k$, since Kalman gain aims at reducing the covariance of the states vector. Before the experiment, we setup the sampling period $\Delta t = 0.01s$, and the initial covariance matrix Q and R are experimentally determined [93].

The results of a static orientation estimation experiment are shown in Figure 3.15. The initial state estimate is chosen to $\mathring{q}_0 = 0 + 0.707\vec{i} + 0.707\vec{j} + 0\vec{k}$, while the actual position

of the sensor is $\mathring{q} = 0.957 + 0.0076\vec{i} + 0.0193\vec{j} - 0.289\vec{k}$. The upper left chart shows the trace tendency of P_k for the first 200 samples, which last only 2 seconds. It is worth noting that the trace of the covariance matrix converges very fast and reaches a stable level at approximately the first 10 samples. The rest charts in Figure 3.15 give the clear illustrations that the state estimate follows the real orientation's track very quickly. Another experiment is designed for dynamic orientation tracking. The subject repeats twice with different rates lifting his right arm from the pose in Figure 3.17(a) to the one in Figure 3.17(c) and lows it back. Figure 3.16 shows the trajectory of angles in three directions.

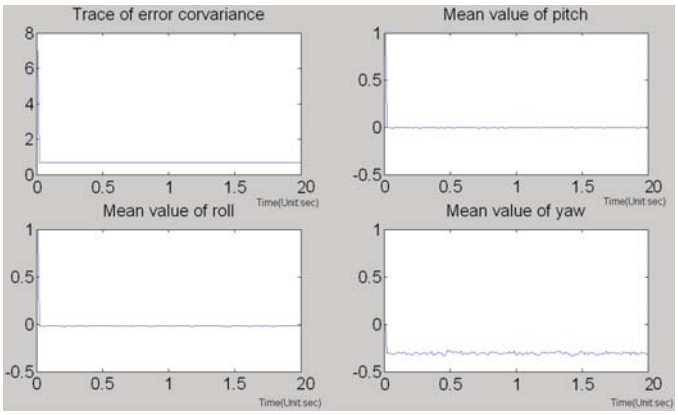

Figure 3.15: The static orientation tracking.

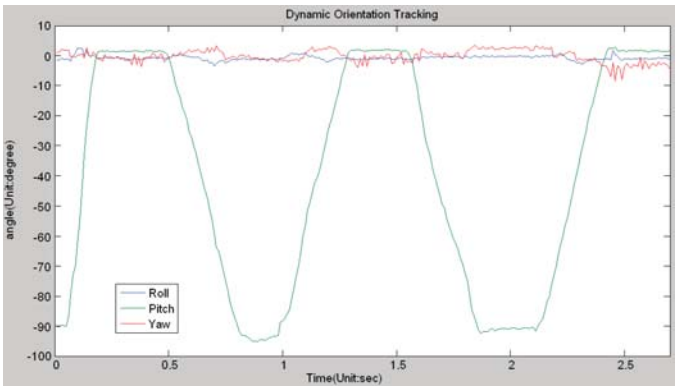

Figure 3.16: The dynamic orientation tracking.

3.6 Applications on PAMS

Long term PA monitoring and accurate human motion analysis have been involved in many applications, such as at-home healthcare, human computer and human robot interactions, etc. Automatic detection of PA types and intensity can provide guidance for various

health assessments [97][98][99][100][101]. Both heuristic and statistical approaches have been proposed in the literatures to achieve activity classification using IMUs. Fall detection can be considered as a special case of activity classifications [102]. Motion capture capability in a free living environment enables interactive control for multi-robot networks in both virtual and real environments. Several strategies for human/robot coordination have been proposed, which cover teleoperations, supervisory control and waypoint control [103][104]. Wii from Nintendo is a successful case in the consumer electronics industry. The Wii-remote with an accelerometer can capture the motion of a single point in the human's body. Being used as a gesture control device, Wii console provides interactions with both abstract objects in virtual environments and robots in real environments. As a general purpose PA system, PAMS has shown prospective future in various applications in assisted living and human robot interactions. In this section, two case studies on body tracking and navigation are presented to demonstrate the flexibility and reliability of proposed PAMS.

3.6.1 Applications on Upper Limb Pose Capture

Recent research shows that the upper limb of the human body could be modeled as a first order linear system containing two rigid segments: the arm and the forearm with two joints (the shoulder and the elbow). Figure 3.17 shows the real pose of the upper limbs and the visualization of its estimation by PAMS. Supposing the origin of the coordinate is setup at the shoulder, and two PAMS wearable sensor nodes are mounted on elbow and wrist respectively, the posture of upper limb can be tracked in real time, while the orientation of these two sensor nodes are estimated. Extensively, PAMS can encode the motion of multiple body parts or even the entire body. Therefore, PAMS can be used as a gesture control device for the interactions with the virtual reality and controlling remote robots in real environments.

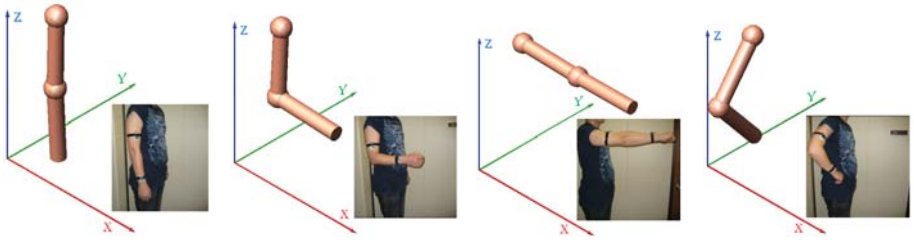

(a) **(b)** **(c)** **(d)**

Figure 3.17: The comparison between the real human poses and the snap shoots of the visualization.

3.6.2 Indoor Environment Navigation

Most navigation approaches nowadays rely on GPS or external landmarks and beacons as references. However, in the buildings or some complex environments where GPS signal is denied, it would be impractical to setup external references, especially in emergency situations. IMU gives an alternative solution to track the subject in indoor environments [105]. However, the single accelerometer in many BSNs only gives the displacement of a point mass by double integrating the linear accelerations along three orthogonal axes, it can not tell the absolute orientation. Fortunately, PAMS can sense the absolute direction of the subject by a magnetometer and have the potential to track and navigate a person in a non-GPS indoor environment with the help of the digital map.

3.7 Summary

PAMS enables continuous longitudinal PA monitoring in free-living environments. This chapter presents both its architecture and the implementation details of the hardware design. For the purpose of power saving and data reliability, an innovative EKF algorithm is also proposed to estimate the human's orientation from the raw inertial sensor readings, and this algorithm is demonstrated in an upper limb motion tracking application.

As the future work, we intend to shrink the dimension of PAMS further to make it more wearable. Moreover, the lifetime would be prolonged further by using more power efficient components and simpler profile algorithms. Additional clinical and robotic applications based on PAMS would be implemented to verify its flexibility and usability.

Chapter 4

CosNet: A Context-aware Sensor Network for Environmental Sensing

4.1 Introduction

4.1.1 Background

Current body sensor networks are concentrating on the issues of body-centric recognition, such as wearable ECG analysis or realtime human motion tracking. However, only body-centric sensing, like physiological signal monitoring and inertial signal tracking, is not enough to understand the human's health status. Consider the following scenario, the wearable sensor may detect the subject's heart beat rate is abnormally high. This would be due to the reason that the subject is suffering a heart attack or maybe he is taking physical exercises. The on-body sensor network can not make the accurate decision whether the alarm should be fired or not. So the knowledge of physical environment is also required for further diagnosis. By this reason, context-aware sensing is being introduced to assist the body sensor networks to provide smarter healthcare service. Context is defined as the environmental information used to identify or characterize the status of a subject, which might be human beings or other physical objects [106]. It may contain all the information of the surrounding environment, such as the environmental weather (temperature, humidity, barometric pressure), environmental noise, the subject's location and so on. In the scenario above, suppose ultrasonic sensors are deployed around, which can track the subject's location in realtime, the system can make the decision based on the localized information: if the subject is lying on the bed, the possibility that he is suffering a heart attack will

increase a lot; nevertheless, if the subject is in a gym, it is highly possible that he is taking the exercises. In summary, the alarm system will make the final decision based on all the valuable knowledge from the subject itself and the environment as well. More information is involved in the health care, the better would the system understand the subject's status.

Therefore, more and more context sensing from static environmental sensor nodes, are being merged into current hybrid body sensor networks. The body sensor networks benefit from the static environmental sensors in two aspects. On one hand, they are able to provide the environmental context information which may be not available to the on-body sensor nodes. Generally the static sensor nodes are deployed all around the living space to collect surrounding information such as temperature, humidity and light. Further, the static sensor can track the location of the subject with ultrasonic transceivers equipped. On the other hand, they are also able to provide networking coverage for the wearable on-body sensor nodes, due to the reason that static sensors can be widely deployed in entire the indoor environment because of its low cost characteristic. Wi-Fi access point might be one competitor, but it suffers from its power budget and robustness. In the Wi-Fi point of view, power consumption is not a critical concern: even a battery support Wi-Fi device still can be loaded with a powerful battery. However this is not true in the static sensor node in body sensor networks, which has more limitation on power budget. In addition, for the access point in Wi-Fi networks, redundancy is not taken into account. Normally it is unnecessary to deploy multiple access points to keep the Wi-Fi networks reliable. In contrast, the static sensor nodes in body sensor networks aim at achieving extremely low manufacturing and operating costs, without sacrificing flexibility or generality, and moreover, the deployment of a number of static sensor nodes guarantees the redundancy of networking, in which single sensor node missing will not affect the networking coverage and performance too much.

4.1.2 Challenges

In practice, the static sensor node differs from others due to variety of environmental settings, diversity of the subject's conditions. Therefore, many challenges arise for those context-aware sensor networks, which may include sensor noise removal, networking coverage and reliability, sensory date integration and power budget limitation.

First, the sensory data in the context-aware sensor networks will be used for critical decision making. Once they are corrupted by the data lost, malicious noise, or uncertainty, the system will lose the fundamental of reasoning, and hence consequential decision will not be reliable for medical usage. So the context-aware sensing should have the robust model against the sensing noise.

Second, the more environmental information are involved during the data processing, the more accurate the sensor network would recognize the context [107]. However, the dimension of the sensing data will increase quickly, once a large number of static sensors are deployed and multiple environmental attributes are monitored. This will arise two potential issues. The first one is that the high dimension of sensing data will place a heavy load on system bandwidth of on-board data processing and wireless data transmission. Another one is that the reasoning rate of the system is going to be slow down while the sensory inputs are increased. Therefore, to keep a good performance of a context-aware sensor network, the system should carefully control the processed data volume, making the system efficient and compressed in data processing and transmission.

Last, the required environmental attributes should also be carefully selected. With more environmental features are monitored, some sensor measurements are related to the specific application, while others are irrelevant or redundant ones. Similar to the constraint of the number of the sensor node, the irrelevant sensory data are limited to be injected into the network, otherwise the wireless transmission will be an unaccepted burden of the power limited sensor networks. Therefore the system is required to filter out the unnecessary sensor readings.

4.1.3 Related Works

The sensor networks for environment monitoring can be classified into two types: one is indoor monitoring and another one is outdoor monitoring for the ecological applications [108]. This subsection mainly concentrates on the sensor networks for indoor environment applications.

CITRIS setups a wireless sensor network including multiple "Smartdust Motes" among the Cory Hall to monitor light and temperature. Some nodes powered by batteries are deployed in office corners, conference rooms, and along hallways, they monitor the realtime distribution on light and temperature conditions among this hall. Additionally, other sensor nodes are placed in the breaker boxes to monitor power consumption. All the sensor measurements are relied to a base station for storage or further data analysis [109]. ASHRAE also uses a sensor network to improve the environmental conditions inside buildings. Multiple sensors are installed in an office building to monitor the operation of heating, ventilation and air condition systems [110]. The data from this sensor network are used to discuss its advantages and disadvantages and survey the trend of wireless technology. Static sensor nodes are also introduced in civil engineering researches [111][112]. Scientists employ static sensor nodes to monitor the health of local structure during the earthquake. They can identify the presence of the vibration, localize the

damage position, and evaluate damage severity. Further after an earthquake, the inspection of a building over the sensor networks will not be limited to evaluation of cracks and damages, but also the real vibration data during the earthquake [113].

To place sensor nodes in the applications above, the research community has developed all sorts of sensor nodes with variety of dimension, weight, and functionality. Most hardware platforms in static sensor networks use off-the-shelf MCUs, even though general purpose computing engines might not be well suited to the event-driven nature of sensor network workloads. Mica2 mote [114] is the prototype in early years which has been widely used by the community. It is based on the 7.3 MHz ATMega 128L microcontroller with 128K code memory and 4K data memory. With a sensing daughter board, Mica2 is loaded with the temperature sensor, light sensor, accelerometer and magnetometer. TmoteSky [115]is another series of sensor node from Crossbow, which is powered by one 16-bit microcontroller MSP430F149 from TI with 512K flash and 2K data memory. It has been integrated with the temperature sensor, light sensor, accelerometer and a acoustic microphone. With the increasing availability and maturity of the underlying technology, more and more state of art sensor nodes have been published. Sun Spot [116] from Oracle is powered by an ARM-based CPU, AT91FR40162S, from Atmel with 2M flash and 256K data memory. The sensor node integrated with sensing daughter board contains a 3D accelerometer, a temperature sensor and a light sensor. More external sensors, such as GPS, humidity, can be enabled with another daughter boards extension. SHIMMER [117] originally developed by Intel Research Labs in 2006, is based on TI MSP430F1611 with 2G flash (by a extendable SD card slot) and 10K data memory. SHIMMER is an open architecture only with a 3D accelerometer. However, with external sensor modules, such as kinematic modules, biophysical modules and ambient modules, it can be expanded to many applications. Table 4.1 lists all the related characteristics of all the popular sensor nodes.

Table 4.1
The comparison of the sensor node prototypes

Prototype	MCU	RAM	Flash	Wireless Module
Mica2	Atmega 128L	4K	128K	CC1000
TelOS/TmoteSky	MSP430F149	2k	60k	CC2420
SunSpot	Atmel AT91FR40162S	256K	2M	CC2420
ECO	nRF24E1	4K	32K	nRF24E1
SHIMMER	MSP430F1611	10K	2G	CC2420
IRIS	ATmega 128L	8K	640K	ATRF230
Ant	MSP430F1232	256	8K	nRF24AP1

The rest of this chapter is organized as follows: the systematical design of CosNet will be discussed first, which includes the major concerns when the static sensor nodes are

brought up. Then we will introduce the hardware design of the static sensor node, from the component selection to the schematic design and to the final layout design. The third section is to discuss the firmware on the senor node, which make this sensor network power efficient. Finally one case study will be described to illustrate how CosNet localizes the subject position.

4.2 Systematical Design

Three major issues are considered during building the static sensor node for context-aware environmental monitoring. First, lifetime is the most critical concern for a battery supported sensor node. Frequent battery replacement during recharging would be unacceptable. Given a budget of battery power, most modules on the node should be able to go into the sleep mode, and be activated when necessary. Second, local preprocessing ability is required to filter out unnecessary sensory data and extract valuable contexts from raw sensor readings, because relaying all the sensing data to a gateway is a heavy load for most battery supported sensor nodes. Finally, the topology of networking should cover the entire indoor environment where the subject may reach in the daily life.

4.3 Hardware Design

Figure 4.1: The static sensor node in CosNet. The front contains the ultrasonic transceiver, the networking module, a temperature sensor, and a photonic sensor.

The static sensor node in CosNet,as shown in Figure 4.1, consists of 7 modules: a MCU, a radio communication module, a storage module, and a suite of environmental sensors

including an ultrasonic transceiver, a humidity sensor, a temperature sensor, and a photonic sensor. The specifications are summarized in Table 4.2.

Table 4.2
The specification of the static sensor node in CosNet

Module	Parameter	MIN	TYP	MAX	Unit
Humidity Sensor	Resolution		0.03		%RH
	Range	0		100	%RH
Temperature Sensor	Resolution		0.01		°C
	Range	-40		124	°C
Photonic Sensor	Response Range	320		730	nm
	Photo Sensitivity		0.3[1]		A/W
Ultrasonic Transceiver	Resolution		147		uS/inch
	Range	0		254	inch
	Sampling Rate		20		Hz

The suite of sensors monitor the environmental attributes, and feed the sensory data to the MCU for processing. The photonic sensor is an analog output, which is acquired via the on-chip ADC; both the humidity sensor and the temperature are direct digital outputs, which is connected to the MCU via an I2C bus; the output of the ultrasonic transceiver has been encoded into a PMW (Pulse-width modulation) signal, in which the width of the pulse is proportional to the sensed distance, so it is fed into a timer on the MCU. After that, MCU can process the data on the specific requirements. The storage module can save all the data on a MicroSD card and the radio module can transmit data wirelessly for monitoring. The block diagram of the static sensor node is shown in Figure 4.2.

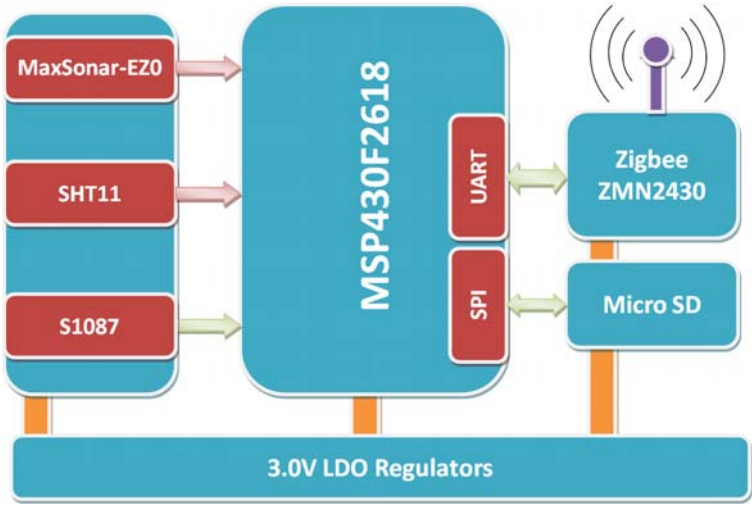

Figure 4.2: The block diagram of the static sensor node in CosNet.

4.3.1 Microcontroller

MCU plays a critical role in the sensor node, which determines the functionality, expansibility and performance of the sensor node. From the system design point of view, MCU should be determined at every beginning by considering its power consumption, expansibility, computational capability and IO resources. Given the applications of CosNet, which keeps monitoring environmental attributes, we balance three major features, power consumption, computational capability and IO resources, and place power consumption as the highest priority: an energy efficient MCU is prerequisite of a battery supported device for a long-term operation, while computational capability is scarified, because it is not required too much calculation in this application. A MCU with rich IO resources will simplify the design, and current existing MCUs on the market have more than enough IO resources, therefore, this factor will be considered at last.

With the three golden rules above, MSP430F2618 [118] from TI is selected to be the main CPU on the static sensor node in CosNet. It embeds a 16-bit RISC MCU with five low-power modes. It is optimized to prolong the battery life in wireless sensor network applications. The device features the digitally controlled oscillator (DCO) which is able to wake up from low-power modes in less than $1\mu s$. MSP430F2618 has two built-in 16-bit timers, one SPI, one I2C bus, and a 12-bit ADC with integrated reference, which can be connected to the suite of sensors directly. MCUs from MSP430 family have been widely applied to various sensor networks, from which the previous reference design helps to cut the developing cost.

4.3.2 Wireless Communication Unit

4.3.2.1 Wireless Communication Protocol

Many protocols exist for short-range wireless communication under different working conditions. Considering the developing cost, power consumption, networking reliability and other factors, the protocol selection is narrowed down to 2.4G based wireless communication protocols. Wi-Fi is excluded first, because it is not designed for the low-speed and low-power communication. Among other protocols in 802.15.X family, Zigbee which lays on IEEE802.15.4 surpasses others concerning the topology, throughput and developing cost. It supports peer-to-peer networking topology, which is the basis of an ad-hoc network, while Bluetooth can only be built into a star-like topology. The star-like

topology is not fit for our situation, which will be discussed in detail in the next subsection. Therefore we choose Zigbee as the wireless communication protocol, considering easy deployment, the proper range of operation and reliable data transfer.

4.3.2.2 Networking Topology

IEEE802.15.4 underlying Zigbee supports two topologies: star-like one and peer-to-peer one. The star-like topology that requires all other nodes in the network should be able to communicate with the coordinate directly, and the commutation between non-coordinate nodes have to be relied over the coordinate, even though they are close to each other in space. Consider the following scenario: in a complex indoor environment, two sensor nodes close to each other are exchanging data. They need the coordinate to rely the data, which is in another room unfortunately. Generally, the wireless communication will be seriously corrupted due to the wall if two nodes are out of line of sight. The only solution under this situation would be increase the transmitting power, which is unacceptable and unnecessary.

On the other hand, peer-to-peer topology can form arbitrary patterns of links, and their extension is only limited by the distance between each pair of nodes. These two points also provide the basis of one self-management and organization ad-hoc network over 802.15.4 protocol. Among this topology, a special node which is connected to the Gateway behaves as the coordinator of the network. It takes in charge of the network, including new node detection and Qos management and other issues, but it will not be involved in the data exchange between other nodes. Other nodes connect to this coordinator over one hop or multi hops.

4.3.3 Wireless Communication Module

ZMN2430 from RFM is a 2.4 GHz transceiver module based on the IEEE 802.15.4 wireless standard and the ZigBee protocol stack [119]. It is a low cost radio chip for peer-to-peer connection, or ad-hoc networks. ZMN2430 has integrated a chip antenna, which requires no more efforts of RF circuit design. Via the provided API over a serial port, the MCU can configure the wireless module and manage the network directly. Last, the low power consumption of the sleep mode provides the possibility to reduced power consumption of sensor node. This off-the-shelf module will greatly reduce the effort working on the wireless subsystem. The key characteristics are listed in Table 4.3.

Table 4.3
The specification of the wireless communication module

Parameter	MIN	TYP	MAX	Unit
Operating Frequency	2405		2475	MHz
Data Transmission Rate		250		kbps
RF Transmit Power			16	dBm
Optimum Antenna Impedance		50		Ω
Response Range	320		730	nm
Receive Mode Current		33		mA
Transmit Mode Current		130		mA
Sleep Mode Current			3	μA

4.3.4 Sensors

4.3.4.1 Ultrasonic Transceiver

MaxSonar-EZ0 from MaxBotix is an ultrasonic range finder, which provides the solution of range detection and ranging from 0-inches to 254-inches. It features that the transmitter and receiver are integrated into one module, which helps to reduce the dimension of the sensor node. Other benefits are summarized as follows:

† It is a very low cost and power-efficient solution of ultrasonic range sensor.

† It is fit for mass deployment in sensor networks.

† It provides reliable and stable range data and there is rarely dead zone.

† It supports a couple of interfaces including pulse width output, analog output and serial port output.

4.3.4.2 Temperature Sensors

SHT11 from Sensirion is a surface mountable sensor module which integrates the temperature sensor and relative humidity sensor. The relative humidity sensor is implemented by a unique capacitive sensor unit, and the temperature is measured by a band-gap sensor unit. A 14bit on-chip ADC guarantees the resolution of the sensing

measurements. A I2C interface circuit is embedded on-chip, such that SHT11 can be connected to the MCU over a I2C bus directly. Each SHT11 is individually calibrated, and the calibration coefficients are archived into non-volatile memory on the chip. Another merit is that the small dimension and low power consumption makes SHT11 the suitable for battery powered sensor nodes.

4.3.4.3 Photonic Sensor

S1087 Hamamatsu Corporation is a Si photodiode for light detection. Its ceramic package will prevent the light coming from the side or backside.

4.3.5 Storage Module and Power Module

The static sensor node does not contain any on-board flash memory but a MicroSD card slot for data storage. First, microSD card has the higher storage density than the normal flash memory. Second, SPI connection will simplify the interface circuit, no extra chip is required to connect between the MCU and the memory module. Last, PC with the SD card socket can dump the data on the SD card easily, while another interface should be designed for on-board flash memory, which could be over the serial port or the wireless module. However, neither of them would be an easy implementation.

The static sensor node in CosNet is powered by a 3.7v rechargeable polymer Li-Ion battery. Compared to other rechargeable batteries cell, polymer Li-Ion battery has much high energy density than other types of batteries. The one used in static sensor nodes contains 1300mAh with only a dimension of $50mm \times 30mm \times 6mm$ and 130g. Other advantages of the polymer Li-Ion battery also include more than 1000 cycle times, low to 2 to 5 percent self discharge per month and better discharge performance.

Due to 3.7v battery voltages, the chips and modules on-board choose 3v as the working voltage and a regulators TPS76430 is plugged in to provide the 3.0v voltage. TPS76430 is a low-dropout (LDO) voltage regulator with a low noise, low-power operation. And multiple TPS76430 are used in the static sensor node for separation of analog circuit power and digital circuit power.

4.4 Software Design

The software contains two parts: the firmware on the static sensor nodes and the application on the Gateway. The firmware on the static sensor node takes in charge of sensing the environmental attributes required by the specific applications and rely them to the coordinate in the ad-hoc networks. The coordinate is associated to a powerful gateway physically, the gateway would make the decision or infer the context according to the valuable data from the static sensor nodes.

4.4.1 Firmware on Static Sensor Nodes

The static sensor node in CosNet is a typical real-time system which contains periodic tasks and sporadic tasks. The periodic tasks include the sensor measurement acquisition, processing and backing-up; the sporadic tasks contain the message handling from the gateway or other sensor nodes. The typical time line of the task processing is shown in 4.3.

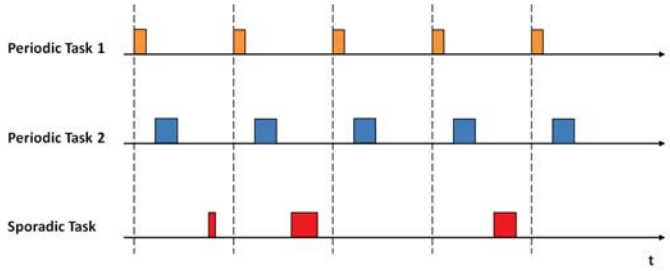

Figure 4.3: The time line of the task processing in CosNet.

The firmware is hierarchized into four layers referring to the popular sensor node design [120]. Figure 4.4 shows the firmware stack in the static sensor node. The hardware modules lies on the bottom layer in the stack. Above that lies the hardware abstract layer. This layer envelops the hardware register operations. Also it provides the basic operations to control the peripheral modules. The layer on that is the driver layer, which provides the operations to the peripheral modules to the middleware. The middleware layer handles three issues, which contains the query processing subsystem, networking management subsystem and the power management subsystem. The top layer is the application layer, it utilizes the APIs from middleware to fulfill the required tasks.

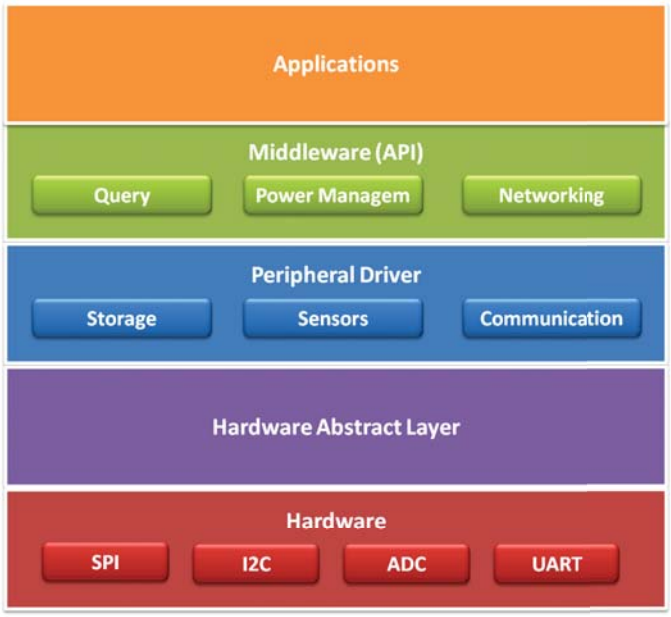

Figure 4.4: The firmware stack in CosNet static sensor node.

4.4.2 Software on Gateway

Applications on Gateway query and manage all the sensor nodes in the network by a set of APIs. The APIs include decoding the commands from the user's application, reporting the errors and abnormalities of the sensor nodes, configuring the sensor nodes and so on.

4.5 A Case Study

In this section, we present a case study of sensor network self-localization using ultrasonic sensor on-board. Sensor networks with ultrasonic ability are applied to the application of moving target tracking [121][122], especially in an indoor environment or the space where the GPS signal is unreliable. Static sensor nodes with the known coordinates utilize the embedded ultrasonic transceiver to measure the distance between the single sensor node and the target. Then the target can be localized using Trilateration approach [123], given the precise locations of more than three static sensor nodes, and their distances to the target.

However, the coordinates of the static sensor nodes should be calibrated in advance, if the static sensor nodes are not deployed regularly in a grid way. Here we employ a moving

triangular trainer installed on a mobile robot to localize these sensor nodes, which is named sensor node self-localization. Figure 4.5 shows the procedure where a triangular trainer localize the entire sensor networks.

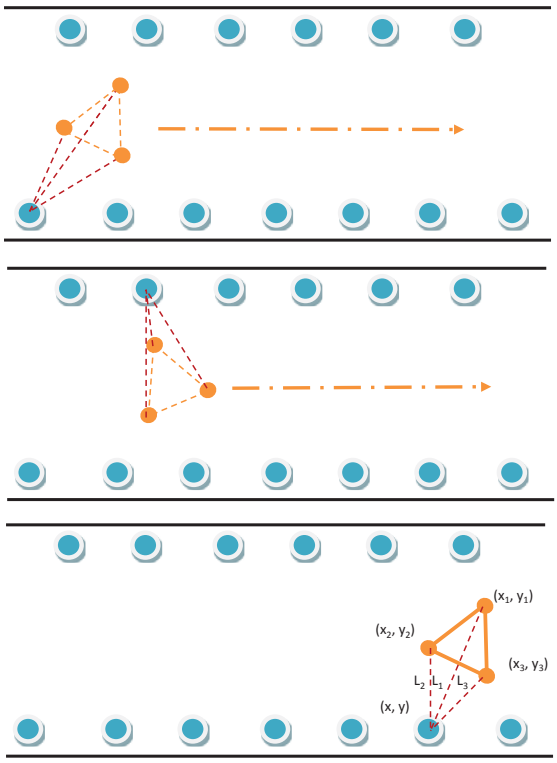

Figure 4.5: Static sensor network self-localization. The Blue nodes are the static sensor nodes deployed in the hallway. The yellow triangular trainer is traversing the entire network. The sensor node measures the distances to the trainer while it is passing by.

It is assumed the mobile triangular trainer integrates an encoder such that it can obtain its realtime location, the location of the static sensor node can also be inferred by the triangular trainer using Trilateration. Suppose the locations of three vertices are (x_1, y_1), (x_2, y_2) and (x_3, y_3). If the distances to one sensor node measured by the ultrasonic transceiver are L_1, L_2 and L_3, the coordinate of one node denoted as (x, y) can be derived as follows:

$$\begin{aligned}(x_1 - x)^2 + (y_1 - y)^2 &= L_1^2 \\ (x_2 - x)^2 + (y_2 - y)^2 &= L_2^2 \\ (x_3 - x)^2 + (y_3 - y)^2 &= L_3^2.\end{aligned} \tag{4.1}$$

If we subtract the first two equations from the last equation, we can obtain a set of linear equations related to x and y.

$$\begin{aligned} 2(x_3-x_1)x+2(y_3-y_1)y &= x_3^2-x_1^2+y3^2-y_1^2-L_3^2+L_1^2 \\ 2(x_3-x_2)x+2(y_3-y_2)y &= x_3^2-x_2^2+y3^2-y_2^2-L_3^2+L_2^2. \end{aligned} \tag{4.2}$$

Convert Equation 4.5 to be a standard matrix form $Au = \beta$. Denote

$$\begin{aligned} A &= \begin{pmatrix} 2(x_3-x_1)x & 2(y_3-y_1)y \\ 2(x_3-x_2)x & 2(y_3-y_2)y \end{pmatrix} \\ \mu &= \begin{pmatrix} x \\ y \end{pmatrix} \\ B &= \begin{pmatrix} x_3^2-x_1^2+y3^2-y_1^2-L_2^2+L_1^2 \\ x_3^2-x_2^2+y3^2-y_2^2-L_3^2+L_2^2 \end{pmatrix}, \end{aligned} \tag{4.3}$$

μ can be written by $\mu = (A^TA)^{-1}A^TB$, which consists the coordinate of one static sensor node.

Figure 4.6 shows the simulation result in the hallway environment. In this simulation setup, the trainer has a triangle with side length 2 feet, and travels through the network with a constant speed of 2 ft/s. The trainer's location is calculated every second, a 5% measurement noise is added to the location computation. The blue triangle is the actual location of the trainer and the red triangle is the calculated trainer position; the circles are the actual sensor location, and the "x"s are the estimated locations of the targets.

4.6 Summary

CosNet is designed for the indoor environment attribute monitoring. The static sensor node arms a suite of sensors including an ultrasonic transceiver, a humidity sensor, a temperature sensor, and a photonic sensor. We develop a prototype of CosNet sensor node, and focus on the minimizing its dimension and energy consumption. The high integration of sensor node leads to a longer life time for a single battery recharge.

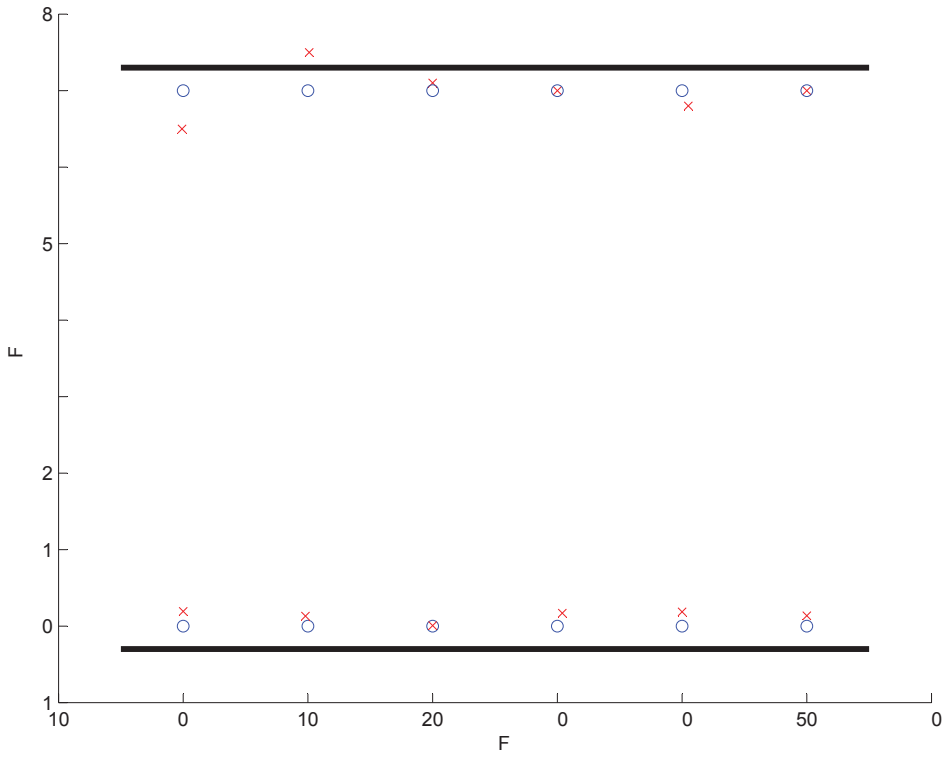

Figure 4.6: The snapshot during the procedure of self-localization.

In this chapter, we introduce the background and motivation of CosNet. Then the related products on the market are compared and we bring up the systematical design of the static sensor node in CosNet. Further, we present the hardware and software design of the static sensor node. Last, a case study is employed to illustrate how CosNet is integrated to the body sensor networks to help localize the subject.

Chapter 5

Conclusions and Future Works

5.1 Conclusion

A BSN designed for in-home personal healthcare named SmartHome is proposed in this dissertation. It contains three subsystems: BioLogger, PAMS, and CosNet. We design their prototypes and apply the proposed algorithms on them. There are two main contributions made to SmartHome.

The first one is the prototype implementation of the wearable sensor networks and the static sensor network: 1) BioLogger is a wearable sensor network for physiological signal monitoring. It aims at monitoring human's physiological signals simultaneously, including ECG, EEG, respiration rate and skin temperature. 2) PAMS is a wearable sensor network designed for inertial signal monitoring. It concentrates on human body's inertial signals, including acceleration, angular rate and magnetic field around human body. The human motion can be inferred by these parameters. 3) The static sensor network is CosNet, a context-aware sensor network for environmental attribute monitoring, which may provide valuable clues for the human's healthcare. To address the challenges discussed in the dissertation, the designs of three types of sensor nodes have the advantages in common. First of all, they detach the sensing unit from the processing unit, and hence the patients or the elders with wearable sensors can be monitored in a free living environment. Moreover, the power efficiency is considered during the hardware and software designs of the wearable sensor node, as the battery-supported device. Therefore, the lifetime of the sensor node can be prolonged into a couple of days, such that the patient's daily life would not be interfered by the battery replacement. Finally, all the sensor nodes are under a stackable structure, which makes it possible to integrate more sensors on the sensor node.

To synthesize the sensing measurements is another contribution. 1) A novel premature contraction classification algorithm is proposed to detect the multiple types of premature contraction. Moreover, the abnormality can be sent to the medical server through an existing telecommunication infrastructure. In the previous works, after the physiological signals are acquired, the analysis and diagnosis are normally performed offline. Fortunately, SmartHome takes the advantage of powerful processing ability of a smartphone, and fulfils the abnormality detection in realtime. Thus, the response time of the emergency will reduce a lot and save more people's lives. 2) We also propose a novel and efficient algorithm of human motion tracking, which can be executed on an embedded devices. It can track the human's gesture in real time rather than activity classification. 3) A static sensor node self localization algorithm is also applied to localize the whole deployed static sensor nodes in CosNet. Meanwhile, the software design make SmartHome open to new healthcare algorithms to rich its application.

5.2 Future Work

The current work can be extended along three axes hardware, software and networking.

5.2.1 Hardware

The sensor node would be minimized further with the release of more integrative IC chips. Up to now, TI released its single solution of complete analog front end chip for ECG/EEG, ADS1298 [124], which reduces components and board size by 95%, reduces solution power by 95%, and increases system reliability and patient mobility. InverSense will publish the world's first and only 9-axis inertial sensor, MPU-9150 [125]. It incorporates one 3-axis gyroscope, one 3-axis accelerometer, one 3-axis digital compass and an onboard Digital Motion Processor (DMP). The on-chip DMP integrates 9-axis MotionFusion algorithms access all internal sensors to gather a full set of sensor data without intervention from the major CPU, which would relief the load of the major CPU on the sensor node. With the latest single-chip solution, the dimension of the sensor node in SmartHome will be greatly slimmed, making them more comfortable when the subject is wearing them. In addition, more and more sensors can be integrated into SmartHome, such that the context-awareness would be more comprehensive.

5.2.2 Software

More efficient and accurate software algorithms will be proposed. First, the sensing data fusion algorithm will benefit from more wearable and static sensor measurements, and will be coordinated with the support of remote database, SmartHome is able to make more accurate diagnosis and has more intelligence. Second, more powerful and efficient middleware will address the query and storage of the sensing data. The SmartHome will provide more valuable information with less power consumption. Last, the graphic user interface will be easier to use and can be implemented on portable devices such as smartphone and tablet.

5.2.3 Networking

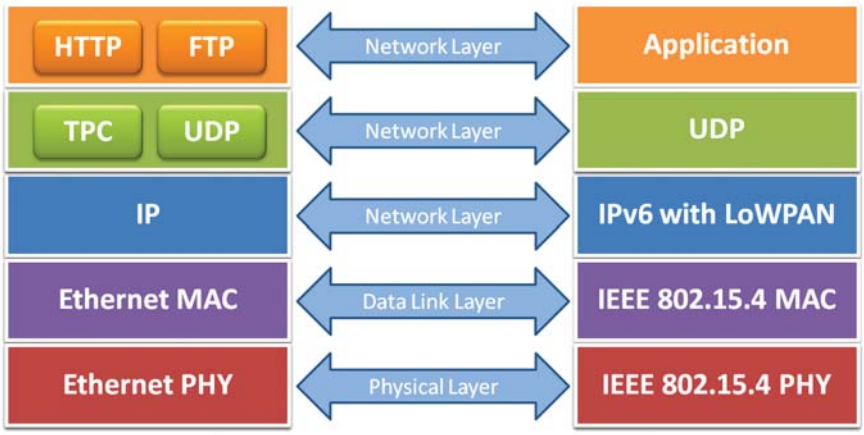

Figure 5.1: The protocol stacks of 6LoWPAN and Ethernet.

As the wireless sensor networks evolve, they represent billions of information devices in the physical world around human beings. Like the web resources on the Internet, the community has proposed a concept "Smart Object" [126] that every wireless sensor node is embedded an IP address. The vision behind that is the road map to merge the isolated wireless sensor networks to be an integral part of the Internet. It has many advantages by associating a sensor node with an IP address. First, Internet is based on TCP/IP protocols. Sensor nodes with an IP address would be easily accessed and connected to the existing the network. Second, established security in IP protocols is able to support the authentication, access control and even firewall mechanism. Third, the wireless sensor networks would benefit naming, discovery, routing and addressing from the existing IP techniques. Last, many networking management tools based on IP have been developed,

such as Ping, Traceroute, SNMP and so on. In summary, the advances of IP based networks in decades would build a solid fundamental for the wireless sensor networks.

6LoWPAN [127] is proposed to address how the wireless sensor nodes are merged to an IP based networks. It enables IP packets carried on the physical layer of low power radio. It solves the incompatibility between the lower level IEEE802.15.4 and current IP protocol and replaces the running short IPv4 address by an IPv6 address. The protocol stack is shown on Figure 5.1. With this technique, the gateway designed to interconnect SmartHome and outside world can be removed, and replaced by any existing hot-spot. In addition, the remote access over Internet will be simple and straightforward for the medicare providers and others.

References

[1] CIA, 2012. [Online]. Available: https://www.cia.gov/library/publications/the-world-factbook/geos/us.html

[2] D. Lloyd-Jones et al., "Heart disease and stroke statistics - 2010 update: a report from the american heart association," *Circulation*, vol. 121, pp. e46–e215, 2010.

[3] T. Dishongh, W. DeLeeuw, and M. Francis, "Adapting technology for personal healthcare," *Intel Technology Journal*, vol. 13, no. 3, pp. 40–57, 2009.

[4] Centers for Medicare And Medicaid Services, 2008. [Online]. Available: NationalHealthExpenditures2008Highlights

[5] US Census Bureau, 2008. [Online]. Available: http://www.census.gov/main/www/cen2000.html

[6] G. Yang, *Body Sensor Networks*. New York, USA: Springer Press, 2006.

[7] M. Kaku, *Visions: How Science Will Revolutionize the Twenty-First Century*. Oxford, UK: Oxford University Press, 1999.

[8] E. Braunwald, *Braunwald's Heart Disease: A Textbook of Cardiovascular Medicine*. philadelphia, USA: W.B. Saunders Co, 2012.

[9] X. Chen, S. Hu, Z. Shao, and J. Tan, "Pedestrian positioning with physical activity classification for indoors," in *Proc. of IEEE Intl. Conf. on Robotics and Automation*, Shang Hai, China, 2011, pp. 1311–1316.

[10] S. Hu, Z. Shao, and J. Tan, "A real-time cardiac arrhythmia classification system with wearable electrocardiogram," in *Proc. of IEEE Intl. Conf. on Body Sensor Networks*, Dallas, USA, 2011, pp. 119–124.

[11] S. Hu, X. Chen, and J. Tan, "Pams: A wearable physical activity monitoring system for continuous motion capture in free-living environments," in *Proc. of IEEE Intl. Conf. on Body Area Networks*, Corfu Island, Greece, 2010, pp. 233–239.

[12] S. Hu and J. Tan, "Biologger: A wireless physiological sensing and logging system with applications in poultry science," in *Proc. of IEEE Intl. Conf. of the IEEE Engineering in Medicine and Biology Society*, Minneapolis, USA, 2009, pp. 4828–4831.

[13] ——, "Biologger: A wireless physiological monitoring and logging system," in *Proc. of IEEE Intl. Conf. on Information Processing in Sensor Networks*, San Francisco, USA, 2009, pp. 383–384.

[14] J. He, S. Hu, and J. Tan, "Layered hidden markov models for real-time daily activity monitoring using body sensor networks," in *Proc. of IEEE Intl. Summer School and Symposium on Medical Devices and Biosensors*, Hong Kong, China, 2008, pp. 326–329.

[15] S. Hu and J. Tan, "Compressive mobile sensing for robotic mapping," in *Proc. of IEEE Intl. Conf. on Automation Science and Engineering*, Arlington, USA, 2008, pp. 139–144.

[16] R. Wong, S. Hu, Cabrera-Mora, J. Xiao, and J. Tan, "A distributed algorithm for mobile robot localization and mapping in wireless sensor networks," in *Proc. of IEEE Intl. Conf. on Information and Automation*, Changsha, China, 2008, pp. 560–566.

[17] Organisation for Economic Co-operation and Development, "Oecd health data 2011," 2011.

[18] C. Otto, A. Milenkovic, C. Sanders, and E. Jovanov, "System architectures of a wireless body area sensor network for ubiquitous health monitoring," *J. of Mobile Multimedia*, vol. 1, no. 4, pp. 307–326, Jan. 2006.

[19] S. N. C. Po, G. Dagang, M. D. B. M. Hapipi, and F. T. E. Hock, "Memswear biomonitoring incorporating sensors into smart shirt for wireless sentinel medical detection and alarm," *J. Phys.: Conf. Ser.*, vol. 34, pp. 1068–1072, 2006.

[20] D. Malan, T. Fulford-Jones, M. Welsh, and S. Moulton, "Codeblue: An ad hoc sensor network infrastructure for emergency medical care," in *Proc. of Intl. Workshop on Wearable and Implantable Body Sensor Networks*, London, United Kingdom, Jun. 2004, pp. 12–14.

[21] T. R. F. F. Jones, G. Y. Wei, and M. Welsh, "A portable, low-power, wireless two-lead ekg system," *The 26th Annual Intl. IEEE EMBS Conference*, vol. 1, no. 1, pp. 2141–2144, Sep. 2004.

[22] B. Liu, Y. Zhang, Z. Liu, and C. Yin, "An Embedded EEG Analyzing System Based on μ C/os-II," *Proc. of IEEE Intl. Conf. of the IEEE Engineering in Medicine and Biology Society*, pp. 2468–2471, Aug. 2007.

[23] B. Winter and J. G. Webster, "Driven-right-leg circuit design," *IEEE Trans. on Biomedical Engineering*, vol. 30, no. 1, pp. 62–66, Jan. 1983.

[24] AAMI, "American national standard for cardiac monitors, heart rate meters, and alarms. ansi/aami ec13:2002/(r)2007," Association for the Advancement of Medical Instrumentation, Tech. Rep., 2007.

[25] A. Vahed, "3-Lead Wireless ECG," 2009. [Online]. Available: http://www.open-ecg-project.org/tiki-index.php?page=3-Lead+Wireless+ECG

[26] A. Savitzky and M. Golay, "Smoothing and differentiation of data by simplified least squares procedures," *Analytical Chemistry*, vol. 36, no. 8, pp. 1627–1639, Jul. 1964.

[27] Laurence M. Hirshberg et al., 2004. [Online]. Available: http://www.neurodevelopmentcenter.com/index.php?id=39

[28] A. Aldenkamp and J. Arends, "The relative influence of epileptic eeg discharges, short nonconvulsive seizures, and type of epilepsy on cognitive function," *Epilepsia*, vol. 45, no. 1, pp. 54–63, Jan. 2004.

[29] K. Vijayalakshmi, S. Sridhar, and P. Khanwani, "Estimation of effects of alpha music on eeg components by time and frequency domain analysis," in *Proc. of Intl. Conf. on Computer and Communication Engineering*, Kuala Lumpur, Malaysia, May 2010, pp. 1–5.

[30] H. Moldofsky and F. Lue, "The relationship of alpha and delta eeg frequencies to pain and mood in fibrositis patients treated with chlorpromazine and l-tryptophan," *Electroencephalography and Clinical Neurophysiology*, vol. 50, no. 1-2, pp. 71–80, Oct. 1980.

[31] E. Smith, 2012. [Online]. Available: http://www.ebme.co.uk/arts/eegintro/index.htm

[32] Cambrige Electronic Design, 2012. [Online]. Available: http://www.ced.co.uk/pru.shtml

[33] Measurement Specialties Inc., "Piezo film sensors technical manual," Measurement Specialties Inc., Tech. Rep., 1999.

[34] *Piezo Film Sensors Technical Manual*, Rev-B ed., Measurement Specialties, Inc., Apr 1999.

[35] W. D. McArdle, F. I. Katch, and V. L. Katch, *Exercise Physiology: Energy, Nutrition, and Human Physiology*. Lippincott Williams & Wilkins, 2006.

[36] P. Lyons and P. Waterw, "The use of ntc thermistors as sensing devices for tec controllers and temperature control integrated circuits," Betatherm Ireland Ltd., Tech. Rep., 2003.

[37] Y. Ephraim and N. Merhav, "Hidden markov processes," *IEEE Trans. on Information Theory*, vol. 48, no. 6, pp. 1518–1569, Jun. 2002.

[38] P. de Chazal, M. O'Dwyer, and R. Reilly, "Automatic classification of heartbeats using ecg morphology and heartbeat interval features," *IEEE Trans. on Biomedical Engineering*, vol. 51, no. 7, pp. 1196–1206, Jul. 2004.

[39] O. Inan, L. Giovangrandi, and G. Kovacs, "Robust neural-network-based classification of premature ventricular contractions using wavelet transform and timing interval features," *IEEE Trans. on Biomedical Engineering*, vol. 53, no. 12, pp. 2507–2515, Dec. 2006.

[40] T. Ince, S. Kiranyaz, and M. Gabbouj, "Automated patient-specific classification of premature ventricular contractions," in *The 30th Annual Ixnternational IEEE EMBS Conference*, Aug. 2008, pp. 5474–5477.

[41] L. Welch, "Hidden markov models and the baum welch algorithm," *IEEE Information Theory Society Newsletter*, vol. 53, no. 4, pp. 10–13, Dec. 2003.

[42] G. Moody, R. Mark, and A. Goldberger, "Physionet: a web-based resource for the study of physiologic signals," *IEEE Engineering in Medicine and Biology Magazine*, vol. 20, no. 3, pp. 70–75, May-Jun. 2001.

[43] MIT, "Mit-bih arrhythmia database." [Online]. Available: http://www.physionet.org/physiobank/database/mitdb/

[44] M. Atzmueller, J. Baumeister, and F. Puppe, "Semi-automatic learning of simple diagnostic scores utilizing complexity measures," *Artificial Intelligence in Medicine*, vol. 37, no. 1, pp. 19–30, May 2006.

[45] O. Inan, L. Giovangrandi, and G. Kovacs, "Robust neural-network-based classification of premature ventricular contractions using wavelet transform and timing interval features," *IEEE Trans. on Biomedical Engineering*, vol. 53, no. 12, pp. 2507–2515, Dec. 2006.

[46] G. Moody and R. Mark, "Development and evaluation of a 2-lead ecg analysis program," in *Proc. of Computers in Cardiology*, Seattle, USA, Sep. 1982, pp. 39–44.

[47] P. de Chazal, M. O'Dwyer, and R. Reilly, "Automatic classification of heartbeats using ecg morphology and heartbeat interval features," *IEEE Trans. on Biomedical Engineering*, vol. 51, no. 7, pp. 1196–1206, Jul 2004.

[48] L.-Y. Shyu, Y.-H. Wu, and W. Hu, "Using wavelet transform and fuzzy neural network for vpc detection from the holter ecg," *IEEE Trans. on Biomedical Engineering*, vol. 51, no. 7, pp. 1269–1273, Jul. 2004.

[49] I. Christov, I. Jekova, and G. Bortolan, "Premature ventricular contraction classification by the kth nearest-neighbours rule," *Physiological measurement*, vol. 26, pp. 123–130, Jan. 2005.

[50] F. Melgani and Y. Bazi, "Detecting premature ventricular contractions in ecg signals with gaussian processes," in *Proc. of Computers in Cardiology*, Bologna, Italy, Sep. 2008, pp. 237–240.

[51] D. Noonan, P. Mountney, D. Elson, A. Darzi, and G. Yang, "A stereoscopic fibroscope for camera motion and 3d depth recovery during minimally invasive surgery," in *Proc. of IEEE Intl. Conf. on Robotics and Automation*, Kobe, Japan, May 2009, pp. 4463–4468.

[52] E.-J. Marey, *La machine animale*. G. Baillie Paris, 1873.

[53] R. B. D. III, S. *Õ*npuu, D. Tyburski, and J. R. Gage, "A gait analysis data collection and reduction technique," *Human Movement Science*, vol. 10, no. 5, pp. 575–587, Oct. 1991.

[54] H. Zhou and H. Hu, "A survey of huuman movement tracking and stroke rehabilitation," Department of Computer Science, University of Essex, Tech. Rep. CSM-420, 2004.

[55] H. Sveistrup, "Motor rehabilitation using virtual reality," *J. of NeuroEngineering and Rehabilitation*, vol. 1, no. 1, p. 10, Dec. 2004.

[56] C. Tercero et al., "Autonomous catheter insertion system using magnetic motion capture sensor for endovascular surgery," *Intl. J. of Medical Robotics and Computer Assisted Surgery*, vol. 3, no. 1, pp. 52–58, Mar. 2007.

[57] K. Kinga, S. Yoonb, N. Perkinsa, and K. Najafib, "Wireless mems inertial sensor system for golf swing dynamics," *Sensors and Actuators A: Physical*, vol. 141, no. 2, pp. 619–630, Feb. 2008.

[58] H. Nunome, T. Asai, Y. Ikegami, and S. Sakurai, "Three-dimensional kinetic analysis of side-foot and instep soccer kicks," *Medicine & Science in Sports & Exercise*, vol. 24, no. 12, pp. 2028–2036, Dec. 2002.

[59] E. A. Suma, B. Lange, S. Rizzo, and D. K. andMark Bolas, "Faast: The flexible action and articulated skeleton toolkit," in *IEEE Virtual Reality Conf.*, Singapore, Mar. 2011, pp. 245–246.

[60] G. B. Guerra-filho, "Optical motion capture: Theory and implementation," *Journal of Theoretical and Applied Informatics (RITA)*, vol. 12, no. 2, pp. 61–89, 2005.

[61] T. B. Moeslund and E. Granum, "A survey of computer vision-based human motion capture," *Computer Vision and Image Understanding*, vol. 81, no. 3, pp. 231–268, Mar. 2001.

[62] XSens, 2012. [Online]. Available: http://www.xsens.com/en/general/products-all

[63] Shin Yabukami et al., "Motion capture system of magnetic markers using three-axial magnetic field sensor," *IEEE Trans. on Magnetics Mag*, vol. 36, no. 5, pp. 3646–3648, Sep. 2000.

[64] G. Welch and E. Foxlin, "Motion tracking: no silver bullet, but a respectable arsenal," *IEEE Computer Graphics and Applications*, vol. 22, no. 6, pp. 24–38, Nov.-Dec. 2002.

[65] C. Langmaid and P. Devon, "Vibrating structure gyroscopes," *Sensor Review*, vol. 16, no. 1, pp. 14–17, 1996.

[66] E. F. Taylor and J. A. Wheeler, *Spacetime Physics*. W. H. Freeman and Company, 1992.

[67] H. Zumbahlen, "Basic linear design," Analog Devices, Tech. Rep., 2007.

[68] M. Clifford and L. Gomez, "Measuring tilt with low-g accelerometers," Freescale Semiconductor, Tech. Rep., 2005.

[69] H. Emmerich and M. Schofthaler, "Magnetic field measurements with a novel surface micromachined magnetic-field sensor," *IEEE Trans. on Electron Devices*, vol. 47, no. 5, pp. 972–977, 2000.

[70] *COMPASS HEADING USING MAGNETOMETERS*, Honeywell, 1995.

[71] J. Checkelsky, "Anisotropic magnetoresistance of $fe_xco_{1-x}s_2$," Harvey Mudd College, Tech. Rep., 2004.

[72] Intersense, 2012. [Online]. Available: http://www.intersense.com/pages/18/59/

[73] XSens, 2012. [Online]. Available: http://www.xsens.com/en/mtw

[74] Trivisio, 2012. [Online]. Available: http://trivisio.com/index.php/products/motiontracking/colibriwireless

[75] Vicon, 2012. [Online]. Available: http://www.vicon.com

[76] Optotrak Certus, 2012. [Online]. Available: http://www.ndigital.com/optotrak-techspecs.php

[77] M. Kusserow, O. Amft, and G. Toster, "Bodyant: Miniature wireless sensors for naturalistic monitoring of daily activity," in *Proc. of IEEE Intl. Conf. on Body Area Networks*, Los Angeles, USA, Apr. 2009, pp. 1–8.

[78] J. Polastre, R. Szewczyk, and D. Culler, "Telos: Enabling ultra-low power wireless research," in *Intl. Sym. on Information Processing in Sensor Networks*, Los Angeles, USA, Apr. 2005, p. 48.

[79] A. Barth, M. Hanson, H. Powell, and J. Lach, "Tempo 3.1: A body area sensor network platform for continuous movement assessment," in *Proc. of Intl. Workshop on Wearable and Implantable Body Sensor Networks*, Berkeley, USA, Jun. 2009, pp. 71–76.

[80] Konrad Lorincz et al., "Mercury: A wearable sensor network platform for high-fidelity motion analysis," in *Proc. of ACM Conf. on Embedded Networked Sensor Systems*, Berkeley, USA, Nov. 2009, pp. 183–196.

[81] Karol O'Donovan et al., "Shimmer: A new tool for temporal gait analysis," in *Proc. of IEEE Intl. Conf. of the IEEE Engineering in Medicine and Biology Society*, Minneapolis, USA, Sep. 2009, pp. 3826–3829.

[82] B. Priyantha, D. Lymberopoulos, and J. Liu, "Little rock: Enabling energy efficient continuous sensing on mobile phones," *IEEE Pervasive Computing*, vol. 10, no. 2, pp. 12–15, Apr.-Jun. 2010.

[83] J. Polastre, J. Hill, and D. Culler, "Versatile low power media access for wireless sensor networks," in *Proc. of Intl. Conf. on Embedded Networked Sensor Systems*, Baltimore, USA, 2004, pp. 95–107.

[84] H. Li and J. Tan, "Heartbeat-driven medium-access control for body sensor networks," *IEEE Trans. on Information Technology in Biomedicine*, vol. 14, no. 1, pp. 44–51, Jan. 2010.

[85] I. Rhee, A. Warrier, M. Aia, J. Min, and M. L.Sichitiu, "Z-mac: a hybrid mac for wireless sensor networks," *IEEE/ACM Trans. on Networking*, vol. 16, no. 3, pp. 511–524, Jun. 2008.

[86] Kwang Yong Lim et al., "A wearable, self-calibrating, wireless sensor network for body motion processing," in *Proc. of IEEE Intl. Conf. on Robotics and Automation*, Pasadena, USA, 2008, pp. 1017–1022.

[87] A. D. Young, "Comparison of orientation filter algorithms for realtime wireless inertial posture tracking," in *Proc. of Intl. Workshop on Wearable and Implantable Body Sensor Networks*, Berkeley, USA, Jun. 2009, pp. 59–64.

[88] J. B. Kuipers, *Quaternions and Rotation Sequences*. Princeton, USA: Princeton University Press, 2002.

[89] E. Hewitt and K. R. Stromberg, *Real and Abstract Analysis: A Modern Treatment of the Theory of Functions of a Real Variable*. New York, USA: Springer, 1965.

[90] E. R. Bachmann, "Inertial and magnetic tracking of limb segment orientation for inserting humans into synthetic environments," Ph.D. dissertation, Naval Postgraduate School, 2000.

[91] X. Yun, E. R. Bachmann, and R. B. McGhee, "A simplified quaternion-based algorithm for orientation estimation from earth gravity and magnetic field measurements," *IEEE Trans. on Instrumentation and Measurement*, vol. 57, no. 3, pp. 638–650, Mar. 2008.

[92] J. Gao, P. Webb, and N. Gindy, "Error reduction for an inertial-sensor-based dynamic parallel kinematic machine positioning system," *Measurement Science and Technology*, vol. 14, no. 5, pp. 543–550, Mar. 2003.

[93] X. Yun and E. R. Bachmann, "Design, implementation, and experimental results of a quaternion-based kalman filter for human body motion tracking," *IEEE Trans. on Robotics*, vol. 22, no. 6, pp. 1216–1227, Dec. 2006.

[94] E. Bachmann, I. Duman, U. Usta, R. McGhee, X. Yun, and M. Zyda, "Orientation tracking for humans and robots using inertial sensors," in *IEEE Intl. Sym. on Computational Intelligence in Robotics and Automation*, Monterey, USA, 1999, pp. 187–194.

[95] R. Zhu and Z. Zhou, "A real-time articulated human motion tracking using tri-axis inertial/magnetic sensors package," *IEEE Trans. on Neural Systems and Rehabilitation Engineering*, vol. 12, no. 2, pp. 295–302, Jun. 2004.

[96] H. Zhou and H. Hu, "Inertial sensor for motion detection of human upper limbs," *Sensor Review*, vol. 27, no. 2, pp. 151–158, Apr.-Jun. 2007.

[97] M. Mathie, B. Celler, N. Lovell, and A. F.Coster, "Classification of basic daily movements using a triaxial accelerometer," *Medical and Biological Engineering and Computing*, vol. 42, no. 5, pp. 679–687, 2004.

[98] D. Karantonis, M. Narayanan, M. Mathie, N. Lovell, and B. Celler, "Implementation of a real-time human movement classifier using a triaxial accelrometer for ambulatory monitoing," *IEEE Trans. on Information Technology in Biomedicine*, vol. 10, no. 1, pp. 156–167, Jan. 2006.

[99] T. Burchfield and S. Venkatesan, "Accelerometer-based human abnormal movement detection in wireless sesor networks," in *Proc. of Intl. Workshop on Systems and Networking Support for Healthcare and Assisted Living Environments*, San Juan, Puerto Rico, Jun. 2007, pp. 67–69.

[100] J. He, H. Li, and J. Tan, "Real-time daily activity classification with wireless sensor networks using hidden markov model," in *Proc. of IEEE Intl. Conf. of the IEEE Engineering in Medicine and Biology Society*, Shanghai, China, Aug. 2007, pp. 3192–3195.

[101] M. Piccardi and O. Perez, "Hidden markov models with kernel density estimation of emission probabilities and their use in activity recognition," in *Proc. of IEEE Intl. Conf. on Computer Vision and Pattern Recognition*, Minneapolis, USA, Jun. 2007, pp. 1–8.

[102] J. Chen, K. Kwong, D. Chang, J. Luk, and R. Bajcsy, "Wearable sensors for reliable fall detection," in *Proc. of IEEE Intl. Conf. of the IEEE Engineering in Medicine and Biology Society*, Shanghai, China, Sep. 2005, pp. 3551–3554.

[103] O. Jenkins, M. Kallmann, and M. Mararic, "Motion capture from inertial sensing for untethered humanoid teleoperation," in *Proc. of IEEE/RAS Intl. Conf. on Humanoid Robots*, Los Angeles, USA, Nov 2004, pp. 547–565.

[104] J. Corrales, F. Candelas, and F. Torres, "Hybrid tracking of human operators using imu/uwb data fusion by a kalman filter," in *Proc. of IEEE/ACM Intl. Conf. on Human Robot Interaction*, Amsterdam, Netherlands, Mar. 2008, pp. 193–200.

[105] L. Ojeda and J. Borenstein, "Personal dead-reckoning system for gps-denied environments," in *IEEE Intl. Workshop on Safety, Security and Rescue Robotics*, Rome, Italy, Sep. 2007, pp. 1–6.

[106] A. K. Dey, D. Salber, G. D. Abowd, and M. Futakawa, "The conference assistant: Combining context-awareness with wearable computing," in *Intl. Sym. on Wearable Computers*, San Francisco, USA, 1999, pp. 21–28.

[107] K. V. Laerhoven, K. Aidoo, and S. Lowette, "Real-time analysis of data from many sensors with neural networks," in *Intl. Sym. on Wearable Computers*, Zurich, Switzerland, 2001, pp. 115–122.

[108] T. Arampatzis, J. Lygeros, and S. Manesis, "A survey of applications of wireless sensors and wireless sensor networks," in *Proc. of IEEE Intl. Sym. on Intelligent Control*, Limassol, Cyprus, Jun. 2005, pp. 719–724.

[109] CITRIS, "Brainy buildings conserve energy," *Bewrkeley Engineering*, vol. 1, no. 1, Jul. 2001.

[110] M. C. Kintner-Meyer and M. Brambley, "Pros & cons of wireless," *ASHRAE Journal*, vol. 44, no. 11, pp. 54–61, Nov 2002.

[111] Q. Ling, Z. Tian, and Y. Li, "Distributed decision-making in wireless sensor networks for online structural health monitoring," *Journal of Communications and Networks*, vol. 11, no. 4, pp. 350–358, Aug. 2009.

[112] Q. Ling, Z. Tian, Y. Yin, and Y. Li, "Localized structural health monitoring using energy-efficient wireless sensor networks," *IEEE Sensors Journal*, vol. 9, no. 11, pp. 1596–1604, Nov. 2009.

[113] A. Rytter, "Vibration based inspection of civil engineering structures," Ph.D. dissertation, Dept. of Building Technology and Structural Engineering, Aalborg University, 1993.

[114] Crossbow, 2012. [Online]. Available: http://bullseye.xbow.com:81/index.aspx

[115] D. Weinberg and J. Zhang, "Sensor wireless network final report," Dept. of ECE, Univ. of Massachusetts, Lowell, Tech. Rep., 2012.

[116] Oracle, 2012. [Online]. Available: http://www.sunspotworld.com

[117] Shimmer Research, 2012. [Online]. Available: http://www.shimmer-research.com

[118] Texas Instruments, 2012. [Online]. Available: http://www.ti.com/product/msp430f2618

[119] *ZMN2430: ZigBee Transceiver Module*, y RF Monolithics, Inc, May 2008.

[120] A. Wood and et al, "Alarm-net: Wireless sensor networks for assisted-living and residential monitoring," Department of Computer Science, University of Virginia, Tech. Rep. CS-2006-13, 2006.

[121] S.-H. Park, Y.-H. Choi, S.-H. Baek, T.-K. Lee, and S.-Y. Oh, "Feature localization using neural networks for cleaning robots with ultrasonic sensors," in *Proc. of Intl. Conf. on Control, Automation and Systems*, Seoul, Korea, Oct. 2007, pp. 449–453.

[122] W. Xiao, J. K. Wu, L. Shue, Y. Li, and L. Xie, "A prototype ultrasonic sensor network for tracking of moving targets," in *Proc. of IEEE Conf. on Industrial Electronics and Applications*, Singapore, May 2006, pp. 1–6.

[123] D. Manolakis, "Efficient solution and performance analysis of 3-d position estimation by trilateration," *IEEE Trans. on Aerospace and Electronic Systems*, vol. 32, no. 4, pp. 1239–1248, Oct. 1996.

[124] Texas Instruments, 2010. [Online]. Available: http://www.ti.com/product/ads1298

[125] InvenSense, 2012. [Online]. Available: http://invensense.com/mems/gyro/mpu9150.html

[126] J. Hui, 2010. [Online]. Available: http://www.cs.berkeley.edu/~jwhui/6lowpan.html

[127] J. Hui and D. Culler, "Ipv6 in low-power wireless networks," *Proc. of the IEEE*, vol. 98, no. 11, pp. 1865–1878, Nov. 2010.

Appendix A

Hardware Design of BioLogger Wearable Sensor Node

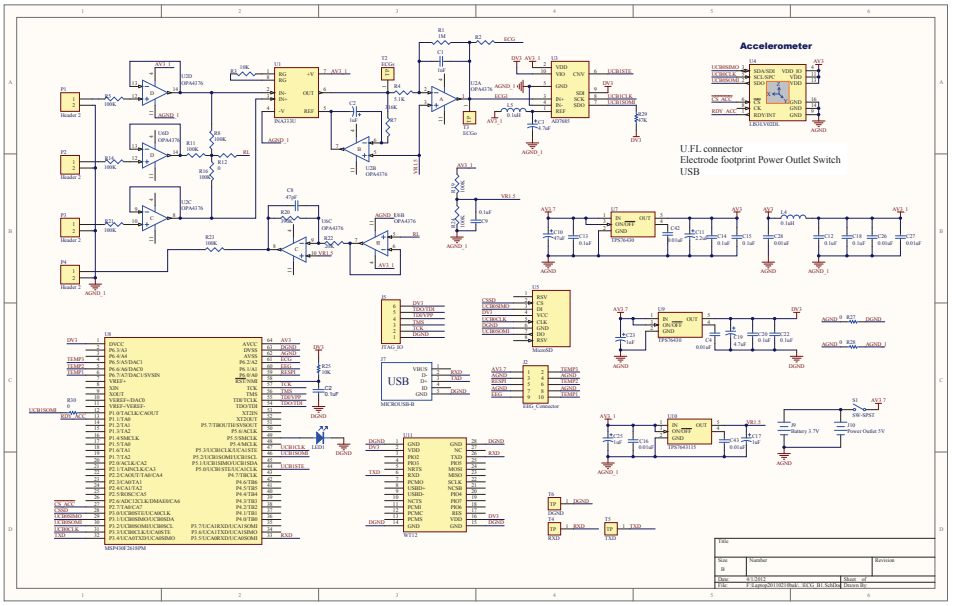

Figure A.1: Schematic design:Part 1.

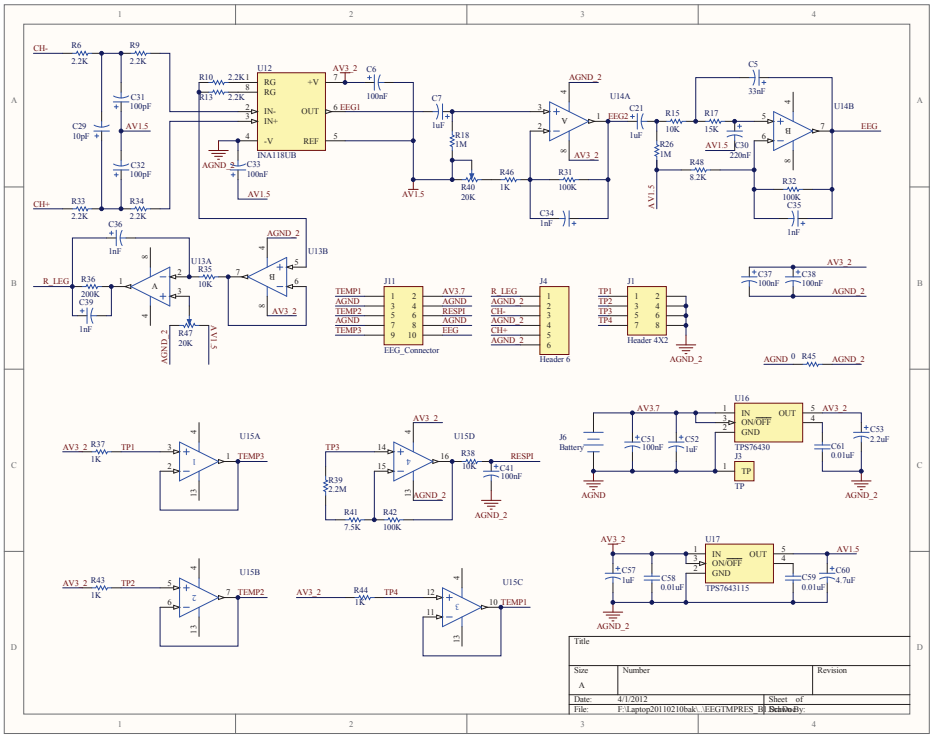

Figure A.2: Schematic design:Part 2.

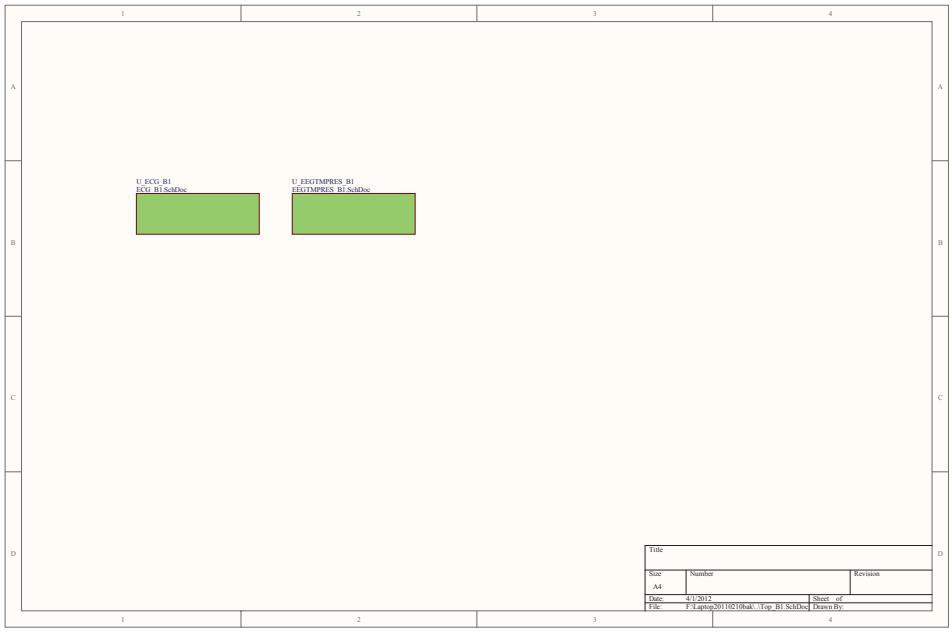

Figure A.3: Schematic design:Part 3.

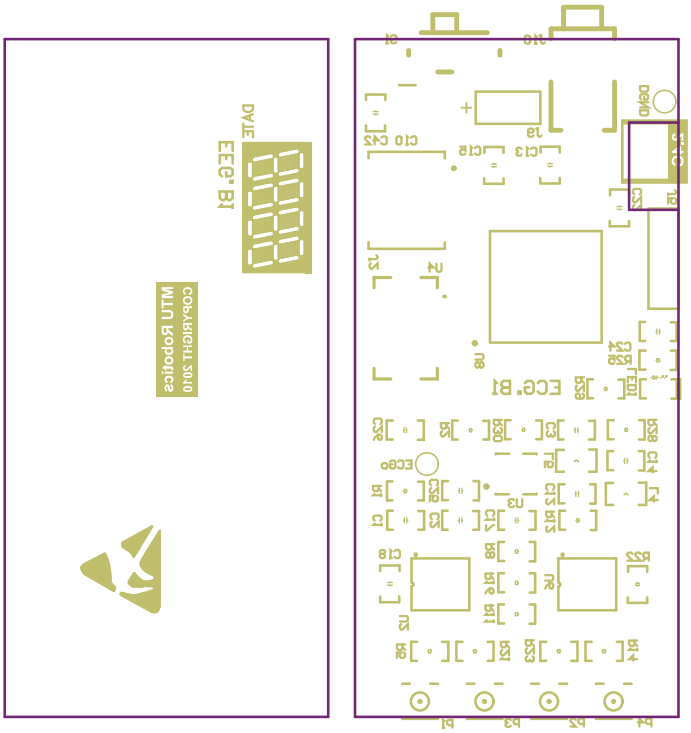

Figure A.4: PCB design:Bottom overlay.

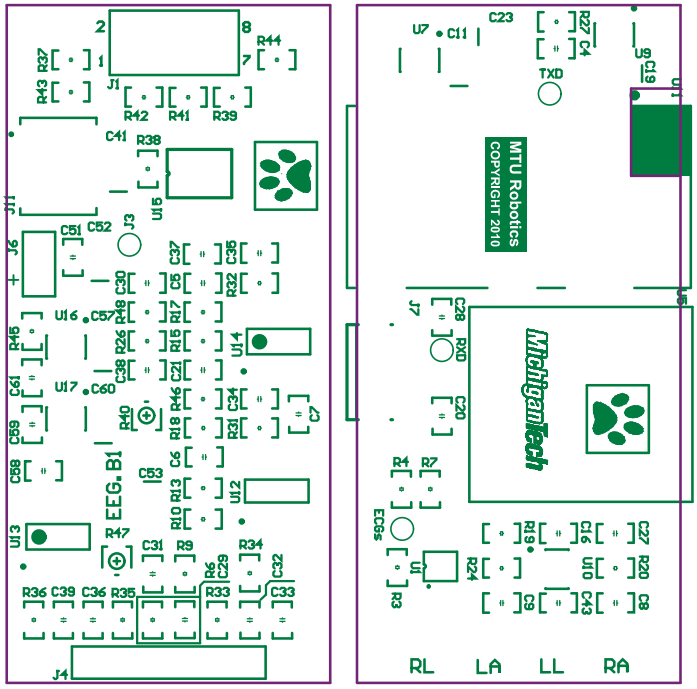

Figure A.5: PCB design:Top overlay.

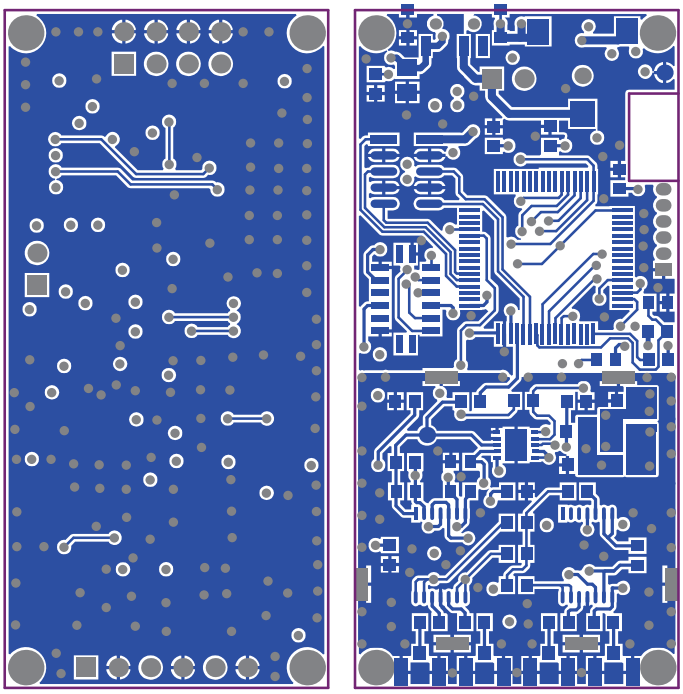

Figure A.6: PCB design: Bottom layer.

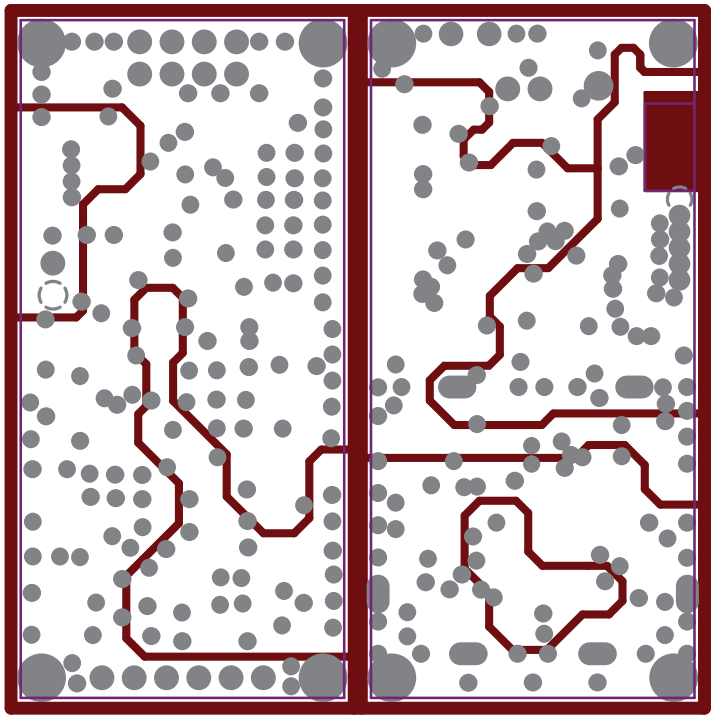

Figure A.7: PCB design: Power plane.

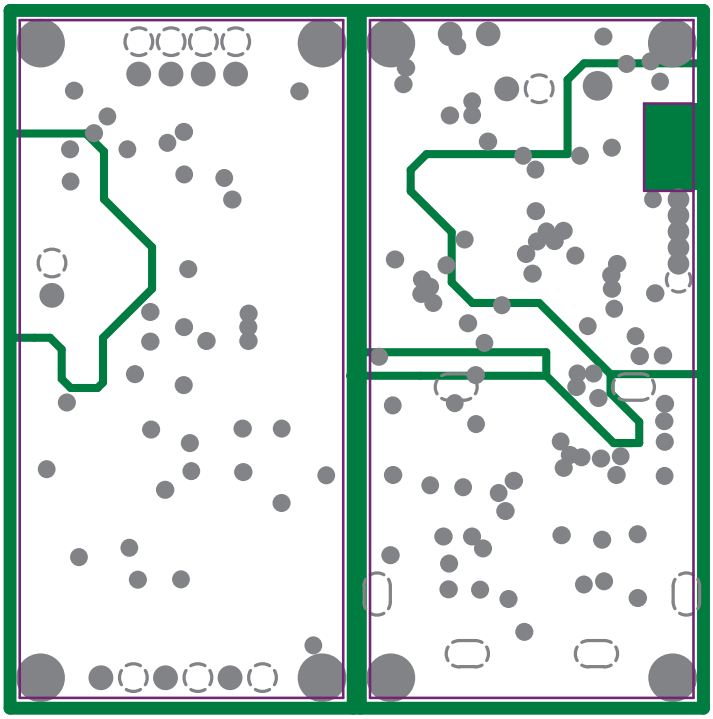

Figure A.8: PCB design: Ground plane.

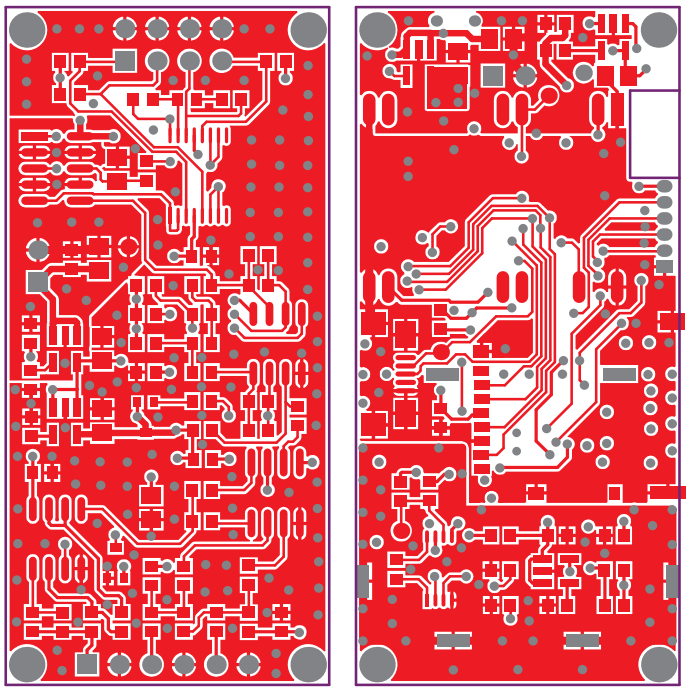

Figure A.9: PCB design: Top layer.

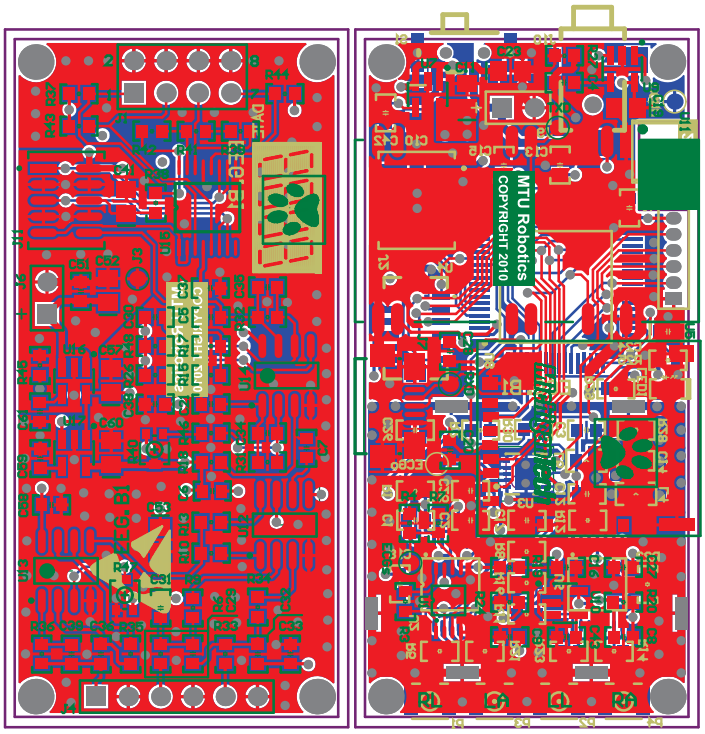

Figure A.10: PCB design: Multiple layers.

Appendix B

Hardware Design of PAMS Wearable Sensor Node

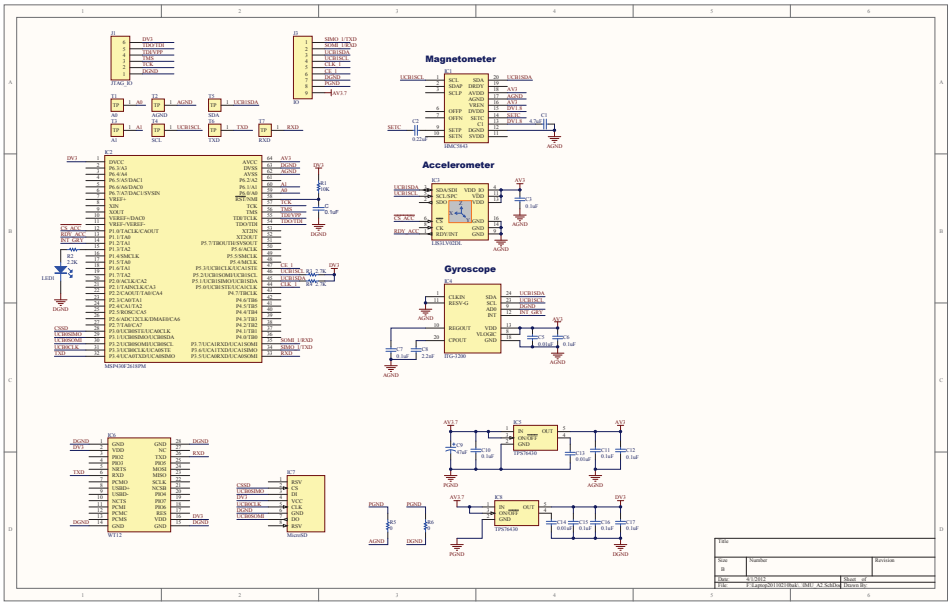

Figure B.1: Schematic design.

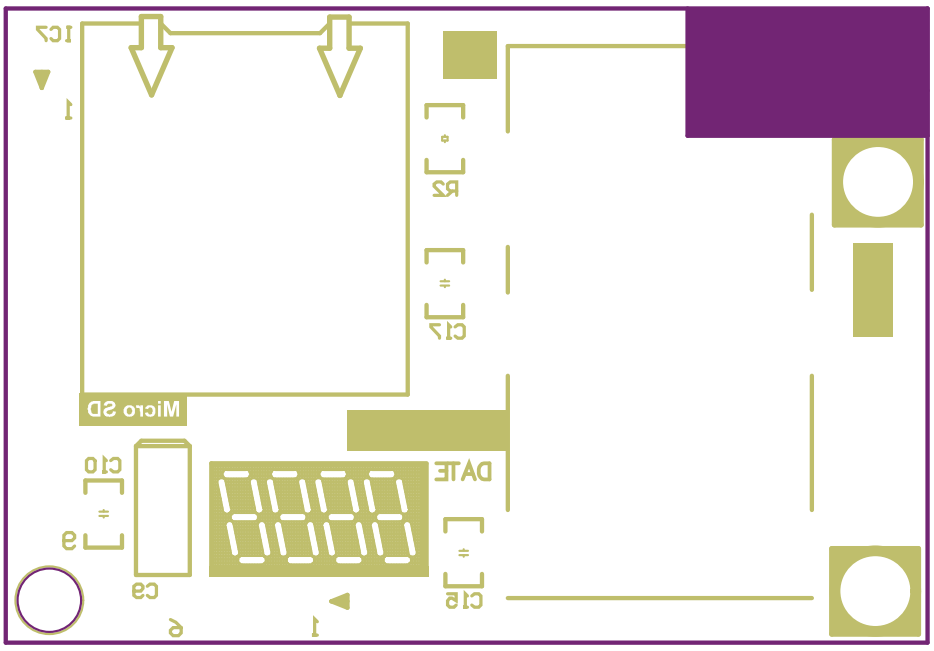

Figure B.2: PCB design:Bottom overlay.

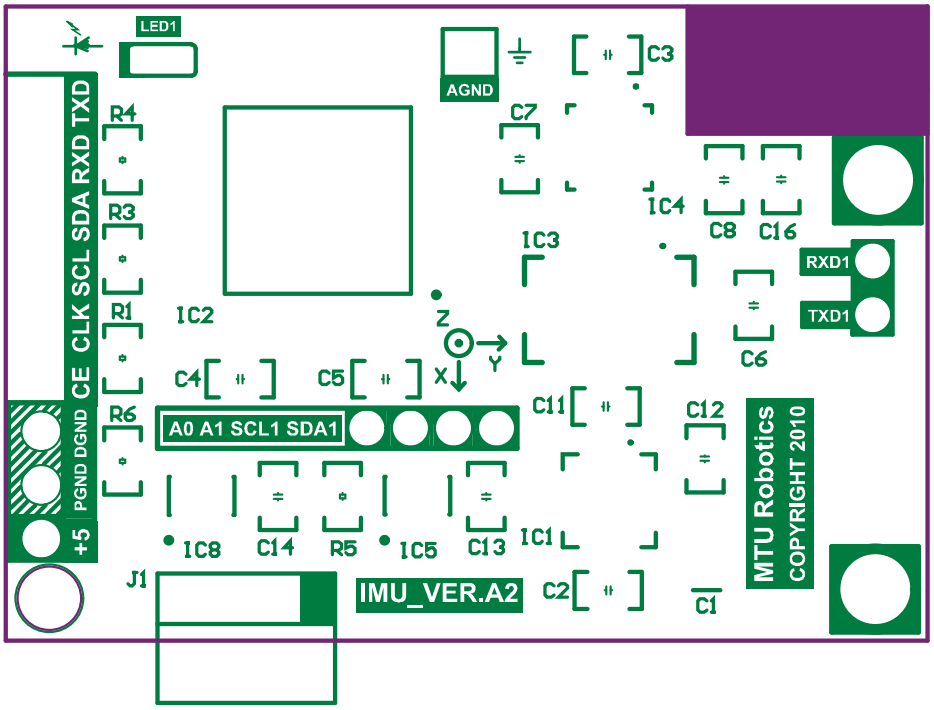

Figure B.3: PCB design:Top overlay.

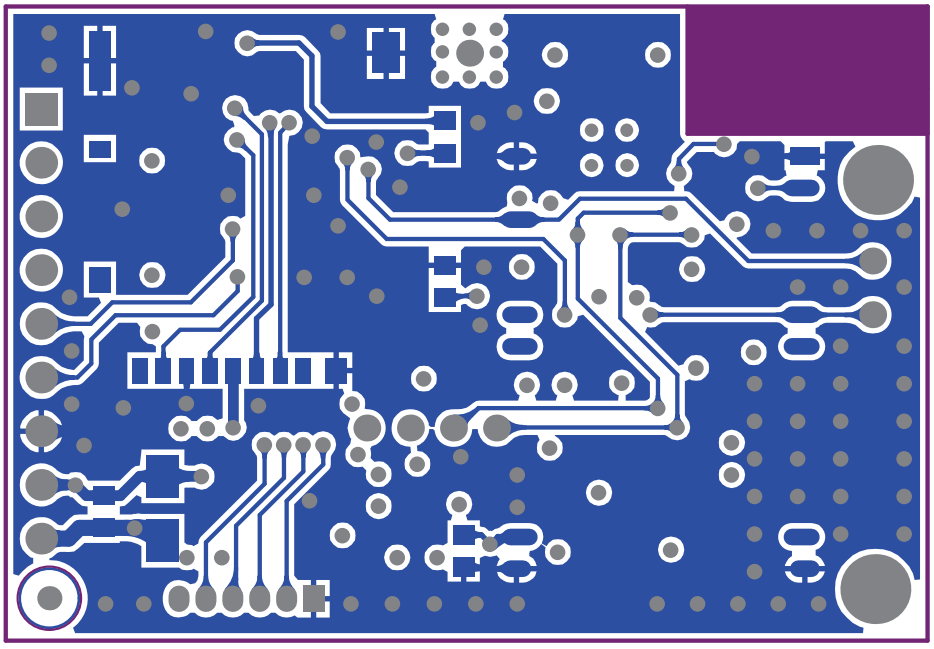

Figure B.4: PCB design: Bottom layer.

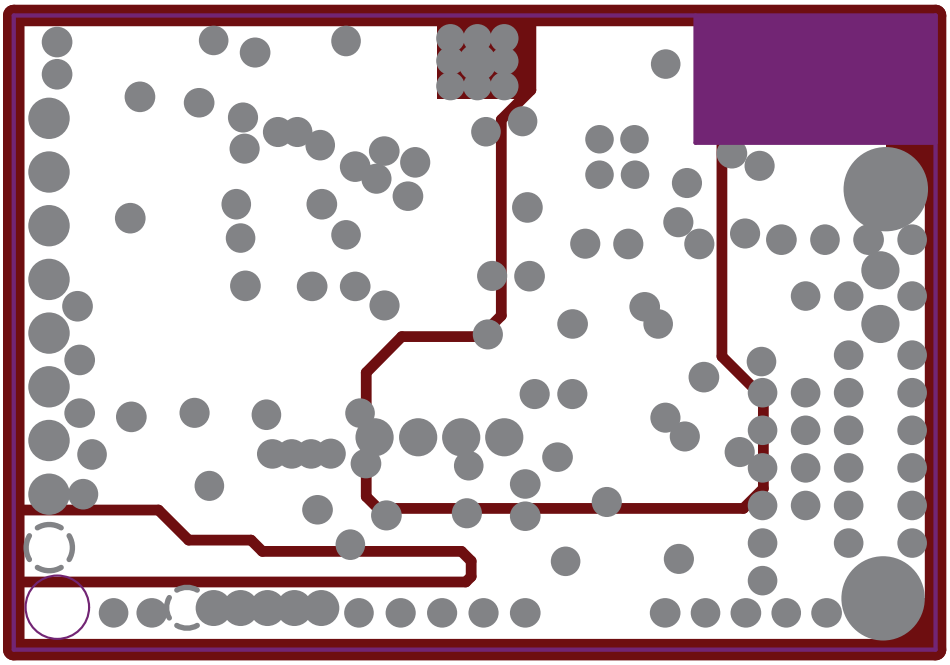

Figure B.5: PCB design: Power plane.

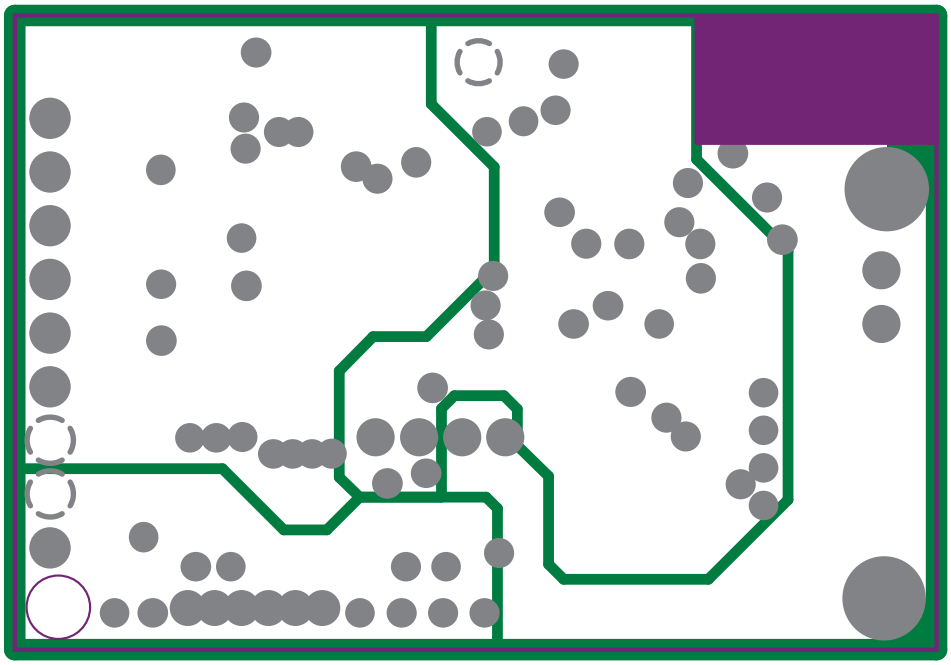

Figure B.6: PCB design: Ground plane.

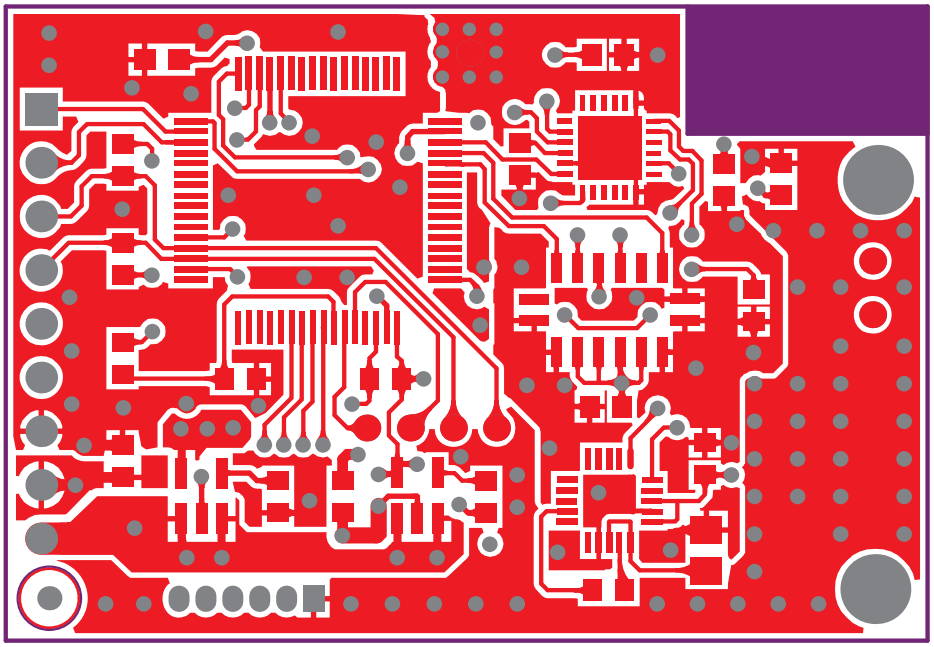

Figure B.7: PCB design: Top layer.

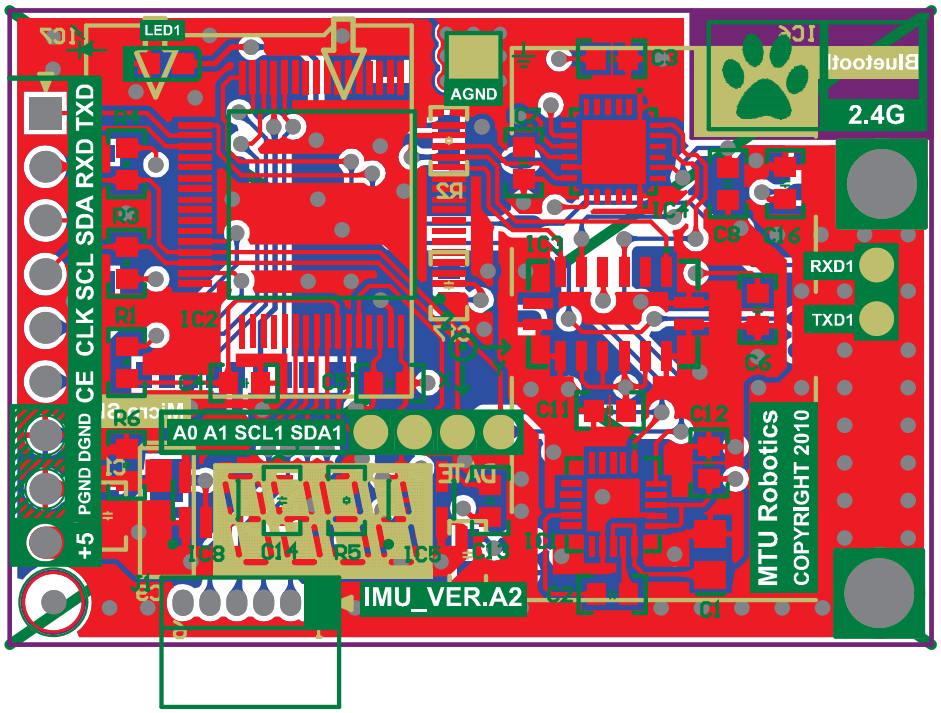

Figure B.8: PCB design: Multiple layers.

Appendix C

Hardware Design of CosNet Static Sensor Node

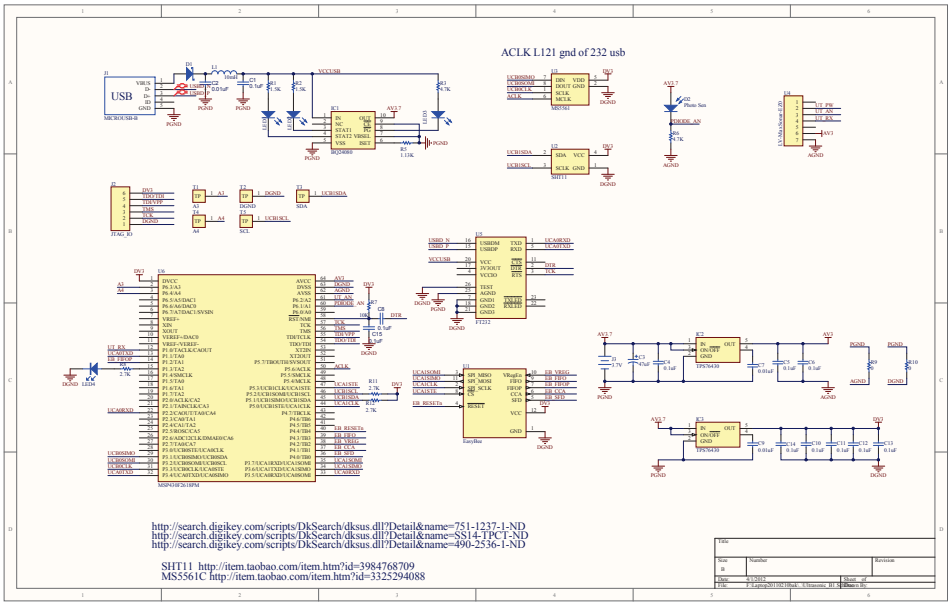

Figure C.1: Schematic design.

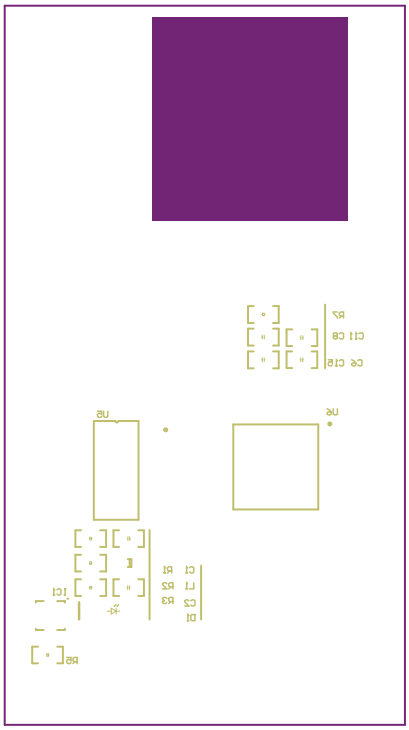

Figure C.2: PCB design: Bottom overlay.

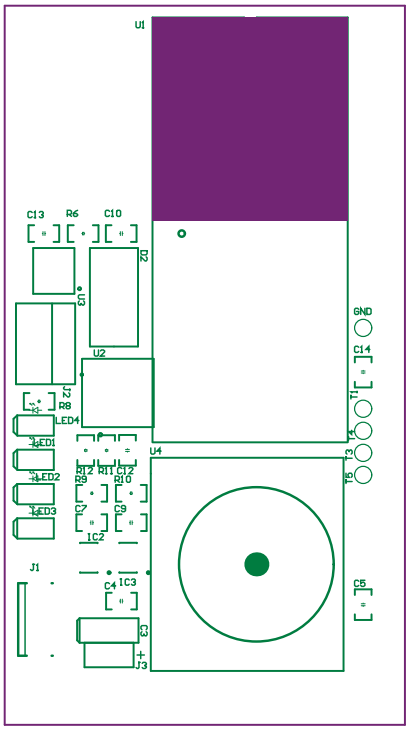

Figure C.3: PCB design: Top overlay.

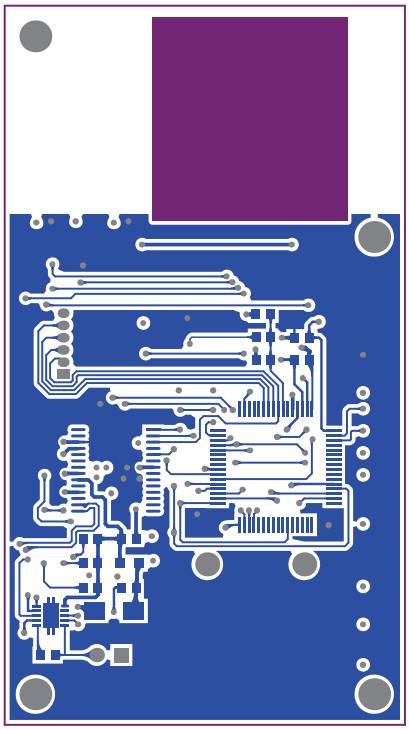

Figure C.4: PCB design: Bottom layer.

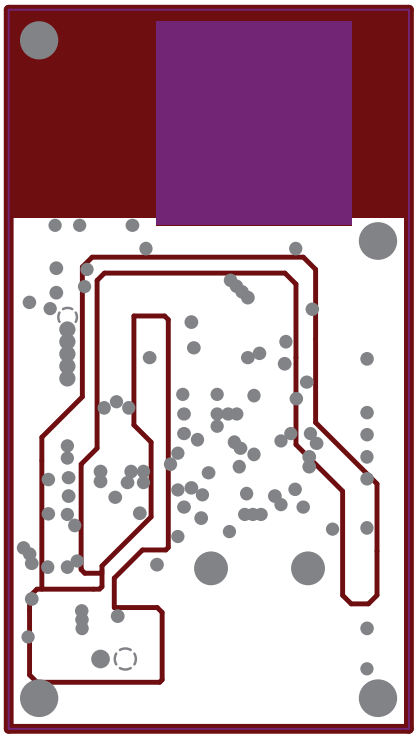

Figure C.5: PCB design: Power Plane.

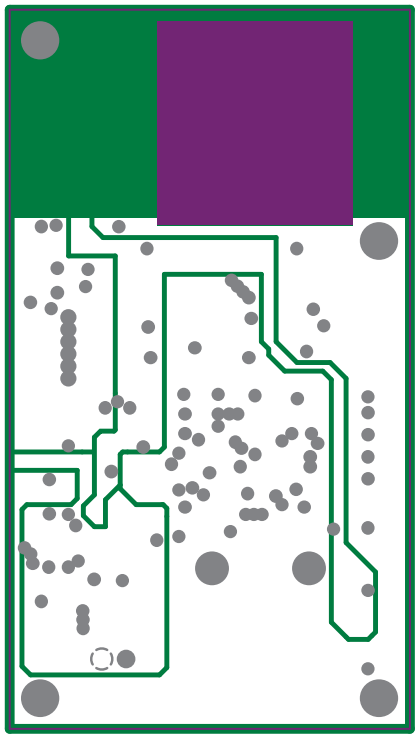

Figure C.6: PCB design: Ground plane.

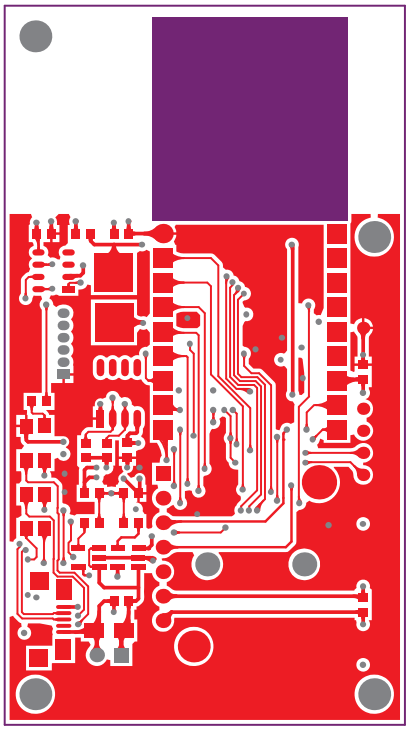

Figure C.7: PCB design: Top layer.

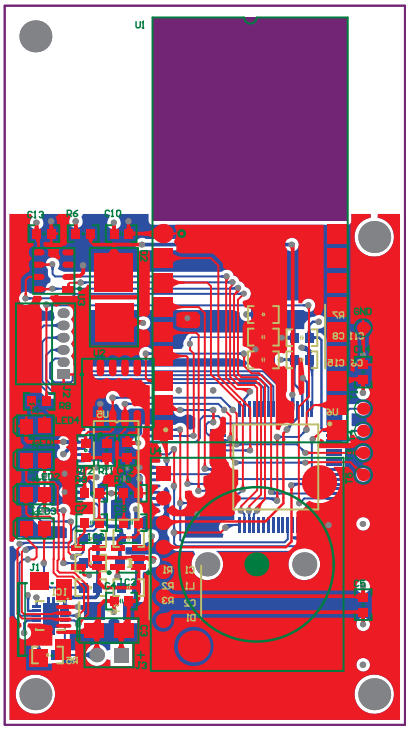

Figure C.8: PCB design: Multiple layers.